Stellingen behorende bij het proefschrift

A Study of In-Plane Dynamics of Tires

van **Sunrong Gong**

1. Tire dynamics can be considered to consist of two different parts: the dynamics of the tire itself and the mechanics of the interaction between the tire and the road. The most efficient way of modeling tire dynamics is to study and model the tire and the tire-road interaction separately and then to combine them into an integrated model. In this way, a wide range of combinations of tires and road conditions can be described by just a few models.

2. In the ring models of tires developed earlier[1], the pretension in the ring was included incorrectly in the equations of motion of the ring.

3. The finite element method is a very powerful tool for solving many static and dynamic problems of complex structures. It can also be applied to the study of tire dynamics. With the rapid development of computer technology, its long-standing disadvantages of requiring large computing power and long computing hours are disappearing.

4. Simulation of vehicle dynamics has become very popular in the past decade for the development of new vehicles. Many advanced simulation softwares and vehicle models have been developed to achieve high simulation accuracy. However, without proper tire modeling, accurate simulation results of vehicle dynamics cannot be obtained.

5. Automation of highway traffic, as envisioned in projects such as IVHS (Intelligent Vehicle-Highway Systems) in the United States and PROMETHEUS in Europe, is a revolutionary idea. However, it would deprive drivers of the control of their own cars, which they have come to enjoy. It is therefore not feasible.

6. With the internationalization of the Delft University of Technology, housing for foreign visiting scholars and students has become an urgent

[1] see References [13,33,44,69,77] of the thesis

issue. A resolution of this would require a consistent and coordinated policy from both the University authorities and the Delft municipal government.

7. One of the main obstacles that foreigners living in The Netherlands encounter in their effort to learn the Dutch language is the amazing ability of the Dutch people to speak English and other languages.

8. With the rapid economic development in China, more and more automobiles are running on its roads and streets. Given the chaotic traffic situation in its big cities, improving traffic control would be a more efficient way of solving the traffic congestion problems than building wider roads and streets.

9. In this information age, too many people waste too much time trying to learn the *new technologies* which often become obsolete before they can be mastered.

10. Unless people are willing to give up the luxuries and conveniences they now enjoy, the issue of environmental pollution cannot be completely resolved.

11. Smoking, eating, using cellular phones, or other similar actions while driving a vehicle, which would divert drivers attention, should be prohibited by law.

A Study of In-Plane Dynamics of Tires

Sunrong Gong

CIP-DATA KONINKLIJKE BIBLIOTHEEK, DEN HAAG

Gong, Sunrong

A Study of In-Plane Dynamics of Tires / Sunrong Gong. -
Delft: Delft University of Technology, Faculty of Mechanical Engineering and Marine Technology. - Ill.
Thesis Technische Universiteit Delft. - With ref. - With summary in Dutch.
ISBN 90-370-0092-4
Subject headings: tires / automobile / dynamics.

Printed in Delft, The Netherlands

A Study of In-Plane Dynamics of Tires

PROEFSCHRIFT

ter verkrijging van de graad van doctor
aan de Technische Universiteit Delft,
op gezag van de Rector Magnificus,
Prof. ir. K.F. Wakker,
in het openbaar te verdedigen
ten overstaan van een commissie
aangewezen door het College van Dekanen
op maandag 20 december 1993 te 10.00 uur

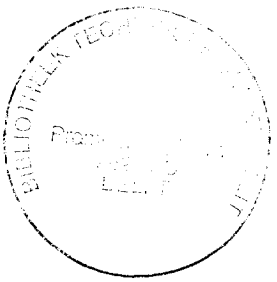

door

Sunrong Gong

Master of Science in Mechanical Engineering

geboren te Zhejiang, China

Dit proefschrift is goedgekeurd door de promotor
Prof. dr. ir. H.B. Pacejka

Dr. ir. A.R. Savkoor
heeft als begeleider in hoge mate bijgedragen
aan het tot standkomen van het proefschrift.
Het College van Dekanen heeft hem als zodanig aangewezen.

to **Caroline** and **Andrew**
to my parents and grandparents

Preface

This thesis describes my work on the in-plane dynamics of tires during my appointment as an AIO (assistant in education) at the Delft University of Technology in The Netherlands. The project was initially entitled *Symmetrisch Dynamisch Bandgedrag* (Symmetric Dynamic Tire Forces). During the course of my research, the emphasis of the project shifted to the development of a tire model suitable for the study of all aspects of in-plane dynamics of tires and to the study of the vibration transmission properties of tires from the road to the wheel. The thesis thus evolved to the form which you see today.

When I began to work on the project, the first task was to establish a mathematical model of the tire. I asked myself the following questions: What approach I should take to model the tire? Theoretical or experimental? Should I model the tire-road system or the tire alone? After spending a couple of months on literature review, I decided to take the theoretical approach and model the tire alone. The idea is to establish separately individual models for the tire alone and for the tire-road interface. By synthesizing the two models, we can obtain models which can characterize systems of various tire-road combinations. The result of adopting this approach was a model which is more versatile in the sense that it can be applied to tires subjected to various boundary conditions at the wheel-axle and the tire-road contact patch and traveling on various road surfaces, at least in theory.

Having established a tire model, the next task was to apply it to solve practical problems of the in-plane dynamics of tires. The simplest mathematical model in our case was sixth order partial differential equations. Trying to solve them for various boundary conditions would not be easy. Fortunately, we had at hand the tool called *modal expansion method*, which simplified the task considerably.

Although the main subject of this thesis is the in-plane dynamics of tires, Chapters 2 and 3 deal with the dynamics of the general ring structure. The analyses and discussions in these two chapters are useful for engineers and researchers interested in similar structures.

During the entire five years spent at the Vehicle Research Laboratory of the Delft University of Technology, I was heavily indebted to my family, colleagues and friends. Without their support and friendship, this thesis would have not been possible. I am especially grateful to my supervisor Prof. dr. ir. Hans B. Pacejka and advisor Dr. ir. Arvin R. Savkoor for giving me the opportunity to pursue my doctorate degree in The Netherlands, and for their invaluable advice and support. Their guidance was indispensable to the completion of this thesis. I would also like to thank Prof. dr. ir. Peter Meijers for thoroughly reviewing my report on the mathematical modeling of tires and the draft thesis. His critical opinions and suggestions proved to be of great value and are reflected in this thesis.

I would like to extend my gratitude to all of my colleagues at the Vehicle Research Laboratory and at the Department of Transport Technology of the Faculty of Mechanical Engineering and Marine Technology, for they created a pleasant working environment for me. Their help and friendship are greatly appreciated. My thanks also go to Professor YU Qun and Professor YU Guyuan at the Beijing Agricultural Engineering University in China for their continuous support and encouragement during the past twelve years.

Finally I would like to thank my wife Caroline for her love, patience and sacrifice. Living in a foreign country has not always been easy for her, especially with a husband whose time was often spent with books and in front of the computer. Hartelijk bedankt, Caroline.

Contents

List of Symbols

Symbol	Description	Unit
A	area of the cross-section of the ring $A = bh$	m^2
b	width of the ring	m
d_0	overall tire deflection	m
E	Young's modulus of the ring material	N/m^2
f_x, f_z	external forces acting at the wheel center in the x, z directions, respectively	N
f_{x^*}, f_{z^*}	external forces acting at the wheel center described in the rotating coordinate system. $f_{x^*} = f_x \cos(\Omega t) + f_z \sin(\Omega t)$, $f_{z^*} = -f_x \sin(\Omega t) + f_z \cos(\Omega t)$	N
h	thickness of the ring	m
I	inertia moment of the cross-section of the ring $I = bh^3/12$	m^4
I_r	moment of inertia of the wheel	$kg \cdot m^2$
k_w, k_v	stiffness of the elastic foundation in the radial and tangential directions, respectively	N/m^2
k_2	stiffness of the tire tread elements in the radial direction	N/m^2
m	mass of the wheel body	kg
m_t	total mass of the tire	kg
n	mode number	
p_0	inflation pressure of the tire	N/m^2
p_w, p_v	point forces acting on the tire at the tire-road contact point in the radial and tangential directions, respectively	N
q_w, q_v	external distributed forces acting on the ring in the radial and tangential directions, respectively	N/m

q	contact pressure of the rolling tire	N/m
R	mean radius of the ring (tire treadband)	m
r	radius of a ring element $r = R + y$	m
$\bar{R}$	free radius of the tire $\bar{R} = R + \tau$	m
T	torque acting on the wheel	N · m
w, v	total displacements of the ring element in the radial and tangential directions, respectively	m
w_r, v_r	displacements of the ring element relative to the wheel center in the radial and tangential directions, respectively	m
x, z	displacement of the wheel center in the longitudinal and vertical directions, respectively	m
x^*, z^*	displacement of the wheel center described in the rotating coordinate system. $x^* = x\cos(\Omega t) + z\sin(\Omega t), z^* = -x\sin(\Omega t) + z\cos(\Omega t)$	m
y	the distance of an element of the ring from the middle surface	m
$\vec{\gamma}$	vector of a point on the middle surface of the ring with respect to the origin of the coordinate system x, z	m
$\dot{\vec{\gamma}}$	speed vector of a point on the middle surface of the ring	m/s
θ	central angle of a point on the ring with respect to the rotating coordinate system	rad
θ_r	angular displacement of the wheel due to the variation of the rotating speed	rad
λ	damping coefficient	
ρ	density of the ring material	kg/m^3
σ_θ^0	prestress in the ring	N/m^2
τ	thickness of the tire tread	m
ϕ	central angle of a point on the ring with respect to the non-rotating coordinate system	rad
ϕ_r, ϕ_f	rear and front central angles of the tire-road contact patch, respectively	rad
Ω	average rotating speed of the tire-wheel system	rad/s
ω_n	natural frequencies of the tire	rad/s

Chapter 1

Introduction

The pneumatic tire is the only component of the automobile which is in contact with the road. It is at the tire-road contact patches that all the forces, except for the aerodynamic ones, are generated, whether desired or not. These forces not only support the weight of the automobile but also control its motion. Therefore the dynamic properties of tires play an important role in the overall performance of the automobile and have received much attention from both automotive and tire engineers since the early 1950s.

From the geometrical viewpoint, a tire has a plane of symmetry perpendicular to the axis of rotation, i.e. the wheel plane. Tire in-plane dynamics deals with the tire motion in the wheel plane. Three aspects of tire in-plane dynamics can be identified: the rolling contact between the tire and the road surface; the force and motion transmission from the contact patch to the wheel axle due to excitation from road irregularities; and the treadband vibration of the tire. The transmission of force and motion is of importance to the overall vehicle dynamics in at least two aspects: the traction/braking performance and the vertical and longitudinal vibrations. The treadband vibration is one of the factors which contribute to the generation of tire noise, and to a lesser extent, affects the durability of the tire. The contact pressure distribution between the tire and the road is one of the major factors affecting the wear of the tire tread and the damage to the road surface caused by automobiles.

1.1 Literature Review

1.1.1 On vibration transmission

Most of the early studies on the vibration transmission properties of tires are mainly of an experimental nature. Among those the work of Chiesa and his colleagues [21, 22] and the work of Barson and Gough et al. [9, 10, 11] are the most prominent. Chiesa et al. observed that when the vibration is transmitted from the road to the wheel, the tire vibrates in two distinct ways. In the middle frequency range (10–20 Hz), the tire vibrates as a whole and acts as a spring and a small damper in parallel. In the high frequency range (50–250 Hz), the tire vibrates in a complex manner with its sidewall and treadband subject to continuous distributed vibrations. They found that the resonant frequency of the first kind (in the middle frequency range) is independent of tire structure and angular speed. The resonant frequencies of the second kind (in the high frequency range) are also independent of speed but are structure-dependent; these of cross-ply tires are higher than those of radial tires. Chiesa et al. also found that there are more than one resonant frequencies of the axle vibration in the high frequency range. By measuring the instantaneous deformation of the tire treadband, Chiesa et al. were able to calculate the vibration transfer functions from the ground to the axle by the summation of the vertical components of the measured treadband displacements along the entire circumference of the tire. This was a very important finding, albeit experimental, because for the first time the tire treadband vibration and the vibration transmission were found to be related. Another contribution of Chiesa and his colleagues is that they demonstrated the importance of proper tire-suspension coupling in order to achieve a good overall vibration performance of an automobile.

Barson and Gough et al. also studied experimentally the tire vibration transmission properties. Instead of using a heavy wheel to apply a static load on the tire, as Chiesa et al. did, they mounted the test tire on a laboratory suspension system through which static load was applied to the tire. In addition to tests using a vibrating platform, they also conducted a large number of tests with the tire running at various speeds on a drum surface fitted with cleats of various shapes and sizes. They found that the frequency response of the axle varies with the wavelength of the road irregularity and with the

rotating speed of the tire. Since the test tire was mounted on a suspension and the input at the tire-road contact patch was not defined (with the exception of the tests with a vibrator), the measured responses do not reflect the vibration transmission properties of the tire alone. Instead, they are the properties of the suspension-tire-road system.

Another significant work on the vibration transmission properties of tires is that of Mills and Dunn [67]. In their tests, the tire was pressed against the smooth surface of a rotating drum by a so-called *air mount pre-loading system* and excited by an electromagnetic vibrator at the axle. Driving point mobility (axle velocity/excitation force) was determined to characterize the vibration transmission properties of the tire. Because the tire was neither mounted on a suspension system nor with a heavy wheel, the measured mobility was free from the influences of components other than the tire with a normal weight wheel and axle and therefore represented only the vibration transmission properties of the tire-wheel system. However, it should be noted here that the constraint conditions of the tire in their tests are different from the ones of a tire on an automobile. In the former case the tire tread elements in the contact patch are constrained from moving in the vertical direction. In the latter case the excitation is applied to the tire by the road irregularities at the contact patch. Therefore the tire tread elements in the contact patch are not subjected to the constraint condition of zero displacement. Mills and Dunn found that in addition to the one low frequency resonance (called *bounce mode*) there exist several high frequency resonances related to the vibration of the tire treadband (called *flexural modes*). This finding coincides with that of Chiesa's. Mills and Dunn also found that resonant frequencies where peaks appear in the mobility curves decrease with the increase of the rotating speed of the tire. This behavior contrasts with that found by Chiesa et al., whose tests showed that the rotating speed has little influence on the vibration transmission properties of the tire.

While the above-mentioned studies are concerned mainly with vibration transmission properties in the range of relatively high frequencies, other studies concentrated on vibration transmissions in the range of low frequencies, such as the *enveloping property* and *dynamic stiffness* of the tire. Lippmann et al. [63] studied experimentally the enveloping property of the tire and proposed that the force response at the axle could be predicted by the product of the road spectrum and the frequency response of the axle force to a single road obstacle of unit size. The latter can be determined exper-

imentally for individual tires. In principle, this method can also be used to predict the high frequency responses of tires to excitations generated by road irregularities, which usually appear at higher rolling speeds. However, the frequency responses of the axle force to a unit obstacle are different from each other when the speed is different.

Pacejka [69] employed a very simple model but successfully predicted the force changes when a tire runs slowly over an obstacle. Davis [25] and others developed a distributed radial spring model to calculate the tire enveloping property. In their model, the radial springs were considered to be independent of each other. Recently, Badalamenti and Doyle [5] improved the distributed radial spring model by adding *inter-radial* springs which connect the neighboring distributed radial springs and act also in the radial direction. Kilner [53] developed yet another tire model for the calculation of tire enveloping forces. He modeled the tire as a toroidal membrane which deflects only in the tire-road contact patch. The tire enveloping force was calculated according to the road profile, the axle position and the consequent tire air volume change (thus the pressure change). The width of the tire-road contact area varies with tire radial deformation. Because it was assumed in the model that the tire deformation at each section is independent of one another, Kilner's model is equivalent to a distributed radial spring model with a non-linear stiffness characteristic.

Rasmussen and Cortese [78] measured the dynamic stiffness of rolling tires. They examined the influences of tire rolling speed, preload, inflation pressure and tire structure on the dynamic stiffness of the tire. They found that substantial differences in stiffness exist between a rolling and non-rolling tire, with the stiffness of the non-rolling tire being higher than that of the rolling tire. They also found that the dynamic stiffness of a rolling tire varies with preload—lighter load results in higher stiffness. In 1974, Captain and Wormley et al. [19] reviewed four tire models for the simulation of vehicles running on uneven roads and evaluated the suitability of those models for low and high frequency simulations. In 1980, Hooker [43] developed a purely empirical model to describe the vertical vibration transmission for low frequencies (0–10 Hz).

More recently, the use of modal analysis and finite element methods for the study of vibration transmission properties of tires has become popular. A team at Goodyear Tire Company conducted both modal testing and FE

analysis of the vibration transmission properties of tires [80, 91]. The resulting tire modal parameters (called *tire modal model*) were applied to the analysis of vehicle noise, vibration and harshness [52]. In their finite element analysis, the tire was modeled as a shell structure with homogeneous anisotropic material properties and the wheel was modeled as a rigid body with six degrees of freedom (DOFs). The FE model was first preloaded to take into account the influences of the inflation pressure, the vertical static load and the constraints at the contact patch. On that basis, small vibrations were assumed. Differences were reported among the results of various tire vibration tests and FE analyses with different tire spindle (axle) and patch (road) constraint conditions [81]. However no effort was made to explain those differences.

Ushijima and Takayama [95] studied the vibration properties of tires using the *constrained modal analysis* method. In their tire modal tests, the tire was mounted on a fixed wheel (has no DOFs) and excited by a vibrating platform on which the tire was placed. The driving point accelerance (acceleration/force) and the constraint force at the axle were used to extract the modal parameters of the tire. These modal parameters obtained from tests of the non-rotating tire were then modified for the rotating tire. This was accomplished by measuring resonant frequencies of the force response at the axle to an impulse force excitation at the treadband when the tire was rotating on a drum. Since the modal parameters were obtained from a tire with a fixed axle, a special modal synthesis method is needed to include the tire model in a complete vehicle model where the axle is moving.

As is evident from this literature review, the vibration transmission properties of a tire are traditionally characterized by two separate properties: stiffness and enveloping properties. The tire stiffness describes the vibration transmission in the low frequency range (< 20 Hz) and it is usually determined by measuring the load-deflection relation of the tire on a flat road surface, either dynamically or statically. The enveloping property of a tire is its ability to cushion a vehicle against road irregularities of short wave length [69]. It is usually measured by the force responses at the axle when a tire with fixed axle height rolls slowly over a short obstacle which extends over the entire width of the tire. Strictly speaking, the enveloping property is a characteristic of the tire-road system, instead of that of the tire alone. Different force responses are expected when the tire rolls over obstacles of different sizes and shapes. Since the enveloping property is obtained in the

state of slow rolling of the tire and no dynamic effects are involved, it is basically a static quantity. However, road irregularities of short wavelength are known to cause high frequency vibrations of tires and vehicles. The force responses of a tire rolling over an obstacle at high speed will be quite different from the ones at very low speed; hence it is not sufficient to describe with the enveloping property the vibration transmission of a tire due to road irregularities of short wavelength.

The subdivision of vibration transmission properties of tires into stiffness and enveloping properties is rather artificial. It is probably because in the early years of tire modeling a tire was often modeled merely as a mass-spring system combined with a filter which filters out the high frequency components of road irregularities. While this kind of tire model gives rather satisfactory results for vibrations at low frequencies , which has been the primary concern in vehicle ride comfort, it is not adequate to represent the vibration transmission properties of tires at higher frequencies.

In addition, most of the previous studies on the vibration transmission of tires were mainly of an experimental nature and concentrated on the vibration transmission in the vertical direction and in the relatively low frequency range. Various constraint conditions of the axle and tire-road contact patch of a tire were applied in these studies described in the preceding paragraphs; thus the results from those studies are not directly comparable with one another.

In order to gain a better understanding of the vibration transmission from the road to the tire-wheel axle, it is desirable to treat the tire in its entirety and study its low and high frequency vibration behaviors comprehensively. Since the tire itself is a very complex entity and the interaction between a tire and the road is also very complicated, it is necessary to study the vibration transmission properties of tires without the influences of the road factors and constraints. Only then can we gain more insight into the mechanism of vibration transmissions of tires.

1.1.2 On treadband vibrations and rolling contact

Most of the early studies on tire treadband vibrations were concerned with the well known standing wave phenomena. Excellent reviews on studies published before 1970 were given by Ames [3] and Pacejka [69]. Several approaches to modeling the standing waves and treadband vibrations of tires have been developed. Clark et al. modeled the tire as a rotating ring supported on radial springs and used this model to calculate the dynamic stiffness of the tire [28], the free vibrations of the treadband [93] and the rolling contact problem [23]. Fiala [35] studied the radial treadband vibrations of radial tires using a tire ring model. Böhm [15] also developed a tire ring model and used it to analyze the free vibrations of the treadband and the standing wave phenomena. He also conducted experiments and compared the test results with the theoretical ones. The tire ring model was later improved by Pacejka [69] with the addition of tangential foundation (sidewall) stiffness and pretension in the ring caused by inflation pressure and centrifugal force. Padovan [71] introduced treadband and sidewall damping into the tire ring model. He demonstrated that standing waves are indeed resonant vibrations of the tire treadband. The internal damping tends to shift the maximum response towards the back of the contact patch and to attenuate the response from the back of the contact patch to the front. In 1977, Potts et al. [77] employed a tire ring model similar to the one proposed by Pacejka to study the free and forced treadband vibrations of tires. They showed that the tire ring model is a very valuable tool for the study of tire vibration properties. Potts et al. also found that the first vibration mode plays an important role in the vibration transmission and that maximum vibration transmission (axle acceleration/footprint displacement) occurs at *antiresonant* frequencies of the corresponding free tire. Yamagishi and Jenkins [99, 100, 50] studied the tire-road contact problem using a tire ring model in which the tread rubber of the tire was modeled as a second set of distributed radial springs to take into account the compliance of the tread elements.

It should be noted here that although the physical structures of the tire ring models mentioned above are similar, the equations of motion derived by the researchers exhibit differences. A preliminary review of the tire ring models can be found in References [36, 37], in which various tire ring models were compared with each other in terms of both the governing equations and the

resulting natural frequencies.

Another approach to modeling a pneumatic tire is to consider it as a thin shell structure. In 1975, Soedel [86] studied the dynamic response of rolling tires by modeling the tire as an equivalent thin shell. Using dynamic Green functions, he showed that all tire responses during steady state (constant speed) rolling are quasi-stationary, and that standing wave phenomena are actually the resonant vibration of the tire treadband. Hirano and Akasaka [42] studied the natural frequencies of a bias tire by modeling it as a composite structure of bias-laminated toroidal membrane shell. Numerical results were compared with experimental data and showed good agreement. In 1977, Padovan [72] again studied the standing wave phenomena with the use of a rotating laminated viscoelastic shell model of the tire. He argued that because the critical speeds of treadband resonant vibrations are so closely spaced that the resonances do not show up on an individual basis, tire standing wave is the result of the superposition of discrete damped harmonics. He therefore concluded that the formation of standing wave is an evolving process instead of a sudden transition. The influence of damping on standing waves was also analyzed by the same author. Hunckler [48] developed a doubly-curved, axisymmetric shell finite element model to study the free vibration of tires. Later, Chang [20] studied the dynamic responses of tires to sinusoidal force excitation using Hunckler's model and the modal expansion method. Kung [59] improved Hunckler's FE model with the integration of computer graphics into the FE program and therefore made it easier to identify the vibration modes of tires.

1.2 Objectives and Scope

While several types of models were developed for the analysis of the treadband vibrations and tire-road contact problem, few analytical models are available for the study of the vibration transmission properties of tires. In most of the literature, the three aspects of tire in-plane dynamics were dealt with as isolated problems without exploring their underlying relations.

The main objective of this study is to develop a tire model which is suitable to study all three aspects of in-plane dynamics of tires in both the low and

high frequency ranges. Emphasis is placed on the analysis of the dynamic properties of the model and the application of the model to the study of practical problems of tire and vehicle dynamics.

To achieve this objective, a ring model is developed in which the tire is modeled as a flexible circular ring on an elastic foundation. The main improvement from ring models developed earlier is that the wheel of the tire in this model is free to translate and rotate in the wheel plane. These degrees of freedom of the wheel make the model suitable for the study of vibration transmission properties of tires operating under more general boundary conditions. This general formulation permits the conversion and comparison of laboratory test data obtained under different boundary conditions and also accommodates the more realistic boundary conditions such as those which occur with tires mounted on a vehicle driving on uneven roads. The modal expansion method is used so that the developed tire model can be easily applied to the study of practical problems of tire and vehicle dynamics.

The tire-road rolling contact and vibration transmission from the ground to the wheel axle are studied using the tire ring model. The study of the contact problem is restricted to the case of a freely rolling tire. The vibration transmission of the tire is studied in the context of point contact assumption.

1.3 Outline of the Thesis

In Chapter 2, a tire ring model is developed. In this model, the tire is modeled as a circular ring supported on an elastic foundation. Three degrees of freedom of the wheel motion in the rotational as well as vertical and longitudinal directions are considered in the model. The model can thus be applied to the study of all three aspects of tire in-plane dynamics. The equations of motion of the tire model are derived in this chapter.

In Chapter 3, the vibration properties of the ring model are analyzed. The natural frequencies and mode shapes are obtained. The influences of the model parameters and rotation on the vibration properties are examined.

In Chapter 4, the equations of motion, which are high order partial differ-

ential equations, are transformed into ordinary differential equations using the modal expansion method. Two sets of the transformed equations are obtained, one using the coordinates defined in the rotating coordinate system and the other using the coordinates defined in the non-rotating coordinate system. Damping is introduced into the model at this stage.

In Chapter 5, the ring model is applied to the study of the contact problem of the tire rolling on a flat road. Secondary radial springs are introduced to take into account the compliance of the tread elements in the radial direction. The numerical results are compared with experimental ones from literature and the general patterns of contact pressure distribution are discussed.

In Chapter 6, the vibration transmission of a free tire-wheel system is studied using the tire ring model developed in Chapter 2. The transfer functions between any two points in the system are obtained using the modal expansion method. The general characteristics of the vibration transmission between the wheel axle and the tire-road contact point are discussed.

Chapter 7 deals with the vibration transmission of a tire-wheel system under various boundary conditions. Three configurations typical to tires in laboratory tests and on the vehicle are discussed. The transfer functions in each case are obtained from those of the corresponding free tire-wheel system using the modal synthesis method. Numerical results are presented and discussed.

In Chapter 8, experimental results obtained from laboratory tests of a tire are presented. The parameters of the tire model are estimated using three measured natural frequencies of the test tire. The theoretical results predicted by the model are compared with the experimental ones of the dynamic tire tests.

Finally, the most important conclusions of this study are given in Chapter 9. Recommendations for further research and possible improvement of the model are mentioned as well.

Chapter 2

The Modeling of Tire-Wheel Systems

2.1 Model Description

The ring model of a tire-wheel system is shown in Figure 2.1. In this model, a pneumatic tire-wheel system is considered to be the assembly of three components: the tire treadband, the sidewall, and the wheel. The tire treadband is idealized as a circular, thin ring with homogeneous material properties. The wheel is modeled as a rigid, axially symmetric body with mass and moment of inertia. The two components, namely the treadband and the wheel, are connected with each other by the third component—sidewall and pressurized air. This third component is modeled as an elastic foundation which consists of radial and tangential springs distributed along the entire circumference of the ring. It is assumed that the springs are connected to the middle surface of the ring. The entire system rotates at an average angular speed Ω around the wheel axis.

In the wheel plane of the tire, the wheel has three degrees of freedom (DOFs)—two translational DOFs and one rotational DOF. The two translational DOFs allow the wheel to move in the vertical and longitudinal directions and the rotational DOF allows the wheel angular speed to vary around

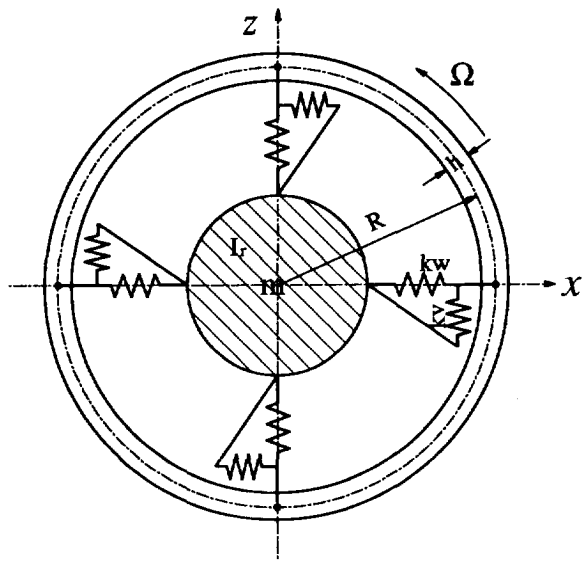

Figure 2.1: The ring model of a tire-wheel system: the tire is modeled as a circular ring supported on an elastic foundation

its mean value. Small variations in the wheel angular speed are assumed so that the equations of motion of the model can be linearized. These three DOFs of the wheel enable the model to be applied to the study of vibration transmission properties of tires in the vertical and longitudinal directions as well as in the rotational direction.

It is understood that the pressurized air in a pneumatic tire is very important to the functioning of the tire. In this model the effects of the pressurized air are introduced in two ways: a) the stiffness of the tangential and radial springs are considered to vary with the inflation pressure of the tire; and b) the circular ring is prestressed by the inflation pressure and centrifugal forces due to rotation.

It is assumed that the in-plane deformation of the tire treadband in planes parallel to the wheel plane is uniform over the tire width. Therefore in-plane dynamics of the tire-wheel system is treated as a two-dimensional problem.

2.2 Coordinate Systems, Displacements and Strains

2.2.1 Coordinate systems

Throughout this thesis, two kinds of coordinate systems are used: one is the space-fixed (non-rotating) coordinate system, the other is the rotating coordinate system. The origins of the two coordinate systems coincide with each other. The translational displacement of the center of the wheel is described in terms of Cartesian coordinates (x, z) in the non-rotating coordinate system, or (x^*, z^*) in the rotating coordinate system. The location of an infinitesimal element of the ring is described in terms of cylindrical coordinates (r, ϕ) in the non-rotating coordinate system, or (r, θ) in the rotating coordinate system, as shown in Figure 2.2. The reason for using two coordinate systems is that the tire-wheel is a rotating system; in order to study the vibrational behavior of the tire treadband it is convenient to have a coordinate system which is rotating with the tire, while for the study of the vibration transmission properties of the system it is more convenient to have a coordinate system which is not rotating. The transformation between the two coordinate systems is as follows (see Figure 2.2):

$$x = x^* \cos(\Omega t) - z^* \sin(\Omega t) \tag{2.1a}$$

$$z = x^* \sin(\Omega t) + z^* \cos(\Omega t) \tag{2.1b}$$

$$\phi = \theta + \Omega t \tag{2.1c}$$

2.2.2 The displacements of ring elements

Figure 2.2 also shows the positions of a point (**A**) on the middle surface of the ring at different stages of the system motion. The absolute displacement of point **A** consists of three parts: one is due to the rotation of the system; another is the rigid body displacement of the system due to the translational motion of the wheel; the third is that due to the deformation of the ring. If we describe the motion of point **A** in the rotating coordinate system, the first part of the displacement can be disregarded. The rigid body displacement is represented by x^* and z^* in the rotating coordinate system (or x and z in the non-rotating coordinate system), which is identical for all points in the system. The displacement components in the rotating coordinate system

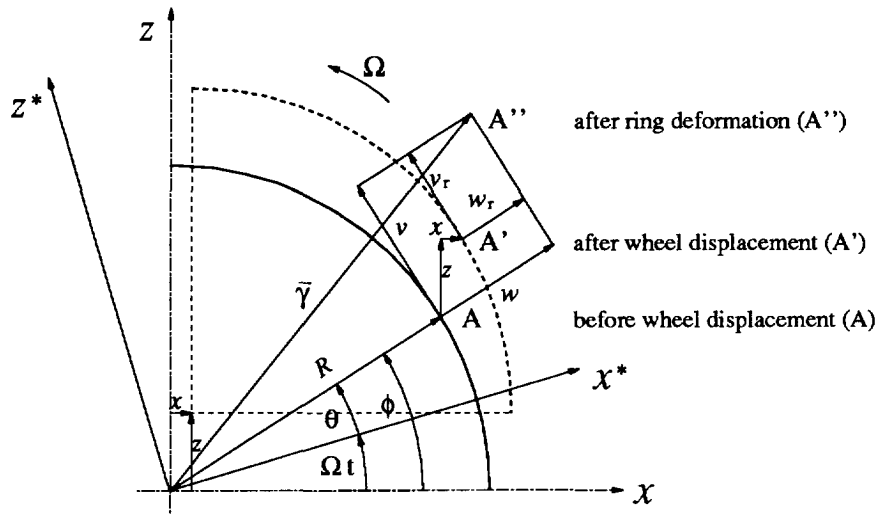

Figure 2.2: The coordinate systems and location of ring elements

due to ring deformation are described by w_r in the radial direction and v_r in the tangential direction, and hereafter will be called relative displacements. The relations between w, v (the total displacement of point **A** with respect to the rotating coordinate system) and w_r, v_r are as follows

$$w = w_r + x^* \cos\theta + z^* \sin\theta \tag{2.2a}$$

$$v = v_r - x^* \sin\theta + z^* \cos\theta \tag{2.2b}$$

The location of point **A** on the ring after deformation (with respect to the non-rotating coordinate system) is described by vector $\vec{\gamma}$, see Figure 2.2.

$$\vec{\gamma} = (R + w)\vec{n}_r + v\vec{n}_\theta \tag{2.3}$$

where $\vec{n}_r, \vec{n}_\theta$ are unit vectors in the radial and tangential directions in the undeformed state, respectively; R is the radius of the middle surface of the ring.

After deformation of the ring, the normal and tangent to the ring surface at point **A** no longer coincide with the unit vectors $\vec{n}_r, \vec{n}_\theta$. Denoting $\vec{n}$ as the unit vector normal to and $\vec{\tau}$ tangent to the deformed ring surface, the

following approximate relations between $\vec{n}, \vec{\tau}$ and $\vec{n}_r, \vec{n}_\theta$ exist [18]:

$$\vec{n} \doteq \left[1 + \frac{1}{R}\left(\frac{\partial v}{\partial \theta} + w\right)\right]\vec{n}_r - \frac{1}{R}\left(\frac{\partial w}{\partial \theta} - v\right)\vec{n}_\theta \tag{2.4a}$$

$$\vec{\tau} \doteq \frac{1}{R}\left(\frac{\partial w}{\partial \theta} - v\right)\vec{n}_r + \left[1 + \frac{1}{R}\left(\frac{\partial v}{\partial \theta} + w\right)\right]\vec{n}_\theta \tag{2.4b}$$

2.2.3 Strain-displacement relations

The general strain-displacement relations of a ring are as follows

$$\epsilon_r = \frac{\partial W_r}{\partial r} \tag{2.5a}$$

$$\epsilon_\theta = \frac{1}{r}\left(W_r + \frac{\partial V_r}{\partial \theta}\right) + \frac{1}{2r^2}\left(\frac{\partial W_r}{\partial \theta} - V_r\right)^2 \tag{2.5b}$$

$$\epsilon_{r\theta} = \frac{\partial V_r}{\partial r} + \frac{1}{r}\left(\frac{\partial W_r}{\partial \theta} - V_r\right) \tag{2.5c}$$

here $\epsilon_r, \epsilon_\theta$ are the normal strains in radial and tangential directions, respectively; $\epsilon_{r\theta}$ is the in-plane shear strain; W_r, V_r are the relative displacements of the point (r, θ) on the ring in the radial and tangential directions, respectively. The derivation of the strain-displacement relations is given in Appendix A. The second order non-linear term in ϵ_θ is retained in order to properly take into account the pretension effect of the ring.

The rigid body displacement does not produce strains in the ring body. Therefore W_r, V_r in Equation (2.5) can be replaced by W, V respectively. Substituting Equation (2.2) in to Equation (2.5), we will see that the terms containing rigid body displacement x^*, z^* cancel each other out and new strain-displacement relations identical to Equation (2.5) result, but now in terms of total displacements W and V.

$$\epsilon_r = \frac{\partial W}{\partial r} \tag{2.6a}$$

$$\epsilon_\theta = \frac{1}{r}\left(W + \frac{\partial V}{\partial \theta}\right) + \frac{1}{2r^2}\left(\frac{\partial W}{\partial \theta} - V\right)^2 \tag{2.6b}$$

$$\epsilon_{r\theta} = \frac{\partial V}{\partial r} + \frac{1}{r}\left(\frac{\partial W}{\partial \theta} - V\right) \tag{2.6c}$$

In our tire model, the ring is considered to be thin. According to the Bernoulli-Euler assumption, the plane cross-sections of the ring remain plane and normal to the middle surface after deformation, and the in-plane shear strain is very small and can be neglected. The only significant strain is therefore the one in the tangential direction. The normal strain in the tangential direction is thus (see Appendix A):

$$\epsilon_\theta = \frac{1}{R}\left(w + \frac{\partial v}{\partial \theta}\right) + \frac{y}{R^2}\left(\frac{\partial v}{\partial \theta} - \frac{\partial^2 w}{\partial \theta^2}\right) + \frac{1}{2R^2}\left(v - \frac{\partial w}{\partial \theta}\right)^2 \tag{2.7}$$

in which y is the distance from the middle surface. The first and third terms represent the extensional deformation of the middle surface of the ring while the second term is the result of bending of the ring.

2.3 Equations of Motion

Hamilton's principle is used for the derivation of the governing equations of the rotating ring on an elastic foundation. Therefore we need first to obtain the expressions of various energy components.

2.3.1 Energy expressions

Strain Energy

In the initial state, it is assumed that the ring is in equilibrium under the action of the inflation pressure and the centrifugal force which induce the prestress σ_θ^0 in the ring. The difference in strain energy between the final state and the initial prestressed state is

$$S_1 = b\int_0^{2\pi}\int_{-h/2}^{h/2}\left[\frac{1}{2}\sigma_\theta\epsilon_\theta + \sigma_\theta^0\epsilon_\theta\right] R\,dy\,d\theta \tag{2.8}$$

in which σ_θ and σ_θ^0 are the incremental and initial normal stress in the tangential direction, respectively; b is the width of the ring. The prestress σ_θ^0 is considered to be a constant which varies only with the inflation pressure

and the rotating speed of the ring. The relation between σ_θ^0 and the rotating speed Ω and the inflation pressure p_0 of the tire is determined by the following equation (see Appendix B):

$$\sigma_\theta^0 A = \left(p_0 bR + \rho A R^2 \Omega^2\right) \tag{2.9}$$

where ρ is the density of the ring; $A = bh$ is the area of the ring cross-section.

Assuming Hooke's law applies to the incremental stress and strain of the ring, the following strain energy expression is obtained, after substituting Equation (2.7) into Equation (2.8) and conducting integration with respect to the ring thickness:

$$S_1 = \int_0^{2\pi} \frac{1}{2}\left\{2\sigma_\theta^0 A\left(w + \frac{\partial v}{\partial \theta}\right) + \frac{\sigma_\theta^0 A}{R}\left(v - \frac{\partial w}{\partial \theta}\right)^2 + \frac{E}{R}\left[A\left(w + \frac{\partial v}{\partial \theta}\right)^2 + \frac{I}{R^2}\left(\frac{\partial v}{\partial \theta} - \frac{\partial^2 w}{\partial \theta^2}\right)^2\right]\right\} d\theta \tag{2.10}$$

in which E is Young's modulus of the ring material; $I = bh^3/12$ is the inertia moment of the ring cross-section. The first two terms of the strain energy are due to the prestress in the ring; the third term is due to the circumferential extension of the ring; the last term in the above expression is due to the change in curvature of the ring (bending deformation).

Kinetic Energy

The kinetic energy of the ring is

$$T_1 = b\int_0^{2\pi}\int_{-h/2}^{h/2} \frac{1}{2}\rho R\left|\dot{\vec{\gamma}}\right|^2 dy\, d\theta \tag{2.11}$$

where $\dot{\vec{\gamma}}$ is the speed vector of the point (r, θ) of the ring. Since the ring is thin, the speed vector of this point can be approximated by that of the middle point **A** of the same cross-section. Differentiating Equation (2.3) with respect to time, we have

$$\dot{\vec{\gamma}} = (\dot{w} - v\Omega)\vec{n}_r + [\dot{v} + (R + w)\Omega]\,\vec{n}_\theta$$

Substituting $\dot{\tilde{\gamma}}$ into the expression of the kinetic energy of the ring body yields

$$T_1 = \int_0^{2\pi} \frac{1}{2}\rho AR\left[(\dot{w} - v\Omega)^2 + (\dot{v} + (R+w)\Omega)^2\right] d\theta \tag{2.12}$$

The kinetic energy stored in the wheel mass reads

$$T_2 = \frac{1}{2}\left[m\left(\dot{x}^2 + \dot{z}^2\right) + I_r\left(\Omega + \dot{\theta}_r\right)^2\right] \tag{2.13}$$

where m is the wheel mass; I_r is the moment of inertia of the wheel; and $\dot{\theta}_r$ is the angular speed variation around the mean value Ω. Substituting Equation (2.1) into the above equation, we have

$$T_2 = \frac{1}{2}\left[m\left((\dot{x}^* - \Omega z^*)^2 + (\dot{z}^* + \Omega x^*)^2\right) + I_r\left(\Omega + \dot{\theta}_r\right)^2\right] \tag{2.14}$$

Elastic Energy of the Foundation

The potential energy stored in the elastic foundation (radial and tangential springs) is

$$\begin{aligned} S_2 = \int_0^{2\pi} \frac{1}{2}\Big[&k_v\left(v + x^*\sin\theta - z^*\cos\theta - R\theta_r\right)^2 \\ &+ k_w\left(w - x^*\cos\theta - z^*\sin\theta\right)^2\Big] R\, d\theta \end{aligned} \tag{2.15}$$

in which θ_r is the angular displacement of the wheel caused by the angular speed variation $\dot{\theta}_r$.

Virtual Work of External Forces

Generally, a tire in working condition is subjected to forces acting at the axle and at the road contact patch. In this tire ring model, these forces are represented by the longitudinal and vertical axle forces f_x, f_z (f_{x^*} and f_{z^*} if converted to the rotating coordinate system); the torque T acting on the wheel; and the external forces q_v, q_w distributed along the ring circumference in the tangential and radial directions, respectively. All of these

external forces as well as the tire inflation pressure will contribute to the tire deformation. The virtual work done by these external forces over virtual displacements $\delta w, \delta v$ and $\delta x^*, \delta z^*, \delta\theta_r$ is

$$\delta E_1 = \int_0^{2\pi} [q_w\, \delta w + q_v\, \delta v]\, R\, d\theta + f_{x^*}\, \delta x^* + f_{z^*}\, \delta z^* + T\, \delta\theta_r \tag{2.16}$$

The inflation pressure always acts on the ring in the direction normal to the deformed ring surface. According to Equation (2.4), the virtual work done by the inflation pressure over the virtual displacement $\delta w, \delta v$ is as follows:

$$\delta E_2 = \int_0^{2\pi} p_0 b \left[\left(1 + \frac{1}{R}\left(\frac{\partial v}{\partial\theta} + w\right)\right)\delta w - \frac{1}{R}\left(\frac{\partial w}{\partial\theta} - v\right)\delta v\right] R\, d\theta \tag{2.17}$$

The total virtual work is thus

$$\delta E = \delta E_1 + \delta E_2 \tag{2.18}$$

The Lagrange function of the tire ring model is

$$L = T_1 + T_2 - S_1 - S_2 \tag{2.19}$$

2.3.2 Equations of motion

According to Hamilton's principle, the time integral over any interval of the sum of virtual kinetic energy change and virtual work vanishes when the virtual displacements are made from configurations of the actual motion and when the final configurations are given [82]. It reads:

$$\int_{t_0}^{t_1} (\delta T + \delta W)\, dt = 0 \tag{2.20}$$

where the virtual work δW consists of two parts—one due to conservative forces and the other due to non-conservative forces. For our tire ring model, Hamilton's principle can be expressed as:

$$\int_{t_0}^{t_1} (\delta L + \delta E)\, dt = 0 \tag{2.21}$$

in which δL is the variation of the Lagrange function. From the above equation the following Euler-Lagrange equations are derived for our ring model:

$$\frac{\partial}{\partial t}\frac{\partial L}{\partial \dot{w}} + \frac{\partial}{\partial \theta}\frac{\partial L}{\partial w'} - \frac{\partial^2}{\partial \theta^2}\frac{\partial L}{\partial w''} - \frac{\partial L}{\partial w} = Q_1 \tag{2.22a}$$

$$\frac{\partial}{\partial t}\frac{\partial L}{\partial \dot{v}} + \frac{\partial}{\partial \theta}\frac{\partial L}{\partial v'} - \frac{\partial L}{\partial v} = Q_2 \tag{2.22b}$$

$$\frac{\partial}{\partial t}\frac{\partial L}{\partial \dot{\theta}_r} - \frac{\partial L}{\partial \theta_r} = Q_3 \tag{2.22c}$$

$$\frac{\partial}{\partial t}\frac{\partial L}{\partial \dot{x}^*} - \frac{\partial L}{\partial x^*} = Q_4 \tag{2.22d}$$

$$\frac{\partial}{\partial t}\frac{\partial L}{\partial \dot{z}^*} - \frac{\partial L}{\partial z^*} = Q_5 \tag{2.22e}$$

Here the raised dot $(\cdot)$ indicates differentiations with respect to time, the prime $(')$ denotes differentiations with respect to θ. Q_i $(i = 1, ..., 5)$ are the generalized forces:

$$Q_1 = \int_0^{2\pi} R\left(q_w + \left(1 + \frac{v' + w}{R}\right) p_0 b\right) d\theta$$

$$Q_2 = \int_0^{2\pi} R\left(q_v - \frac{w' - v}{R} p_0 b\right) d\theta$$

$$Q_3 = T$$

$$Q_4 = f_{x^*}$$

$$Q_5 = f_{z^*}$$

Substituting the Lagrange function (Equation (2.19)) into Equations (2.22), the equations of motion of the tire ring model are obtained:

$$\begin{aligned}
&\frac{EI}{R^4}\left(\frac{\partial^4 w}{\partial \theta^4} - \frac{\partial^3 v}{\partial \theta^3}\right) + \frac{EA}{R^2}\left(w + \frac{\partial v}{\partial \theta}\right) + \frac{\sigma_\theta^0 A}{R^2}\left(\frac{\partial v}{\partial \theta} - \frac{\partial^2 w}{\partial \theta^2}\right) \\
&\quad + k_w\left(w - x^* \cos\theta - z^* \sin\theta\right) + \rho A\left(\ddot{w} - 2\Omega\dot{v} - \Omega^2 w\right) \\
&\quad - \frac{p_0 b}{R}\left(\frac{\partial v}{\partial \theta} + w\right) = q_w
\end{aligned} \tag{2.23a}$$

$$\begin{aligned}
&\frac{EI}{R^4}\left(\frac{\partial^3 w}{\partial \theta^3} - \frac{\partial^2 v}{\partial \theta^2}\right) - \frac{EA}{R^2}\left(\frac{\partial w}{\partial \theta} + \frac{\partial^2 v}{\partial \theta^2}\right) + \frac{\sigma_\theta^0 A}{R^2}\left(v - \frac{\partial w}{\partial \theta}\right) \\
&\quad + k_v\left(v + x^* \sin\theta - z^* \cos\theta - R\theta_r\right) + \rho A\left(\ddot{v} + 2\Omega\dot{w} - \Omega^2 v\right)
\end{aligned}$$

$$+\frac{p_0 b}{R}\left(\frac{\partial w}{\partial \theta} - v\right) = q_v \tag{2.23b}$$

$$I_r \ddot{\theta}_r + 2\pi k_v R^3 \theta_r - R^2 \int_0^{2\pi} k_v v \, d\theta = T \tag{2.23c}$$

$$\begin{aligned} &m(\ddot{x}^* - 2\Omega \dot{z}^* - \Omega^2 x^*) + \pi R (k_w + k_v) x^* \\ &\quad - R \int_0^{2\pi} (k_w w \cos\theta - k_v v \sin\theta) \, d\theta = f_{x^*} \end{aligned} \tag{2.23d}$$

$$\begin{aligned} &m(\ddot{z}^* + 2\Omega \dot{x}^* - \Omega^2 z^*) + \pi R (k_w + k_v) z^* \\ &\quad - R \int_0^{2\pi} (k_w w \sin\theta + k_v v \cos\theta) \, d\theta = f_{z^*} \end{aligned} \tag{2.23e}$$

2.3.3 The in-extensibility assumption

The governing equations of the tire ring model can be simplified with the introduction of the so-called *in-extensibility assumption*, which means that the circumferential length of the middle surface of the ring is constant during the deformation. This assumption is usually valid for rings with high extensional stiffness, which is the case with the most widely used radial tires.

At the middle surface, the tangential normal strain is

$$\epsilon_\theta = \frac{1}{R}\left(w + \frac{\partial v}{\partial \theta}\right)$$

With this we get under the in-extensibility assumption:

$$w = -\frac{\partial v}{\partial \theta} \tag{2.24}$$

Substituting Equation (2.24) into Equations (2.23), then differentiating Equation (2.23a) with respect to θ and adding it to Equation (2.23b) we obtain the equations of motion of the tire ring model under the in-extensibility assumption:

$$\begin{aligned} &-\frac{EI}{R^4}\left(\frac{\partial^2 v}{\partial \theta^2} + 2\frac{\partial^4 v}{\partial \theta^4} + \frac{\partial^6 v}{\partial \theta^6}\right) + \frac{\sigma_\theta^0 A}{R^2}\left(v + 2\frac{\partial^2 v}{\partial \theta^2} + \frac{\partial^4 v}{\partial \theta^4}\right) - \frac{p_0 b}{R}\left(v + \frac{\partial^2 v}{\partial \theta^2}\right) \\ &\quad - k_w \frac{\partial^2 v}{\partial \theta^2} + k_v (v - R\theta_r) + (k_w + k_v)(x^* \sin\theta - z^* \cos\theta) \end{aligned}$$

$$+\rho A\left[\ddot{v}-\frac{\partial^2\ddot{v}}{\partial\theta^2}-4\Omega\frac{\partial\dot{v}}{\partial\theta}+\Omega^2\left(\frac{\partial^2 v}{\partial\theta^2}-v\right)\right]=q_v+\frac{\partial q_w}{\partial\theta} \tag{2.25a}$$

$$I_r\ddot{\theta}_r+2\pi k_v R^3\theta_r-R^2\int_0^{2\pi}k_v v\,d\theta=T \tag{2.25b}$$

$$m(\ddot{x}^*-2\Omega\dot{z}^*-\Omega^2x^*)+\pi R(k_w+k_v)x^* -R\int_0^{2\pi}\left(-k_w\frac{\partial v}{\partial\theta}\cos\theta-k_v v\sin\theta\right)d\theta=f_{x^*} \tag{2.25c}$$

$$m(\ddot{z}^*+2\Omega\dot{x}^*-\Omega^2z^*)+\pi R(k_w+k_v)z^* -R\int_0^{2\pi}\left(-k_w\frac{\partial v}{\partial\theta}\sin\theta+k_v v\cos\theta\right)d\theta=f_{z^*} \tag{2.25d}$$

Up to this point, we have already derived the equations of motion of the tire ring model with the inclusion of the coriolis effect and the two translational and one rotational DOFs of the wheel (Equation (2.23)). And we have further simplified the equations of motion by introducing the in-extensibility assumption (Equation (2.25)). The inclusion of the two translational and one rotational DOFs of the wheel in the current model makes it possible to study the vibration transmission properties of tires under various constraint conditions and therefore can simulate the operation conditions of tires on an automobile on actual road surfaces.

Chapter 3

Natural Frequencies and Modes

3.1 The Natural Frequencies

The displacements of the ring w in the radial direction and v in the tangential direction are periodic functions of the angular coordinate θ or ϕ. Therefore we may expand w, v into complex Fourier series:

$$w(\theta,t) = \sum_{n=-\infty}^{+\infty} w_n(t) e^{jn\theta} \tag{3.1a}$$

$$v(\theta,t) = \sum_{n=-\infty}^{+\infty} v_n(t) e^{jn\theta} \tag{3.1b}$$

where $n = -\infty, ..., -1, 0, +1, ... + \infty$; $j = \sqrt{-1}$ is the imaginary unit. Note that the following relations exist:

$$\cos\theta = \frac{1}{2}\left(e^{j\theta} + e^{-j\theta}\right) = \frac{1}{2}\sum_{n=-\infty}^{+\infty}\left(e^{jn\theta}\delta_{|n|1}\right)$$

$$\sin\theta = \frac{1}{2j}\left(e^{j\theta} - e^{-j\theta}\right) = -\frac{1}{2}\sum_{n=-\infty}^{+\infty}\left(jne^{jn\theta}\delta_{|n|1}\right)$$

$$\int_0^{2\pi} e^{jn\theta}\cos\theta\, d\theta = \pi\delta_{|n|1}$$

$$\int_0^{2\pi} e^{jn\theta} \sin\theta \, d\theta = jn\pi\delta_{|n|1}$$

here δ_{pq} is the Kronecker delta function whose value equals 1 when $p = q$ or 0 when $p \neq q$.

Inserting Equation (3.1) into Equations (2.23), we obtain,

$$\rho A\ddot{w}_n - 2\rho A\Omega\dot{v}_n + \left[\frac{EI}{R^4}n^4 + \frac{EA}{R^2} + \frac{\sigma_\theta^0 A}{R^2}n^2 - \frac{p_0 b}{R} + k_w - \rho A\Omega^2\right] w_n$$
$$+j\left[\frac{EI}{R^4}n^3 + \frac{EA}{R^2}n + \frac{\sigma_\theta^0 A}{R^2}n - \frac{p_0 b}{R}n\right] v_n - \frac{1}{2}k_w(x^* - jnz^*)\delta_{|n|1} = 0 \tag{3.2a}$$

$$\rho A\ddot{v}_n + 2\rho A\Omega\dot{w}_n - j\left[\frac{EI}{R^4}n^3 + \frac{EA}{R^2}n + \frac{\sigma_\theta^0 A}{R^2}n - \frac{p_0 b}{R}n\right] w_n$$
$$+\left[\left(\frac{EI}{R^4} + \frac{EA}{R^2}\right)n^2 + \frac{\sigma_\theta^0 A}{R^2} - \frac{p_0 b}{R} + k_v - \rho A\Omega^2\right] v_n$$
$$-\frac{1}{2}jnk_v(x^* - jnz^*)\delta_{|n|1} - k_v R\theta_r\delta_{|n|0} = 0 \tag{3.2b}$$

$$I_r\ddot{\theta}_r + 2\pi k_v R^3\theta_r - 2\pi R^2 k_v v_0 = 0 \tag{3.2c}$$

$$m\left(\ddot{x}^* - 2\Omega\dot{z}^* - \Omega^2 x^*\right) + \pi R(k_w + k_v)x^*$$
$$-\pi R[k_w(w_1 + w_{-1}) - jk_v(v_1 - v_{-1})] = 0 \tag{3.2d}$$

$$m\left(\ddot{z}^* + 2\Omega\dot{x}^* - \Omega^2 z^*\right) + \pi R(k_w + k_v)z^*$$
$$-\pi R[jk_w(w_1 - w_{-1}) + k_v(v_1 + v_{-1})] = 0 \tag{3.2e}$$

The external forces were set to zero in the above equations.

Before going further with the analysis of natural frequencies, we may first manipulate Equations (3.2d, 3.2e) so that w_{-1}, v_{-1} can be decoupled from w_1, v_1. Adding Equation (3.2e) multiplied by j to Equation (3.2d), we have

$$m[(\ddot{x}^* + j\ddot{z}^*) + j2\Omega(\dot{x}^* + j\dot{z}^*)] + \left[\pi R(k_w + k_v) - m\Omega^2\right](x^* + jz^*)$$
$$-2\pi R(k_w w_{-1} + jk_v v_{-1}) = 0$$

Subtracting Equation (3.2e) multiplied by j from Equation (3.2d) yields

$$m[(\ddot{x}^* - j\ddot{z}^*) - j2\Omega(\dot{x}^* - j\dot{z}^*)] + \left[\pi R(k_w + k_v) - m\Omega^2\right](x^* - jz^*)$$
$$-2\pi R(k_w w_1 - jk_v v_1) = 0$$

We may now introduce a new variable $u_n = x^* - j\,\mathrm{sign}(n)\,z^*$. The above two equations then can be expressed as follows:

$$m\ddot{u}_n - j2n\Omega m\dot{u}_n + \left[\pi R(k_w + k_v) - m\Omega^2\right] u_n - 2\pi R(k_w w_n - jnk_v v_n) = 0 \tag{3.2f}$$

Note that $n = -1$ or 1 in the above equation.

For $|n| \neq 0, 1$, Equations (3.2) can be rewritten as

$$\begin{bmatrix} m_{11}^{(n)} & 0 \\ 0 & m_{22}^{(n)} \end{bmatrix} \begin{Bmatrix} \ddot{w}_n \\ \ddot{v}_n \end{Bmatrix} + \begin{bmatrix} 0 & g_{12}^{(n)} \\ g_{21}^{(n)} & 0 \end{bmatrix} \begin{Bmatrix} \dot{w}_n \\ \dot{v}_n \end{Bmatrix} + \begin{bmatrix} k_{11}^{(n)} & jk_{12}^{(n)} \\ jk_{21}^{(n)} & k_{22}^{(n)} \end{bmatrix} \begin{Bmatrix} w_n \\ v_n \end{Bmatrix} = \mathbf{0} \tag{3.3}$$

where

$$\begin{aligned}
m_{11}^{(n)} &= m_{22}^{(n)} = \rho A \\
g_{12}^{(n)} &= -g_{21}^{(n)} = -2\rho A\Omega \\
k_{11}^{(n)} &= \frac{EI}{R^4}n^4 + \frac{EA}{R^2} + \frac{\sigma_\theta^0 A}{R^2}n^2 - \frac{p_0 b}{R} + k_w - \rho A\Omega^2 \\
k_{22}^{(n)} &= \left(\frac{EI}{R^4} + \frac{EA}{R^2}\right)n^2 + \frac{\sigma_\theta^0 A}{R^2} - \frac{p_0 b}{R} + k_v - \rho A\Omega^2 \\
k_{12}^{(n)} &= -k_{21}^{(n)} = \frac{EI}{R^4}n^3 + \frac{EA}{R^2}n + \frac{\sigma_\theta^0 A}{R^2}n - \frac{p_0 b}{R}n
\end{aligned}$$

For $|n| = 1$, Equations (3.2) now become

$$\begin{bmatrix} m_{11}^{(n)} & 0 & 0 \\ 0 & m_{22}^{(n)} & 0 \\ 0 & 0 & m_{33}^{(n)} \end{bmatrix} \begin{Bmatrix} \ddot{w}_n \\ \ddot{v}_n \\ \ddot{u}_n \end{Bmatrix} + \begin{bmatrix} 0 & g_{12}^{(n)} & 0 \\ g_{21}^{(n)} & 0 & 0 \\ 0 & 0 & jg_{33}^{(n)} \end{bmatrix} \begin{Bmatrix} \dot{w}_n \\ \dot{v}_n \\ \dot{u}_n \end{Bmatrix} + \begin{bmatrix} k_{11}^{(n)} & jk_{12}^{(n)} & k_{13}^{(n)} \\ jk_{21}^{(n)} & k_{22}^{(n)} & jk_{23}^{(n)} \\ k_{31}^{(n)} & jk_{32}^{(n)} & k_{33}^{(n)} \end{bmatrix} \begin{Bmatrix} w_n \\ v_n \\ u_n \end{Bmatrix} = \mathbf{0} \tag{3.4}$$

where

$$\begin{aligned}
m_{33}^{(n)} &= \frac{m}{4\pi R} \\
g_{33}^{(n)} &= -n2\Omega\frac{m}{4\pi R}
\end{aligned}$$

$$k_{13}^{(n)} = k_{31}^{(n)} = -\frac{1}{2}k_w$$
$$k_{23}^{(n)} = -k_{32}^{(n)} = -\frac{1}{2}k_v n$$
$$k_{33}^{(n)} = \frac{1}{4}(k_w + k_v) - \frac{m}{4\pi R}\Omega^2$$

For $n = 0$, Equations (3.2) become

$$\begin{bmatrix} m_{11}^{(0)} & 0 & 0 \\ 0 & m_{22}^{(0)} & 0 \\ 0 & 0 & m_{33}^{(0)} \end{bmatrix} \begin{Bmatrix} \ddot{w}_n \\ \ddot{v}_n \\ \ddot{\theta}_r \end{Bmatrix} + \begin{bmatrix} 0 & g_{12}^{(0)} & 0 \\ g_{21}^{(0)} & 0 & 0 \\ 0 & 0 & 0 \end{bmatrix} \begin{Bmatrix} \dot{w}_n \\ \dot{v}_n \\ \dot{\theta}_r \end{Bmatrix}$$
$$+ \begin{bmatrix} k_{11}^{(0)} & jk_{12}^{(0)} & 0 \\ jk_{21}^{(0)} & k_{22}^{(0)} & k_{23}^{(0)} \\ 0 & k_{32}^{(0)} & k_{33}^{(0)} \end{bmatrix} \begin{Bmatrix} w_n \\ v_n \\ \theta_r \end{Bmatrix} = \mathbf{0} \tag{3.5}$$

where

$$m_{33}^{(0)} = \frac{I_r}{2\pi R}$$
$$k_{23}^{(0)} = k_{32}^{(0)} = -k_v R$$
$$k_{33}^{(0)} = k_v R^2$$

Equations (3.3, 3.4 and 3.5) can be written in a unified form:

$$\mathbf{M}_n \ddot{\mathbf{x}}_n + \mathbf{G}_n \dot{\mathbf{x}}_n + \mathbf{K}_n \mathbf{x}_n = 0 \tag{3.6}$$

in which $\mathbf{x}_n = \{w_n, v_n\}^T$ for $|n| \neq 0, 1$; $\mathbf{x}_n = \{w_n, v_n, u_n\}^T$ for $|n| = 1$; and $\mathbf{x}_n = \{w_n, v_n, \theta_r\}^T$ for $n = 0$.

for $|n| \neq 0, 1$

$$\mathbf{M}_n = \begin{bmatrix} m_{11}^{(n)} & 0 \\ 0 & m_{22}^{(n)} \end{bmatrix} \tag{3.7a}$$

$$\mathbf{G}_n = \begin{bmatrix} 0 & g_{12}^{(n)} \\ g_{21}^{(n)} & 0 \end{bmatrix} \tag{3.7b}$$

$$\mathbf{K}_n = \begin{bmatrix} k_{11}^{(n)} & jk_{12}^{(n)} \\ jk_{21}^{(n)} & k_{22}^{(n)} \end{bmatrix} \tag{3.7c}$$

for $|n| = 1$

$$\mathbf{M}_n = \begin{bmatrix} m_{11}^{(n)} & 0 & 0 \\ 0 & m_{22}^{(n)} & 0 \\ 0 & 0 & m_{33}^{(n)} \end{bmatrix} \tag{3.8a}$$

$$\mathbf{G}_n = \begin{bmatrix} 0 & g_{12}^{(n)} & 0 \\ g_{21}^{(n)} & 0 & 0 \\ 0 & 0 & jg_{33}^{(n)} \end{bmatrix} \tag{3.8b}$$

$$\mathbf{K}_n = \begin{bmatrix} k_{11}^{(n)} & jk_{12}^{(n)} & k_{13}^{(n)} \\ jk_{21}^{(n)} & k_{22}^{(n)} & jk_{23}^{(n)} \\ k_{31}^{(n)} & jk_{32}^{(n)} & k_{33}^{(n)} \end{bmatrix} \tag{3.8c}$$

for $n = 0$

$$\mathbf{M}_n = \begin{bmatrix} m_{11}^{(0)} & 0 & 0 \\ 0 & m_{22}^{(0)} & 0 \\ 0 & 0 & m_{33}^{(0)} \end{bmatrix} \tag{3.9a}$$

$$\mathbf{G}_n = \begin{bmatrix} 0 & g_{12}^{(0)} & 0 \\ g_{21}^{(0)} & 0 & 0 \\ 0 & 0 & 0 \end{bmatrix} \tag{3.9b}$$

$$\mathbf{K}_n = \begin{bmatrix} k_{11}^{(0)} & jk_{12}^{(0)} & 0 \\ jk_{21}^{(0)} & k_{22}^{(0)} & k_{23}^{(0)} \\ 0 & k_{32}^{(0)} & k_{33}^{(0)} \end{bmatrix} \tag{3.9c}$$

By assuming that

$$\mathbf{x}_n = \mathbf{X}_n e^{j\omega_n t} \tag{3.10}$$

$$\mathbf{X}_n = \begin{cases} \{A_n, B_n\}^T, & \text{for } |n| \neq 0, 1 \\ \{A_n, B_n, C_n\}^T & \text{for } |n| = 1 \\ \{A_n, B_n, \Theta_r\}^T & \text{for } n = 0 \end{cases}$$

the characteristic equations which determine the natural frequencies of the tire-wheel system can be obtained. Substituting Equation (3.10) into Equation (3.6) yields

$$\left\{\mathbf{M}_n\left(-\omega_n^2\right) + j\mathbf{G}_n\omega_n + \mathbf{K}_n\right\}\mathbf{X}_n = \mathbf{0} \tag{3.11}$$

In order to get a non-trivial solution, the determinant of the coefficient matrix of Equation (3.11) must be zero. With this condition, the characteristic equation of the ring model which determines the natural frequencies of the tire-wheel system is obtained.

$$\left|\mathbf{M}_n\left(-\omega_n^2\right) + j\mathbf{G}_n\omega_n + \mathbf{K}_n\right| = 0 \tag{3.12}$$

For $|n| \neq 0, 1$ the tire treadband displacements are decoupled from the wheel displacements. The characteristic equation of the system thus obtained is:

$$a_4\omega_n^4 + a_3\omega_n^3 + a_2\omega_n^2 + a_1\omega_n + a_0 = 0 \tag{3.13}$$

where

$$\begin{aligned}
a_4 &= (\rho A)^2 \\
a_3 &= 0 \\
a_2 &= -\left[\rho A\left(k_{11}^{(n)} + k_{22}^{(n)}\right) + (2\rho A\Omega)^2\right] \\
a_1 &= 4\rho A\Omega k_{12}^{(n)} \\
a_0 &= k_{11}^{(n)}k_{22}^{(n)} - k_{12}^{(n)2}
\end{aligned}$$

The solutions of Equation (3.13) are the natural frequencies of the nth (except for the zeroth and first) mode vibration of the ring body. In general, there exist four natural frequencies corresponding to each n number.

For $|n| = 1$, the tire treadband deformation and wheel displacement are coupled with each other. The characteristic equation of the entire system is then

$$b_6\omega_n^6 + b_5\omega_n^5 + b_4\omega_n^4 + b_3\omega_n^3 + b_2\omega_n^2 + b_1\omega_n + b_0 = 0 \tag{3.14}$$

where

$$\begin{aligned}
b_6 &= -m_{33}^{(n)}a_4 \\
b_5 &= -g_{33}^{(n)}a_4 \\
b_4 &= k_{33}^{(n)}a_4 - m_{33}^{(n)}a_2 \\
b_3 &= -g_{33}^{(n)}a_2 - m_{33}^{(n)}a_1 \\
b_2 &= k_{33}^{(n)}a_2 - g_{33}^{(n)}a_1 - m_{33}^{(n)}a_0 + m_{11}^{(n)}k_{23}^{(n)2} + m_{22}^{(n)}k_{13}^{(n)2} \\
b_1 &= k_{33}^{(n)}a_1 - g_{33}^{(n)}a_0 - 2g_{12}^{(n)}k_{13}^{(n)}k_{23}^{(n)} \\
b_0 &= k_{33}^{(n)}a_0 - k_{11}^{(n)}k_{23}^{(n)2} - k_{22}^{(n)}k_{13}^{(n)2} - 2k_{12}^{(n)}k_{13}^{(n)}k_{23}^{(n)}
\end{aligned}$$

The solutions of Equation (3.14) are the natural frequencies corresponding to the $|n| = 1$ vibration modes of the tire ring model.

For $n = 0$, the characteristic equation of the entire system is

$$\omega_n^2 \left(c_6 \omega_n^4 + c_4 \omega_n^2 + c_2 \right) = 0 \tag{3.15}$$

where

$$\begin{aligned} c_6 &= -m_{33}^{(0)} a_4 \\ c_4 &= -m_{33}^{(0)} a_2 + k_{33}^{(0)} a_4 \\ c_2 &= -m_{33}^{(0)} a_0 + k_{33}^{(0)} a_2 + m_{11}^{(0)} k_{23}^{(0)^2} \end{aligned}$$

The solutions of Equation (3.15) are the natural frequencies corresponding to the zeroth order vibration modes of the tire ring model. The $\omega_n^2 = 0$ solution of Equation (3.15) corresponds to the rigid body rotational mode of the system.

3.2 The Natural Modes

From Equation (3.11), the relationship between A_n, B_n and C_n or Θ_r can be determined. For $|n| \neq 0, 1$,

$$D_{ni} = j\frac{B_{ni}}{A_{ni}} = -\frac{-m_{11}^{(n)}\omega_{ni}^2 + k_{11}^{(n)}}{g_{12}^{(n)}\omega_{ni} + k_{12}^{(n)}} = \frac{g_{12}^{(n)}\omega_{ni} + k_{12}^{(n)}}{-m_{22}^{(n)}\omega_{ni}^2 + k_{22}^{(n)}} \tag{3.16}$$

in which $\omega_{ni} (i = 1, 2, 3, 4)$ are the solutions of the characteristic equation (Equation (3.13)).

For $|n| = 1$,

$$D_{ni} = j\frac{B_{ni}}{A_{ni}} = -\frac{\left(-m_{11}^{(n)}\omega_{ni}^2 + k_{11}^{(n)}\right)\left(-m_{33}^{(n)}\omega_{ni}^2 - g_{33}^{(n)}\omega_{ni} + k_{33}^{(n)}\right) - k_{13}^{(n)}k_{31}^{(n)}}{\left(g_{12}^{(n)}\omega_{ni} + k_{12}^{(n)}\right)\left(-m_{33}^{(n)}\omega_{ni}^2 - g_{33}^{(n)}\omega_{ni} + k_{33}^{(n)}\right) - k_{13}^{(n)}k_{32}^{(n)}} \tag{3.17a}$$

$$E_{ni} = \frac{C_{ni}}{A_{ni}} = -\frac{k_{31}^{(n)} + k_{32}^{(n)} D_{ni}}{-m_{33}^{(n)}\omega_{ni}^2 - g_{33}^{(n)}\omega_{ni} + k_{33}^{(n)}} \tag{3.17b}$$

in which $i = 1, 2, ..., 6$ since there are in general six natural frequencies for $|n| = 1$ according to Equation (3.14).

For $n = 0$,

$$D_{ni} = j\frac{B_{ni}}{A_{ni}} = -\frac{-m_{11}^{(n)}\omega_{ni}^2 + k_{11}^{(n)}}{g_{12}^{(n)}\omega_{ni} + k_{12}^{(n)}} = \frac{g_{12}^{(n)}\omega_{ni} + k_{12}^{(n)}}{-m_{22}^{(n)}\omega_{ni}^2 + k_{22}^{(n)} + k_{23}^{(n)}F_{ni}} \tag{3.18a}$$

$$F_{ni} = \frac{\Theta_{ri}}{B_{ni}} = -\frac{k_{32}^{(n)}}{-m_{33}^{(n)}\omega_{ni}^2 + k_{33}^{(n)}} \tag{3.18b}$$

where $i = 1, 2, 3$.

Equations (3.16), (3.17), and (3.18) together with Equation (3.1) determine the mode shapes of the tire ring model.

Examining the expressions of the coefficients of the characteristic equations, we find that upon replacing n by $-n$, coefficients a_1 and b_1, b_3, b_5 change sign but their magnitudes remain unchanged while coefficients a_4, a_2, a_0 and b_6, b_4, b_2, b_0 remain unchanged. Therefore we have

$$\omega_{ni} = -\omega_{-ni} \qquad n = 1, 2, ..., \infty \tag{3.19}$$

Examining Equations (3.16) and (3.17), we find

$$D_{ni} = -D_{-ni} \qquad E_{ni} = E_{-ni} \tag{3.20}$$

With this nature of the eigenvalues of the system, we may combine the complex eigenfunctions for n and $-n$ into real eigenfunctions. The complex eigenfunctions are (Equations (3.1), (3.10)):

$$w_{ni} = A_{ni}e^{j(n\theta+\omega_{ni}t)} \qquad n = -\infty, ..., 0, ..., +\infty \tag{3.21a}$$

$$v_{ni} = B_{ni}e^{j(n\theta+\omega_{ni}t)} \qquad n = -\infty, ..., 0, ..., +\infty \tag{3.21b}$$

$$u_{ni} = C_{ni}e^{j\omega_{ni}t} \qquad n = -1, 1 \tag{3.21c}$$

$$\theta_{ri} = \Theta_{ri}e^{j\omega_{ni}t} \qquad n = 0 \tag{3.21d}$$

Note that for the complex eigenfunctions w_{ni}, v_{ni}, n is from minus infinity to plus infinity. Assuming $A_{ni} = A_{-ni}$, then we have $B_{ni} = -B_{-ni}, C_{ni} = C_{-ni}$.

The complex eigenfunctions w_{ni}, w_{-ni} and v_{ni}, v_{-ni} can be combined to form new real eigenfunctions:

$$w_{ni} = 2A_{ni}\cos(n\theta + \omega_{ni}t) \tag{3.22a}$$

$$v_{ni} = 2A_{ni}D_{ni}\sin(n\theta + \omega_{ni}t) \tag{3.22b}$$

Now $n = 0, 1, 2, ..., \infty$. Combining u_{1i} and u_{-1i} (remember $u_1 = x^* - jz^*$, $u_{-1} = x^* + jz^*$) yields

$$x_i^* = A_{ni}E_{ni}\cos(\omega_{ni}t), \qquad z_i^* = -A_{ni}E_{ni}\sin(\omega_{ni}t) \tag{3.22c}$$

in which $n = 1$.

In the above equations, D_{ni}, E_{ni} are defined by Equation (3.16) for $n \neq 0, 1$ and Equation (3.17) for $n = 1$.

$n = 0$ is a special case. There are no eigenfunctions of the same order but opposite sign to combine with and the corresponding eigenfunctions remain unchanged. However, for $n = 0$, the motion of the ring is independent of the space coordinate θ. The complex eigenfunctions thus can be substituted by the same real eigenfunctions as Equations (3.22a, 3.22b).

Equations (3.22) and (3.16, 3.17, 3.18) define the complete natural modes of the tire ring model. However, it should be noted that the term "mode" here has a meaning different from its conventional definition in modal analysis in which the modes are time-independent. Instead, the modes here are time-dependent and are neither stationary nor rotating with the same speed Ω as the ring. As pointed out by Huang et al. [44], the effect of rotation makes it difficult to separate the space and time coordinates in the usual manner.

3.3 Alternative Definition of Natural Frequencies and Modes

In this section, we would like to clarify one issue concerning the definitions of natural frequencies and modes. As we have seen in the previous section, the analyses of the natural frequencies and modes are all conducted in the rotating coordinate system. In other words, the natural frequencies and

modes are defined in the rotating coordinate system. This is proper and also convenient when we study the flexural vibrations of the ring, i. e., the tire treadband vibrations. However, for the study of the vibration transmission properties of the tire, the wheel motion and the forces acting on the wheel and treadband are usually described in the non-rotating coordinate system. Therefore the natural frequencies and modes are better defined in the non-rotating coordinate system instead of in the rotating coordinate system.

With Equation (2.1) being substituted into Equation (3.22), we obtain

$$w_{ni} = 2A_{ni}\cos(n\phi + \omega'_{ni}t) \qquad n = 0, 1, ..., +\infty \qquad (3.23a)$$

$$v_{ni} = 2A_{ni}D_{ni}\sin(n\phi + \omega'_{ni}t) \qquad n = 0, 1, ..., +\infty \qquad (3.23b)$$

$$x_i = A_{ni}E_{ni}\cos(\omega'_{ni}t) \qquad n = 1 \qquad (3.23c)$$

$$z_i = -A_{ni}E_{ni}\sin(\omega'_{ni}t) \qquad n = 1 \qquad (3.23d)$$

where

$$\omega'_{ni} = \omega_{ni} - n\Omega \qquad n = 0, 1, ..., +\infty \qquad (3.24)$$

Equations (3.23) and (3.24) define the natural frequencies and modes of the ring model in the non-rotating coordinate system. It will be seen that this alternative definition of natural frequencies and modes is very useful for the study of the vibration transmission properties of tires. The zeroth order modes ($n = 0$) and natural frequencies remain unchanged by this change of definition.

3.4 The Influence of Extensional Stiffness of the Ring

In Chapter 2, simplified equations of motion of the ring model were also derived using the in-extensibility assumption of the ring. It is important to determine under what circumstances and to what extent this assumption is valid to permit the simplification of the tire model. In order to do so, we shall first analyze the influences of the extensional stiffness on the vibration properties of the system.

To analyze the vibration properties of the tire ring model, we will focus our attention on the system characteristic equations (Equations (3.13), (3.14)

and (3.15)) and the corresponding coefficient expressions. Because the characteristic equations are high order (fourth order for $n \neq 0, 1$ and sixth order for $n = 0, 1$ respectively) polynomials, it is difficult, even impossible, to obtain closed form solutions for the natural frequencies of the system. However, by comparing the relative values of the polynomial coefficients, it is still possible to qualitatively analyze the influences of system parameters on the vibrational properties of the tire ring model.

The characteristic equations and the corresponding coefficient expressions presented in the previous sections can be rewritten in forms easy to analyze. Substituting $k_{11}^{(n)}, k_{12}^{(n)}$ and $k_{22}^{(n)}$ into the coefficient expressions, we have for $n \neq 0, 1$

$$a_4 = (\rho A)^2 \tag{3.25a}$$

$$a_3 = 0 \tag{3.25b}$$

$$a_2 = -\rho A \left[K_e \left(1 + n^2\right) - \frac{p_0 b}{R} \left(1 - n^2\right) + k_w + k_v + 2\rho A \Omega^2 \right] \tag{3.25c}$$

$$a_1 = 4\rho A n \Omega K_e \tag{3.25d}$$

$$a_0 = K_e K_i + \left(k_w - K_1 - \rho A \Omega^2\right) \left(k_v + K_1 - \frac{p_0 b}{R} \left(1 - n^2\right) - \rho A \Omega^2 \right) \tag{3.25e}$$

in which

$$K_e = \frac{EI}{R^4} n^2 + \frac{EA}{R^2} + \frac{\sigma_\theta^0 A}{R^2} - \frac{p_0 b}{R}$$

$$K_i = \left(\frac{EI}{R^4} n^2 + \frac{\sigma_\theta^0 A}{R^2} \right) \left(1 - n^2\right)^2 - \frac{p_0 b}{R} \left(1 - n^2\right) + k_w n^2 + k_v - \rho A \left(1 + n^2\right) \Omega^2$$

$$K_1 = \left(\frac{EI}{R^4} n^2 + \frac{\sigma_\theta^0 A}{R^2} \right) \left(1 - n^2\right)$$

For $n = 1$, the characteristic equation can be rewritten as

$$(\omega_n - \Omega)^2 \left[d_4 (\omega_n - \Omega)^4 + d_3 (\omega_n - \Omega)^3 + d_2 (\omega_n - \Omega)^2 + d_1 (\omega_n - \Omega) + d_0 \right] = 0 \tag{3.26}$$

in which

$$d_4 = -(\rho A)^2 \frac{m}{4\pi R}$$

$$
\begin{aligned}
d_3 &= 4\Omega d_4 \\
d_2 &= \rho A\left[\frac{\rho A}{4}\left(k_w + k_v\right) + \frac{m}{4\pi R}\left(2K_e + k_w + k_v\right)\right] \\
d_1 &= \rho A\left(\rho A + \frac{m}{2\pi R}\right)\left(k_w + k_v\right)\Omega \\
d_0 &= -\frac{1}{2}\left(\rho A + \frac{m}{2\pi R}\right)\left[K_e\left(k_w + k_v\right) + k_w k_v\right]
\end{aligned}
$$

in which

$$
K_e = \frac{EI}{R^4} + \frac{EA}{R^2} - \rho A\Omega^2
$$

3.4.1 Qualitative analysis

Looking into the coefficient expressions (3.25), we can see that the only term which is related to the extensional stiffness is K_e. Since the ring is assumed to be thin, K_e is predominated by the extensional stiffness of the ring and the pretension in the ring due to inflation pressure and centrifugal force. Only when n is very large, then the bending stiffness term in the K_e expression becomes comparable with the other two terms. If we divide Equation (3.13) by K_e (note this operation does not affect the solutions of the equation), then it can be seen that the coefficient of the fourth order term of the polynomial is very small compared with the other coefficients. This means that of the four solutions of the characteristic equation, two will be very large in value while the other two are much smaller. If $EA \gg \frac{EI}{R^2}n^2$, then the lower two of the four natural frequencies can be approximated by the following equation:

$$
a_2'\omega_n^2 + a_1'\omega_n + a_0' = 0 \tag{3.27}
$$

in which

$$
\begin{aligned}
a_2' &= -\rho A\left[\left(1 + n^2\right) + \frac{1}{K_e}\left(\frac{p_0 b}{R}\left(n^2 - 1\right) + k_w + k_v + 2\rho A\Omega^2\right)\right] \\
a_1' &= 4\rho A n\Omega \\
a_0' &= K_i + \frac{1}{K_e}\left(k_w - K_1 - \rho A\Omega^2\right)\left(k_v + K_1 - \frac{p_0 b}{R}\left(1 - n^2\right) - \rho A\Omega^2\right)
\end{aligned}
$$

It is obvious from Equation (3.27) that the two lower natural frequencies (the low set) do vary with the extensional stiffness of the ring. However, if K_e is

much larger than k_w and k_v, and the rotating speed is limited and does not reach the level comparable with K_e, then the terms involving K_e ($\frac{1}{K_e}$) in the coefficients a_2', a_0' all have very small values and can be neglected. Only then can the two lower natural frequencies of the ring model for each n number be considered to be independent of the extensional stiffness of the ring, and be accurately approximated by the natural frequencies of the corresponding in-extensible ring model. Let $EA \to +\infty$, then Equation (3.27) becomes

$$-\rho A\left(1+n^2\right)\omega_n^2 + 4\rho A n\Omega\omega_n + \left(\frac{EI}{R^4}n^2 + \frac{\sigma_\theta^0 A}{R^2}\right)\left(1-n^2\right)^2 - \frac{p_0 b}{R}\left(1-n^2\right) + k_w n^2 + k_v - \rho A\left(1+n^2\right)\Omega^2 = 0 \qquad (3.28a)$$

in which $n \neq 0, 1$.

For $n = 1$, the characteristic equation (Equation (3.14)) simply becomes

$$(\omega_n - \Omega)^2\left[2\rho A m\left(\omega_n - \Omega\right)^2 - \left(2\pi R\rho A + m\right)\left(k_w + k_v\right)\right] = 0 \qquad (3.28b)$$

For $n = 0$, the characteristic equation becomes

$$\omega_n^2\left[m_{33}\rho A\omega_n^2 - \left(m_{33} + \rho A R^2\right)k_v\right] = 0 \qquad (3.28c)$$

Equations (3.28) are the same as the characteristic equations derived directly from the in-extensible ring model (see Reference [38]).

To summarize the above qualitative analysis, we may conclude that of the four natural frequencies of the ring model for each n ($n \neq 0, 1$) number, two are much higher than the other two and are strongly influenced by the extensional stiffness of the ring. The natural modes associated with these two high frequencies (the high set) will be called *extensional modes* hereafter. The lower two (the low set) natural frequencies of each n number are also influenced by the extensional stiffness in general. But the degree of influence of the extensional stiffness on the low set natural frequencies depends on the relative magnitude of K_e and k_w, k_v. If the extensional stiffness of the ring is sufficiently large so that K_e is much larger than k_w or k_v, then the two lower frequencies can be accurately represented by the natural frequencies of the corresponding in-extensible ring model and thus can be considered to be independent of the extensional stiffness of the ring.

Table 3.1: Model parameters for the numerical examples

ring mean radius R:	0.273 m
ring width b:	0.075 m
ring density ρA:	1.59 kg/m
wheel mass m:	10 kg
wheel moment of inertia I_r:	0.25 kgm^2
bending stiffness EI:	0.706 Nm^2
extensional stiffness EA:	6×10^5 N
radial stiffness k_w:	7.63×10^5N/m^2
tangential stiffness k_v:	1.30×10^5N/m^2
inflation pressure p_0:	1.25×10^5N/m^2

The above discussion concerning the influence of extensional stiffness on the natural frequencies for $n \neq 0, 1$ are equally applicable for $n = 0, 1$.

3.4.2 Numerical examples and discussion

Numerical examples are shown in Figure 3.1 to Figure 3.3. Table 3.1 lists the basic parameter values used for the numerical examples, which are taken from Reference [15], except for the mass and moment of inertia of the wheel.

Figure 3.1 is the numerical result showing the influences of the extensional stiffness on both the high set and the low set natural frequencies of the ring model. It can be seen that with the increase of extensional stiffness, the high set natural frequencies increase proportionally without limit, while the low set natural frequencies initially increase but soon approach the maximum values, which are the natural frequencies of the corresponding in-extensible ring model. It can also be seen that with increasing n, the influence of extensional stiffness on the low set natural frequencies decreases while the influence on the high set natural frequencies increases. Note that the negative natural frequencies shown in the figures do not have the same values as the positive ones due to the coriolis effect of rotation.

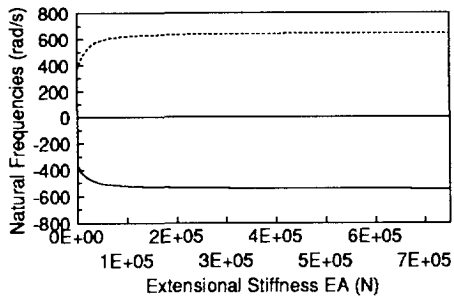

(a) $n = 1$, low set

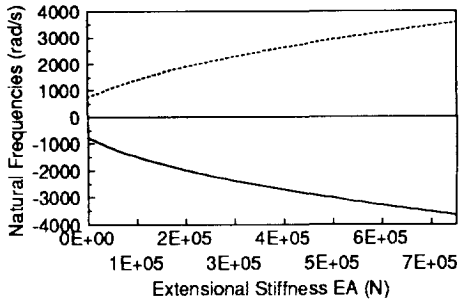

(b) $n = 1$, high set

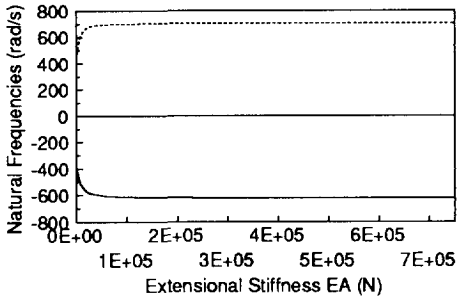

(c) $n = 2$, low set

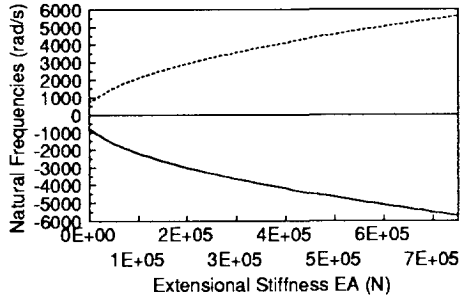

(d) $n = 2$, high set

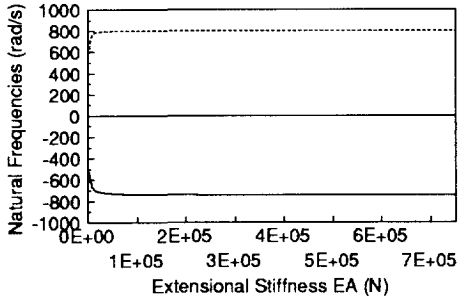

(e) $n = 3$, low set

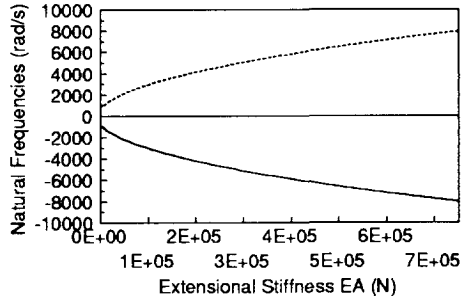

(f) $n = 3$, high set

Figure 3.1: The influence of extensional stiffness on the natural frequencies ω_{ni} ($\Omega = 50$ rad/s) (*cont.*)

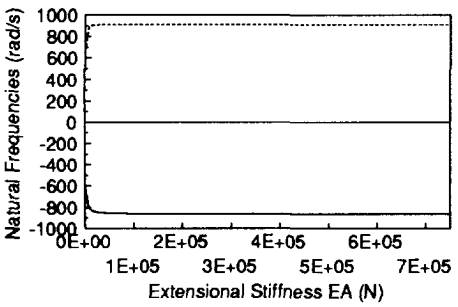

(g) $n = 4$, low set

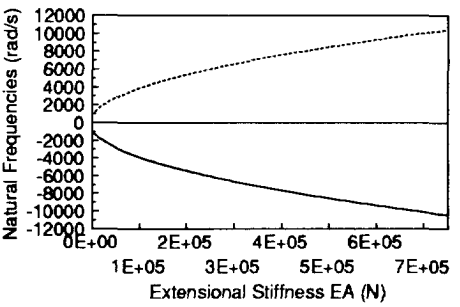

(h) $n = 4$, high set

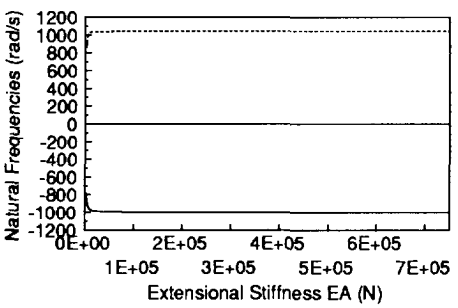

(i) $n = 5$, low set

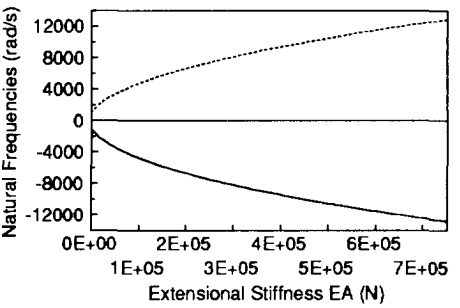

(j) $n = 5$, high set

Figure 3.1 (*cont.*): The influence of extensional stiffness on the natural frequencies ω_{ni} ($\Omega = 50$ rad/s)

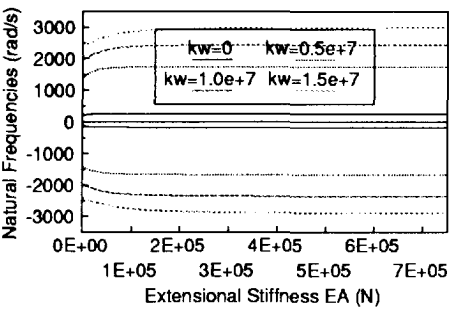

(a) $n = 2$, low set

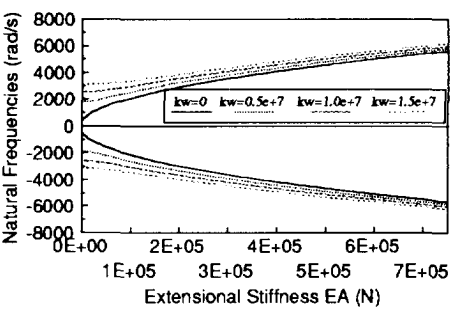

(b) $n = 2$, high set

Figure 3.2: The influence of foundation stiffness on the ω_{ni}–EA relations ($k_v = 0.6k_w$, $\Omega = 50$ rad/s)

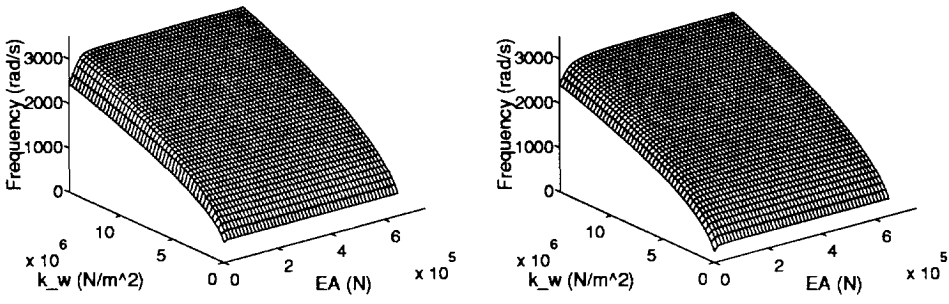

Figure 3.3: Three dimensional description of the effect of foundation stiffness on the ω_{ni}–EA relations ($k_v = 0.6k_w$, $n = 3$, $\Omega = 100$ rad/s, low set)

Figure 3.2 is an example which shows the influence of foundation stiffness of the model on the relations between the natural frequencies and the extensional stiffness ($n = 2$). As is expected, with the increase of foundation stiffness, the influence range of the extensional stiffness on the low set natural frequencies increases too. Figure 3.3 is a three-dimensional picture which more clearly shows the interactive effect of the foundation and extensional stiffnesses on the low set natural frequencies of the model. Note that the right side of Figure 3.3 shows the natural frequencies with negative values.

The high set natural frequencies are usually one order higher than the corresponding low set natural frequencies. If the lowest frequency of the high set is well beyond the frequency range in which we are interested, then we are confident that the in-extensibility assumption is valid. In the numerical examples presented here, the lowest frequency of the high set is about 3500 rad/s (560 Hz), which is well above the frequency range in most problems concerning the vibration transmission to the vehicle through tires.

3.5 The Influences of Other Parameters

3.5.1 The influence of the bending stiffness

The effect of the bending stiffness of the ring on the vibrational properties of the system can also be analyzed by looking at the coefficient expressions of the characteristic equations of the system. It is quite obvious from Equation (3.25) that the effect of the bending stiffness depends on the relative values of the bending stiffness, the extensional stiffness and the foundation stiffnesses, and on the mode order n. When n is small, the bending stiffness of the ring is usually very low compared with the extensional stiffness and foundation stiffnesses of the ring model, $\frac{EI}{R^4}n^6$ is thus much smaller than $k_w n^2 + k_v$. Therefore we do not expect that the bending stiffness will have much influence on both the low and high set natural frequencies of the ring model. But for large n numbers, the term involving EI becomes large in the K_i expression (see Equation (3.25)). Therefore it is expected that the low set natural frequencies of the ring model will change with the bending stiffness.

Figure 3.4 is the numerical result showing the relations between the natural frequencies and the bending stiffness of the ring model. As can be seen from the figures, the bending stiffness has little influence on natural frequencies of the low order (small n) vibrational modes of the model. However, for high order modes we can see that the low set natural frequencies change with the increase of the bending stiffness.

3.5.2 The influence of the foundation stiffnesses

As was pointed out in the preceding section, the foundation stiffnesses influence the relations between the low set natural frequencies and the extensional and bending stiffnesses. In addition, Figure 3.5 shows the changes of the low set natural frequencies of the ring model with the increase of radial and tangential foundation stiffnesses. The natural frequencies increase with the increase of foundation stiffnesses. It is evident that the radial stiffness has more influence on the vibrational properties of the model than the tangential stiffness has. Again, the right side of the figure shows the negative branch

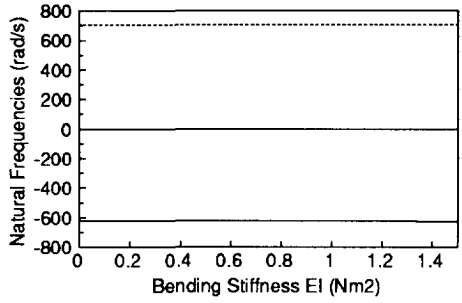

(a) $n = 2$, low set

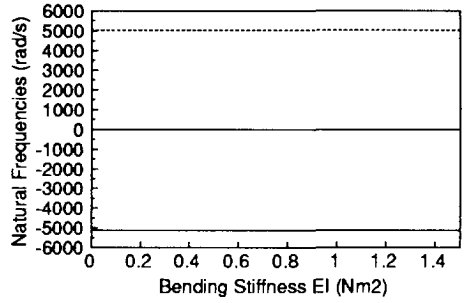

(b) $n = 2$, high set

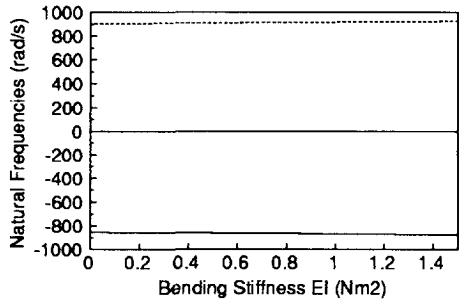

(c) $n = 4$, low set

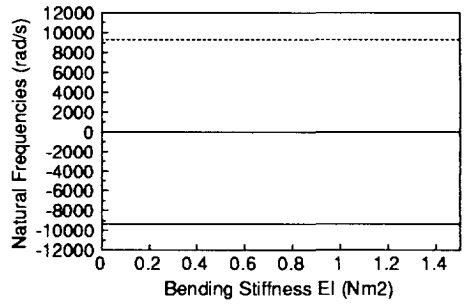

(d) $n = 4$, high set

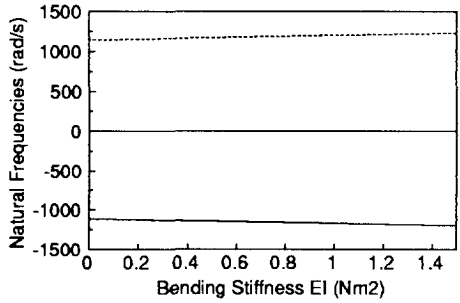

(e) $n = 6$, low set

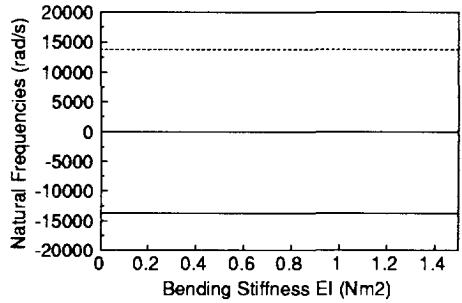

(f) $n = 6$, high set

Figure 3.4: The influence of bending stiffness on the natural frequencies ω_{ni} ($\Omega = 50$ rad/s) (*cont.*)

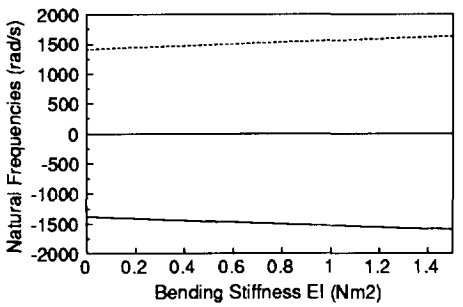

(g) $n = 8$, low set

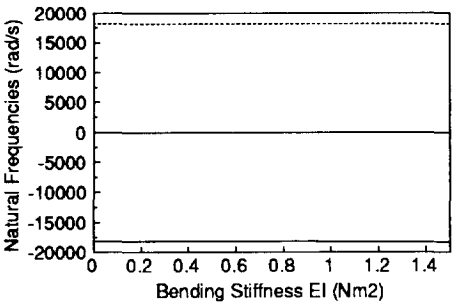

(h) $n = 8$, high set

Figure 3.4 (*cont.*): The influence of bending stiffness on the natural frequencies ω_{ni} ($\Omega = 50$ rad/s)

of the natural frequencies.

3.6 The Effect of Tire Rotation and Rotating Speed

The effect of wheel rotation on the vibrational properties is the so-called *bifurcation* of natural frequencies. When the system is in the non-rotating state, i.e. $\Omega = 0$, the coefficients a_3, a_1 in Equation (3.13) and b_5, b_3, b_1 in Equation (3.14) are equal to zero, the characteristic equations are therefore reduced to second and third order polynomials in terms of ω_n^2, respectively. As a consequence, there are only three and two natural frequencies for the first order and the other order vibration modes, respectively. When the system is in the rotating state, the coefficients a_1 and b_5, b_3, b_1 of the characteristic equations are not equal to zero; therefore six or four natural frequencies exist for the $n \neq 0$ vibration modes of the ring model in the rotating state. That is to say, the number of the natural frequencies of each order of modes doubles when the system rotates. The doubling of the natural frequencies due to rotation is sometimes called frequency bifurcation in literature [44]. However, it should be noted that the term bifurcation used here does not have exactly the same meaning as it has when used in Non-linear Dynamics. It is noted that the coefficients a_1 and b_5, b_3, b_1 are linearly proportional to the rotating speed Ω of the system, which is recognized as the coriolis

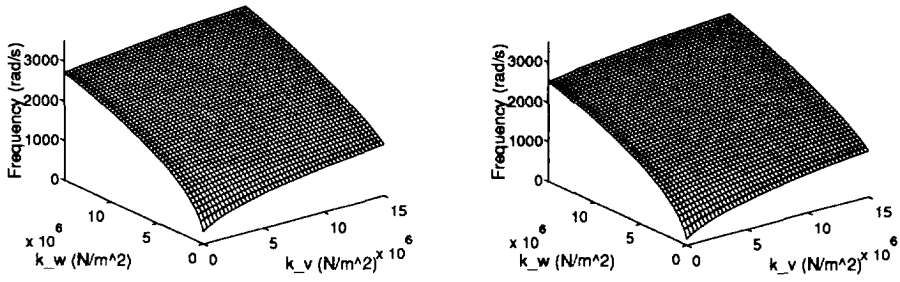

(a) $n = 2$

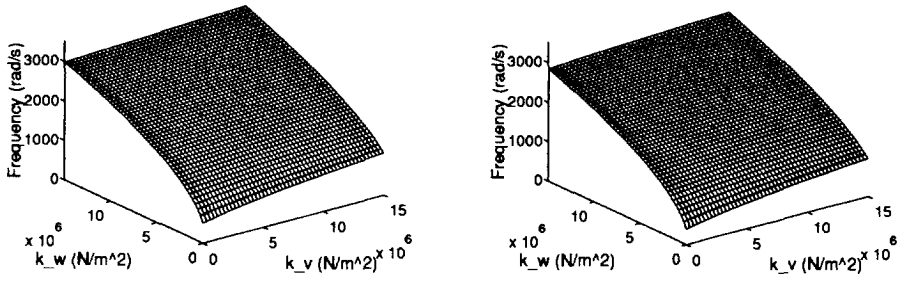

(b) $n = 3$

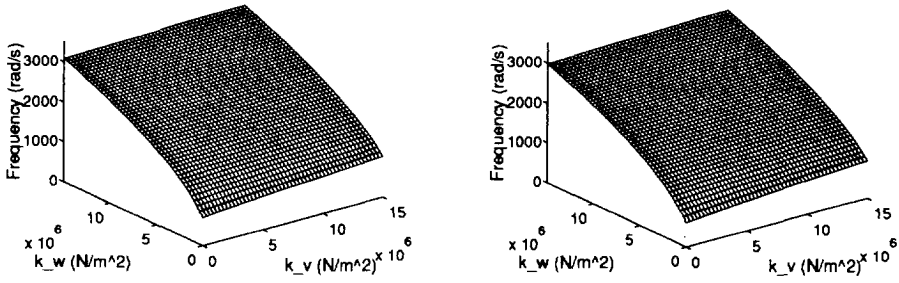

(c) $n = 4$

Figure 3.5: The influence of foundation stiffnesses on natural frequencies ω_{ni} ($\Omega = 100$ rad/s, low set)

acceleration of the rotating system. Therefore the doubling of the numbers (or bifurcation) of natural frequencies of the system from the non-rotating to rotating state is the result of the coriolis effect.

For the zeroth order vibration modes, it can be seen from Equation (3.15) that the characteristic equation is not changed due to rotation. Therefore the frequency bifurcation due to rotation does not apply to the zeroth order modes. However, the tire rotation does affect the coefficients of the characteristic equation, thus affecting the values of the natural frequencies of the zeroth order modes.

In order to investigate the natural frequency changes of the system with the rotating speed, we may look at the characteristic equations of the system under the in-extensibility assumption. Equations (3.28) can be solved and explicit expressions of the natural frequencies can be obtained.

For $n \neq 0, 1$

$$\omega_{n1,2} = \frac{2n\Omega}{1+n^2} \pm \left\{ \left[\left[\left(\frac{EI}{R^4} + \frac{\rho A \Omega^2}{1+n^2} \right) \left(1-n^2\right) - \frac{p_0 b}{R} \right] \right.\right.$$
$$\left.\left. n^2\left(1-n^2\right) + k_v + k_w n^2 \right] \frac{1}{\rho A \left(1+n^2\right)} \right\}^{\frac{1}{2}} \tag{3.29}$$

and for $n = 1$, the natural frequencies corresponding to flexible modes are

$$\omega_{n1,2} = \Omega \pm \sqrt{\frac{(2\pi R\rho A + m)(k_w + k_v)}{2\rho A m}} \tag{3.30}$$

For $n = 0$, the non-zero solution of the characteristic equation is

$$\omega_n = \sqrt{\frac{I_r + 2\pi\rho A R^3}{I_r \rho A} k_v} \tag{3.31}$$

which is independent of the rotating speed Ω. Note in the above equations, $\sigma_\theta^0 A$ has been substituted by Equation (2.9).

It can be proved that for $n \neq 0, 1$, one of the natural frequencies of each order increases monotonously with the rotating speed, while the other one first decreases and then increases after reaching a minimum with the increase

of rotating speed. The rotating speed at which one of the natural frequencies reaches a minimum can be derived from Equation (3.29). We find

$$\Omega^2 = \frac{4\left(1+n^2\right)}{\rho A\left(1-n^2\right)^2 n^2\left(n^4-2n^2-3\right)} \left[\left(\frac{EI}{R^4}\left(1-n^2\right)-\frac{p_0 b}{R}\right) n^2\left(1-n^2\right)+k_v+k_w n^2\right] \tag{3.32}$$

For $n = 1$, the situation is different. The two natural frequencies are merely equal to the rotating speed Ω minus/plus a constant, which is recognized as the first order natural frequency of the ring model without rotation, ω_1^0. Therefore, of the two first order natural frequencies, one increases and the other decreases linearly with the rotating speed. When the rotating speed is equal to ω_1^0, one of the first order natural frequencies of the rotating ring model becomes zero. It should be reminded here that the natural frequencies we are discussing are defined in the rotating coordinate system. If we use the alternative definition which is discussed in Section 3.3, we will find that the first order natural frequency under the alternative definition is independent of the rotating speed; and there is only one, instead of two, first order natural frequency.

Figure 3.6 shows the bifurcation of the natural frequencies of the in-extensible ring model due to rotation. It should be noted that dashed lines in Figure 3.6 correspond to the negative branch of the natural frequencies. We present them here as positive ones to better illustrate the doubling nature of the natural frequencies due to rotation. The natural frequencies represented by the dashed lines correspond to the natural modes which travel backwards, as will be explained in Section 3.8.

3.7 The Influence of the DOFs of the Wheel

The influence of the translational and rotational degrees of freedom of the wheel is obvious from the characteristic equations of the model. The vibration modes other than those of the zeroth and first order are not affected by the release of the DOFs of the wheel; the corresponding natural frequencies are not influenced by the mass and moment inertia of the wheel. For the

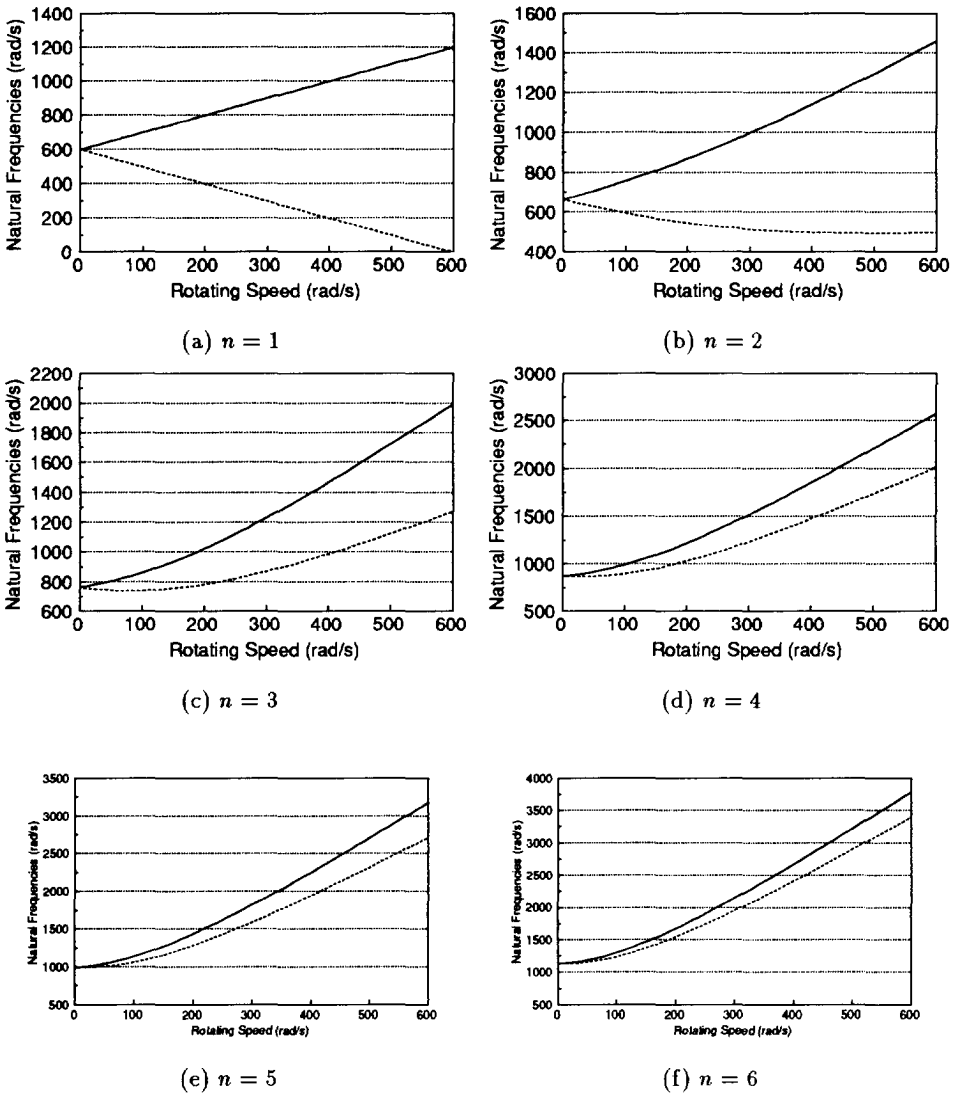

(a) $n = 1$ (b) $n = 2$

(c) $n = 3$ (d) $n = 4$

(e) $n = 5$ (f) $n = 6$

Figure 3.6: The bifurcation effect of natural frequencies (ω_{ni}) due to rotation (low set)

zeroth and first order vibration modes of the system, the wheel motion and the ring deformation are coupled with each other. Therefore releasing the wheel DOFs affects the natural frequencies of the system for those modes. In addition to the rigid body modes, there are two natural frequencies for the zeroth order vibration modes and four for the first order modes in which the rotating ring and wheel are vibrating together as a system (two for the non-rotating system).

Table 3.2 shows the low set natural frequencies calculated from this tire ring model. The model parameters used for the calculation are the same as those listed in Table 3.1. The natural frequencies of this model are compared with those of the corresponding ring model with a fixed wheel in order to illustrate the influence of the wheel DOFs on the system dynamic behavior. As has been observed, the natural frequencies other than the zeroth and first order ones are not affected by the DOFs of the wheel. The zeroth and first order natural frequencies, however, are influenced by the wheel DOFs. For $n = 0, 1$, the wheel motion and ring deformation are coupled with each other. As a result, the natural frequencies of the system are no longer equal to the natural frequencies of the ring with a fixed wheel. The zeroth and first order natural frequencies shown in Table 3.2 are the ones corresponding to the vibration modes with the ring body and the wheel moving in opposite directions, i.e., the flexible mode. The natural frequencies corresponding to the rigid body modes, which are equal to 0 for $n = 0$ and equal to the system rotating speed in value for $n = 1$, are not included in the table.

3.8 Numerical Examples of The Natural Modes

Figure 3.7 illustrates the mode shapes corresponding to the low set natural frequencies calculated according to Equations (3.22). Up to the fourth order natural modes are shown in the figure. It should be noted that the mode shapes are rotating, according to the definition in Section 3.2. For the same order n, there are two similar in-extensional mode shapes. One travels forward, which corresponds to the higher one of the two natural frequencies of the low set. The other travels backward, which corresponds to the lower one (i.e., the solutions of the characteristic equations with negative values, as noted in Section 3.6). If the mode shapes are viewed from a stationary

Table 3.2: Natural frequencies ω_{ni} of the ring model with and without wheel DOFs (low set)

Ω (rad/s)	n	Natural Frequencies without Wheel DOFs (rad/s)		Natural Frequencies with Wheel DOFs (rad/s)	
0	0	285.94	285.94	385.02	385.02
	1	529.92	529.92	597.83	597.83
	2	663.10	663.10	663.10	663.10
	3	763.47	763.47	763.47	763.47
	4	871.34	871.34	871.34	871.34
50	0	285.94	285.94	385.02	385.02
	1	579.92	479.92	647.83	547.83
	2	705.81	625.81	705.81	625.81
	3	802.85	742.85	802.85	742.85
	4	912.56	865.50	912.56	865.50
100	0	285.94	285.94	385.02	385.02
	1	629.92	429.92	697.83	497.83
	2	753.87	593.87	753.87	593.87
	3	860.31	740.31	860.31	740.31
	4	987.17	893.05	987.17	893.05
150	0	285.94	285.94	385.02	385.02
	1	679.92	379.92	747.83	447.83
	2	807.10	567.10	807.10	567.10
	3	934.09	754.09	934.09	754.09
	4	1090.15	948.98	1090.15	948.98
200	0	285.94	285.94	385.02	385.02
	1	729.92	329.92	797.83	397.83
	2	865.20	545.20	865.20	545.20
	3	1021.83	781.83	1021.83	781.83
	4	1215.50	1027.27	1215.50	1027.27

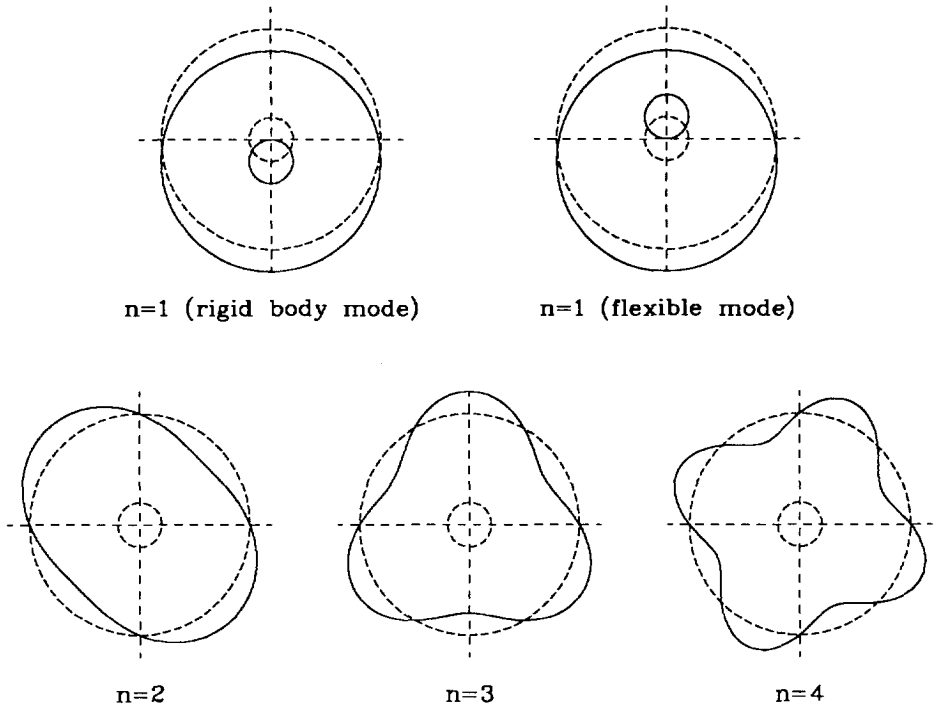

Figure 3.7: Mode shapes of the ring model

observer, the forward traveling ones rotate with speeds higher than Ω while the backward traveling ones rotate with speeds lower than Ω, or even rotate opposite to the rotating direction of the ring. It should be noted that for $n = 1$, in addition to the flexible mode, there is a rigid body mode whose natural frequency equals to Ω if defined in the rotating coordinate system or 0 if defined in the non-rotating coordinate system.

3.9 About the 0th Vibration Modes of the Ring Model

Until now, little attention has been paid to the discussion of the natural frequencies and modes of the zeroth order. But they do exist. Examining Equation (3.15), we will see that the coefficients c_5 and c_3 of the polynomial are equal to zero. If we disregard the solution $\omega_n = 0$, which corresponds to

the rigid body rotational mode of the system, it is found that the characteristic equation is a quadratic equation in terms of ω_n^2. Therefore there exist only two natural frequencies for $n = 0$, instead of four in the general case.

Let us look at the special case when the model is not rotating($\Omega = 0$). In this case the natural frequencies of the zeroth order mode are

$$\omega_{01} = \sqrt{\frac{1}{\rho A}\left(\frac{EA}{R^2} - \frac{p_0 b}{R} + k_w\right)} \tag{3.33a}$$

$$\omega_{02} = \sqrt{\frac{I_r + 2\pi\rho A R^3}{I_r \rho A} k_v} \tag{3.33b}$$

The corresponding mode shapes are according to Equation (3.18)

$$\begin{aligned} &\text{at } \omega_{01}, \qquad D_n = 0 \\ &\text{at } \omega_{02}, \qquad 1/D_n = 0 \end{aligned}$$

Since the extensional stiffness of the ring is usually much larger than the foundation stiffnesses k_w and k_v, ω_{01} is much larger than ω_{02}.

It can be seen that the radial and tangential vibrations of the model are completely decoupled from each other for $n = 0$. This means that at ω_{01} the ring motion occurs only in the radial direction, while at ω_{02} the ring motion occurs only in the tangential direction. In other words, the higher one of the two natural frequencies corresponds to the vibration mode in which the ring expands and contracts while keeping the circular shape. Needless to say it is the extensional vibration of the ring. The other corresponds to the vibration mode in which the ring vibrates relative to the wheel in the tangential direction while keeping its original shape and size, i.e., the ring rotates as a rigid body relative to the wheel (the tangential springs). The vibration mode at ω_{01} is called in literature the *breathing mode* [89]. The vibration mode at ω_{02} will be called *rotational mode* in this thesis.

For the rotating ring model, the above statement also applies. However, due to the coriolis effect, the radial and tangential vibration are no longer decoupled from each other (see Equation (3.15)). Figure 3.8 shows the zeroth modes of the ring model.

The rotational mode of the ring model is important to vehicle dynamics in that this vibration mode of the tire will transmit the excitations at the tire-

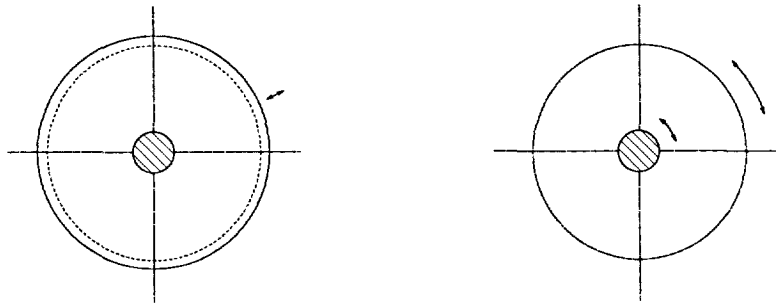

(a) breathing mode (b) rotational mode

Figure 3.8: The zeroth mode shapes of the ring model

road contact patch due to road unevenness to the vehicle powertrain and causes the rotational vibrations of the power transmission parts of vehicles. The rotational mode is also important to the design of the modern anti-lock braking and traction control systems.

3.10 Conclusions

- In this chapter, the characteristic equations of the tire ring model are obtained, which determine the natural frequencies of the model;
- Because of the difficulties encountered in separating the space and time coordinates for the rotating ring model, the time-dependent mode concept is adopted, which was first suggested by Huang and Soedel [44];
- It has been shown that the extensional stiffness of the ring contributes mainly to the high frequency vibrations of the model. But it has also been found that the extensional stiffness does influence the low set natural frequencies at which the bending deformation of the ring dominates. The dependence of the low set natural frequencies on the extensional stiffness is related to the relative magnitude of the extensional stiffness, bending stiffness and foundation stiffnesses of the model;
- The influence of the bending stiffness on the natural frequencies depends on the relative values of $\frac{EI}{R^4}n^6$ and $k_w n^2 + k_v$. Under normal circumstances it has little influence on the low order vibration modes

of the model. However, it does affect the vibration properties of the high order vibration modes;

- With the increase of the radial and tangential foundation stiffnesses, the natural frequencies of the ring model also increase. Therefore the foundation stiffnesses are very important parameters which influence the vibrational properties of the ring model;

- The effect of rotation of the ring model is to double the natural frequencies of the model, which is caused by the coriolis acceleration. However, this *bifurcation* of natural frequencies due to rotation does not apply for the zeroth order vibration modes.

- Releasing the rotational and translational DOFs of the wheel of the model affects only the zeroth and first order vibration modes, namely the change of the natural frequencies of the zeroth and first order vibration modes of the ring model. This finding is important since it shows that the vibration transmission properties of a tire/wheel assembly are governed only by the zeroth and first order vibration modes of the system;

- Of the two zeroth order vibration modes, one has a very large natural frequency and corresponds to the extensional deformation of the ring. The other corresponds to the state in which the ring moves as a rigid body relative to the wheel in the rotational direction. The latter (the rotational mode) is important to the vibrations of the powertrains of vehicles and to the design of modern anti-lock braking and traction control systems.

Chapter 4

Equations of Motion in Mixed Modal and Physical Coordinates

It has been shown in the previous chapter that the extensional vibration modes of the ring model have very high natural frequencies, which normally contribute very little to the overall vibrations of the tire and vehicle. Therefore in the following chapters, we will be using the in-extensibility assumption of the ring model. That is, the analysis in the rest of this study will be based on Equation (2.25).

The *Modal Expansion Method* is used to simplify the analysis. The basic idea behind the modal expansion method is that the response of a linear system to any external excitation force can be expressed as a weighted summation of the natural mode shapes of the system. The mode shapes of a system are usually time independent while the weight factors are space independent. Since the mode shapes of the tire model have been obtained, we are able to simplify the equations of motion of the tire model, which are sixth order partial differential equations, into ordinary differential equations which involve only first and second order differentiations with respect to time.

4.1 Equations in the Rotating Coordinate System

According to the modal expansion method, the tangential displacement of the ring can be expressed as follows:

$$v(\theta,t)=\sum_{n=0}^{+\infty}\zeta_n(t)\cos(n\theta+\omega_n t) \tag{4.1}$$

where $\zeta_n(t)$ are the modal participation factors. The above expression can be rearranged as

$$v(\theta,t)=\sum_{n=0}^{+\infty}[a_n(t)\cos(n\theta)+b_n(t)\sin(n\theta)] \tag{4.2}$$

Substituting Equation (4.2) into (2.25) yields:

$$\mathbf{M}_n\ddot{\mathbf{u}}_n+\mathbf{G}_n\dot{\mathbf{u}}_n+\mathbf{K}_n\mathbf{u}_n=\mathbf{f}_n \tag{4.3}$$

in which $n=0,1,2,...,+\infty$. Three different cases exist for Equations (4.3) depending on the mode number n. When $n=0$,

$$\mathbf{M}_n=\begin{bmatrix} m_n & 0 & 0\\ 0 & m_n & 0\\ 0 & 0 & m_r\end{bmatrix}$$

$$\mathbf{G}_n=\begin{bmatrix} 0 & g_n & 0\\ -g_n & 0 & 0\\ 0 & 0 & 0\end{bmatrix}$$

$$\mathbf{K}_n=\begin{bmatrix} k_n & 0 & k_{0r}\\ 0 & k_n & 0\\ k_{0r} & 0 & k_r\end{bmatrix}$$

$$\mathbf{u}_n=\{a_n,\ b_n,\ \theta_r\}^T$$

$$\mathbf{f}_n=\{\xi_n,\ \eta_n,\ T/(2\pi R)\}^T$$

When $n=1$,

$$\mathbf{M}_n=\begin{bmatrix} m_n & 0 & 0 & 0\\ 0 & m_n & 0 & 0\\ 0 & 0 & m_a & 0\\ 0 & 0 & 0 & m_a\end{bmatrix}$$

$$\mathbf{G}_n = \begin{bmatrix} 0 & g_n & 0 & 0 \\ -g_n & 0 & 0 & 0 \\ 0 & 0 & 0 & -g_a \\ 0 & 0 & g_a & 0 \end{bmatrix}$$

$$\mathbf{K}_n = \begin{bmatrix} k_n & 0 & 0 & -k_{12} \\ 0 & k_n & k_{23} & 0 \\ 0 & k_{23} & k_a & 0 \\ -k_{12} & 0 & 0 & k_a \end{bmatrix}$$

$$\mathbf{u}_n = \{a_n,\ b_n,\ x^*,\ z^*\}^T$$

$$\mathbf{f}_n = \{\xi_n,\ \eta_n,\ f_{x^*}/(\pi R), f_{z^*}/(\pi R)\}^T$$

and when $n \neq 0, 1$,

$$\mathbf{M}_n = \begin{bmatrix} m_n & 0 \\ 0 & m_n \end{bmatrix}$$

$$\mathbf{G}_n = \begin{bmatrix} 0 & g_n \\ -g_n & 0 \end{bmatrix}$$

$$\mathbf{K}_n = \begin{bmatrix} k_n & 0 \\ 0 & k_n \end{bmatrix}$$

$$\mathbf{u}_n = \{a_n, b_n\}^T$$

$$\mathbf{f}_n = \{\xi_n, \eta_n\}^T$$

The elements in the above matrices are as follows:

$$\xi_0 = \frac{1}{2\pi}\int_0^{2\pi}\left(q_v + \frac{\partial q_w}{\partial \theta}\right)d\theta$$

$$\xi_n = \frac{1}{\pi}\int_0^{2\pi}\left(q_v + \frac{\partial q_w}{\partial \theta}\right)\cos n\theta d\theta$$

$$\eta_n = \frac{1}{\pi}\int_0^{2\pi}\left(q_v + \frac{\partial q_w}{\partial \theta}\right)\sin n\theta d\theta$$

$$m_n = \rho A(1 + n^2)$$

$$m_r = \frac{I_r}{2\pi R}$$

$$m_a = \frac{m}{\pi R}$$

$$g_n = -4\rho A n\Omega$$

$$g_a = \frac{2m\Omega}{\pi R}$$

$$k_n = \left(\frac{EI}{R^4}n^2 + \frac{\sigma_\theta^0 A}{R^2}\right)\left(1-n^2\right)^2 - \frac{p_0 b}{R}\left(1-n^2\right)$$
$$+k_v + k_w n^2 - \rho A\left(1+n^2\right)\Omega^2$$
$$k_r = k_v R^2$$
$$k_{0r} = -k_v R$$
$$k_a = k_w + k_v - \frac{m\Omega^2}{\pi R}$$
$$k_{12} = k_{23} = k_w + k_v$$

Two things should be noted here. First, in Equation (4.2) of the modal expansion of the tangential displacement of the ring, the mode shapes are defined in the rotating coordinate system which is attached to the ring. As was pointed out in Section 3.3 of Chapter 3, it is possible to define the natural frequencies and mode shapes of the tire ring model in a non-rotating coordinate system. According to the problem the model is intended to be applied to, one of the two definitions of natural frequencies and mode shapes is preferred. In the case of vibration transmission from the ground to the vehicle, it is more desirable to have the mode shapes defined in the non-rotating coordinate system.

Secondly, the transformed equations of motion are based on mixed modal and physical coordinates. The motion of the ring is expressed in terms of modal coordinates while the motion of the wheel-axle assembly is described with physical coordinates. Though it is possible to transform the equations of motion of the system into equations in terms of complete modal coordinates, it does not simplify the analysis. It is the author's opinion that retaining the physical coordinates of the wheel-axle assembly is more straight forward.

4.2 Equations in the Non-Rotating Coordinate System

As was mentioned in the previous section, for the study of the vibration transmission properties of tires, it is more desirable to write the transformed equations of motion in the non-rotating coordinate system.

The tangential displacement of the ring when expanded in the non-rotating coordinate system is as follows:

$$v(\phi,t)=\sum_{n=0}^{+\infty}\left[a'_n(t)\cos(n\phi)+b'_n(t)\sin(n\phi)\right] \tag{4.4}$$

The following relations exist between the rotating and non-rotating coordinate systems (see Chapter 2):

$$x^*=x\cos(\Omega t)+z\sin(\Omega t) \tag{4.5a}$$
$$z^*=-x\sin(\Omega t)+z\cos(\Omega t) \tag{4.5b}$$
$$\theta=\phi-\Omega t \tag{4.5c}$$

Substituting Equation (4.5c) into Equation (4.2) and comparing it with Equation (4.4), we have

$$a_n=a'_n\cos(n\Omega t)+b'_n\sin(n\Omega t) \tag{4.5d}$$
$$b_n=-a'_n\sin(n\Omega t)+b'_n\cos(n\Omega t) \tag{4.5e}$$

Substituting Equation (4.5c) into the expressions of ξ_n,η_n yields:

$$\xi_n=\xi'_n\cos(n\Omega t)+\eta'_n\sin(n\Omega t) \tag{4.5f}$$
$$\eta_n=-\xi'_n\sin(n\Omega t)+\eta'_n\cos(n\Omega t) \tag{4.5g}$$

where ξ'_n,η'_n are the generalized forces defined in the non-rotating coordinate system.

$$\xi'_0=\frac{1}{2\pi}\int_0^{2\pi}\left(q_v+\frac{\partial q_w}{\partial\phi}\right)d\phi \tag{4.6a}$$
$$\xi'_n=\frac{1}{\pi}\int_0^{2\pi}\left(q_v+\frac{\partial q_w}{\partial\phi}\right)\cos n\phi\,d\phi \tag{4.6b}$$
$$\eta'_n=\frac{1}{\pi}\int_0^{2\pi}\left(q_v+\frac{\partial q_w}{\partial\phi}\right)\sin n\phi\,d\phi \tag{4.6c}$$

Equation (4.5) can be rewritten in matrix form:

$$\mathbf{u}_n=\mathbf{R}_n\mathbf{u}'_n \tag{4.7a}$$
$$\mathbf{f}_n=\mathbf{R}_n\mathbf{f}'_n \tag{4.7b}$$

in which,

$$\mathbf{R}_n = \begin{cases} \begin{bmatrix} 1 & 0 & 0 \\ 0 & 1 & 0 \\ 0 & 0 & 1 \end{bmatrix} & \text{for } n = 0 \\ \begin{bmatrix} \cos\Omega t & \sin\Omega t & 0 & 0 \\ -\sin\Omega t & \cos\Omega t & 0 & 0 \\ 0 & 0 & \cos\Omega t & \sin\Omega t \\ 0 & 0 & -\sin\Omega t & \cos\Omega t \end{bmatrix} & \text{for } n = 1 \\ \begin{bmatrix} \cos n\Omega t & \sin n\Omega t \\ -\sin n\Omega t & \cos n\Omega t \end{bmatrix} & \text{for } n \neq 0, 1 \end{cases}$$

$$\mathbf{u}'_n = \begin{cases} \{a'_n,\ b'_n,\ \theta_r\}^T & \text{for } n = 0 \\ \{a'_n,\ b'_n,\ x,\ z\}^T & \text{for } n = 1 \\ \{a'_n,\ b'_n\}^T & \text{for } n \neq 0, 1 \end{cases}$$

$$\mathbf{f}'_n = \begin{cases} \{\xi'_n,\ \eta'_n,\ T/(2\pi R)\}^T & \text{for } n = 0 \\ \{\xi'_n,\ \eta'_n,\ f_x/(\pi R),\ f_z/(\pi R)\}^T & \text{for } n = 1 \\ \{\xi'_n,\ \eta'_n\}^T & \text{for } n \neq 0, 1 \end{cases}$$

Substituting Equation (4.7) into Equation (4.3), we obtain the new transformed equations of motion, in which the generalized coordinates are defined in the non-rotating coordinate system.

$$\mathbf{M}'_n \ddot{\mathbf{u}}'_n + \mathbf{G}'_n \dot{\mathbf{u}}'_n + \mathbf{K}'_n \mathbf{u}'_n = \mathbf{f}'_n \tag{4.8}$$

The coefficient matrices have the same form as the ones in Equation (4.3), only the elements are different.

$$m'_n = m_n = \rho A(1 + n^2)$$
$$m'_r = m_r = \frac{I_r}{2\pi R}$$
$$m'_a = m_a = \frac{m}{\pi R}$$
$$g'_n = 2n\rho A\Omega(n^2 - 1)$$
$$g'_a = 0$$

$$k'_n = \left(\frac{EI}{R^4}n^2 + \frac{\sigma_\theta^0 A}{R^2}\right)\left(1-n^2\right)^2 - \frac{p_0 b}{R}\left(1-n^2\right)$$
$$+k_v + k_w n^2 - \rho A\Omega^2\left(1-n^2\right)^2$$
$$k'_r = k_v R^2$$
$$k'_{0r} = -k_v R$$
$$k'_a = k_w + k_v$$
$$k'_{12} = k'_{23} = k_w + k_v$$

4.3 Damping Effect

In deriving the mathematical model described in the previous sections, the tire-wheel system is considered as an undamped vibration system, but in reality, damping exists both in the treadband and in the sidewall of tires. And it is well known that damping in tires is important to explain some aspects of tire behavior such as standing waves.

We may introduce damping effects into our analysis by adding a damping factor to the matrix $\mathbf{G}_n$ or $\mathbf{G}'_n$, depending on the problem at hand. For the problem of vibration transmission, we may add the damping factor to the matrix $\mathbf{G}'_n$. After introducing damping the matrix becomes

$$\mathbf{G}'_n = \begin{bmatrix} c'_n & g'_n & 0 \\ -g'_n & c'_n & 0 \\ 0 & 0 & c'_r \end{bmatrix} \qquad \text{for } n = 0 \tag{4.9a}$$

$$\mathbf{G}'_n = \begin{bmatrix} c'_n & g'_n & 0 & 0 \\ -g'_n & c'_n & 0 & 0 \\ 0 & 0 & c'_a & -g'_a \\ 0 & 0 & g'_a & c'_a \end{bmatrix} \qquad \text{for } n = 1 \tag{4.9b}$$

$$\mathbf{G}'_n = \begin{bmatrix} c'_n & g'_n \\ -g'_n & c'_n \end{bmatrix} \qquad \text{for } n \neq 0, 1 \tag{4.9c}$$

in which $c'_n = 2\lambda\sqrt{m'_n k'_n}$, $c'_r = 2\lambda\sqrt{m'_r k'_r}$, $c'_a = 2\lambda\sqrt{m'_a k'_a}$. λ is the dimensionless damping coefficient. The damping coefficient λ has in general

different values for different modes but is assumed to be the same for all modes here.

In the following analysis, the prime sign ($'$) will be left out of the equations for the sake of simplicity.

Chapter 5

Rolling Contact between a Tire and a Flat Road

5.1 Introduction

Tire-flat road contact is an important problem in tire mechanics and has been the subject of many theoretical and experimental studies. However, no analytical solutions can be obtained because the tire is structurally complex and composite materials are involved. It is not a solid body so its contact with the road surface is non-Hertzian. The tire-road contact pressure distribution directly affects the development of the shear forces in the contact area and consequently influences the vehicle handling and braking/traction performance. The contact pressure distribution is also one of the main factors which determine the wear of the tire tread and the damage to the road surface caused by automobiles.

Much experimental work has been done to measure the tire-road contact areas and contact pressure distributions. The main findings of these experiments can be summarized as follows:

1. The contact length between a tire and a flat road is basically determined by the tire deflection. For constant tire deflection, the contact

length remains effectively constant when the load and inflation pressure change simultaneously;

2. The increase of rotating speed generally tends to increase the contact length slightly for a given normal load and inflation pressure;

3. Increasing the speed causes a corresponding increase in contact pressure in the front part of the contact area and a decrease in the rear portion of the contact area;

4. For small normal loads, the distribution of contact pressure along the contact length is a convex curve with the maximum pressure at the center of the contact area. At high normal loads, the pressure distribution has a dip at the center of the contact area.

Clark, using a tire ring model, studied the contact problem of a rolling tire under load [23]. In his study, the equation of motion of the tire model was first reduced to static state. Then by assuming that the part of the tire treadband which is in contact with the road is deformed to a flat plate, the radial displacement of the ring was determined and substituted into the governing equation. The tire-road contact pressure was thus obtained. The contact length was determined by finding the angular coordinates of the two points at which the contact pressure solution changes sign. Boundary conditions at the tire entry and exit points were not imposed. Clark was able to describe the effects of the change of the tire rotating speed on the contact pressure distribution. Clark later pointed out [24] that in order to get more realistic dynamic pressure distributions, the shear deformation of the treadband must be included in the model so that the shear and bending moment continuity at the edges of the contact region can be assured.

Yamagishi and Jenkins adopted a different approach to the tire-road contact problem. In their study [99, 100, 50], the tire treadband was also modeled as an elastic circular ring and the sidewalls were modeled as radial springs. In addition, the tread rubber was modeled as secondary radial springs attached to the outside of the ring. Under a certain tire deflection value, the relation between the deformation of the secondary radial springs (thus the contact pressure) and the radial displacement of the treadband was derived according to the geometric relations. The governing equation was solved separately for the contact part and for the free part of the treadband. The

two solutions were matched by the continuity conditions at the edges of the contact region, which state that at the contact edge, the displacements of the free and contact part and their derivatives up to the fourth order must be equal to each other. But because the bending stiffness of a tire treadband is very small compared with the pre-tension in the treadband and the spring stiffnesses, numerical difficulties are encountered when attempting to obtain exact solutions [99]. Therefore the perturbation method was used to obtain approximate solutions [100, 50]. The contact area was further divided into three regions: a boundary layer closest to the edge; an intermediate layer, which is a little further from the edge; and the outer region, which is furthest from the edge and closest to the center of contact. The procedure is rather complicated and involves the matching of many constants and equations. Only static tire-road contact was dealt with in their study. When the model parameters were given properly, the numerical results were able to reproduce the typical contact pressure distribution curves observed from experiments [50].

In a recent paper, Akasaka studied the two-dimensional contact problem of a radial tire [1]. The tire was also modeled as a circular ring on an elastic foundation. However, different mathematical models were developed separately for the contact-free region and the contact region of the tire. In the contact-free region, the governing equation was derived for the ring in which the lateral deformation was neglected. In the contact region, the tire treadband was considered as a flat plate subjected to three-dimensional deformation. The tire deformation in these two regions was solved separately and boundary conditions were applied to the solutions in the contact-free region. Those boundary conditions are stated as: at the contact edge the belt should have a horizontal tangential line and the bending moment should be equal to the initial value to flatten the contact part of the belt. The continuity conditions at the contact edges are not completely satisfied by this kind of treatment; in particular, the continuity conditions in the lateral direction were not imposed at all.

In summary, with the conventional method of dealing with the tire-road contact problem, a tire is divided into contact-free and contact regions. These two regions are analyzed separately. In the contact-free region, the problem is defined as pre-described loads and unknown tire deformation. The equations of motion are solved to obtain the unknown tire deformation. In the contact region, the problem is defined as pre-described tire deformation

and unknown loads (the contact pressure). The equations are solved for the contact pressure. The solutions of these two separate problems are finally matched by the continuity conditions at the contact edges, which involves the determination of many constants. As was shown by Yamagishi and Jenkins, numerical difficulties will be encountered in the matching process.

In this chapter, a new method is developed to solve the tire-road rolling contact problem. The basic idea is that the tire deformation is continuous along its circumference; the tire can and should be treated as one entity instead of dividing it into two separate parts. Therefore a unified solution can be found for both the contact region and the contact-free region. The periodic property of the tire treadband displacement in terms of angular coordinate θ is utilized. The tire model developed in Chapter 2 is used.

The uniqueness of the tire-road rolling contact problem is analyzed first. A small modification to the ring model is then introduced especially for the contact problem in order to take into consideration the stiffness of the tire tread rubber. The rolling contact problem is thus formulated. Later, the tire response to a stationary concentrated load is studied with the ring model. Tire response to distributed forces in a finite contact area are then considered. A method is thus developed for solving the tire-road contact problem. The convergence of this method is also examined. The constraint conditions are discussed and an algorithm is developed to determine the boundaries at which the tire tread elements enter and leave the contact area. Finally, numerical examples are presented and the results are analyzed.

5.2 Formulation of the Rolling Contact Problem

We now examine the tire-road contact problem. Usually, a tire is far more flexible than both the road and the metal wheel and the axle supporting it so that when a tire comes into contact with the road surface the deformation is almost entirely contributed by the tire deformation. For a tire which is in contact with a rigid road surface at constant axle height, the external forces are the forces acting on the part of the tire tread in the tire-road contact area, which deform the tire, and the constraint forces at the axle, which is required to balance the contact forces in order to maintain certain tire-wheel

position or motion. The relations between the tire deformation (radial and tangential displacements of the treadband) and the contact forces (radial and tangential pressures) are governed by the equations of motion. If we know the contact forces, then the tire treadband displacements can be obtained by solving the governing equations of motion. Alternatively, if the treadband displacements are known, then the contact pressure distribution can be obtained by solving the governing equations. Clark [23] dealt with the tire-road contact problem by assuming that the part of the treadband in contact with the road is flat (thus known radial displacement). In reality, because of the existence of the tire tread rubber, the part of the treadband in contact with the road is not flat. Therefore, both the treadband displacements and the contact force distributions are unknown. In a typical tire-road rolling contact problem, the tire deflection (which is defined as the difference between the radius of a free tire and the axle height of a loaded tire), or alternatively, the total vertical force acting on the tire-wheel axle, is prescribed. The contact pressure distributions and the contact length (thus the treadband displacements) are the ones that need to be determined. Therefore, an additional set of relations between the tire treadband displacements and the contact forces is needed to solve the tire-road contact problem.

To serve this purpose, a small modification to the physical model of the tire is made to take into account the flexibility of the tire tread rubber, i.e., a fourth component—radial springs distributed along the outer edge of the ring circumference—is added to the original ring model to represent the tire tread rubber. This type of treatment was first proposed by Akasaka and employed by Yamagishi and Jenkins [99] to solve the tire-road static contact problem. The modified ring model is shown in Figure 5.1.

When the tire is rolling steadily on a flat road, the tire-road contact area should be constant. Suppose the tire-road contact angles ϕ_f (front) and ϕ_r (rear) are already known, then the geometric relation between the radial displacement w of the treadband and the deformation κ of the tread springs is approximately (see Figure 5.2):

$$\kappa(\phi) = w(\phi) + d_0 - \bar{R}(1 - \cos\phi) \qquad \phi_f \le \phi \le \phi_r \tag{5.1}$$

where $\bar{R} = R + \tau$. τ is the thickness of tire tread rubber; w is the radial displacement of the tire treadband; and d_0 is the overall tire deflection. The contact angle is assumed to be small. Note κ is equal to zero outside the contact area. It should be mentioned that the tangential displacement of

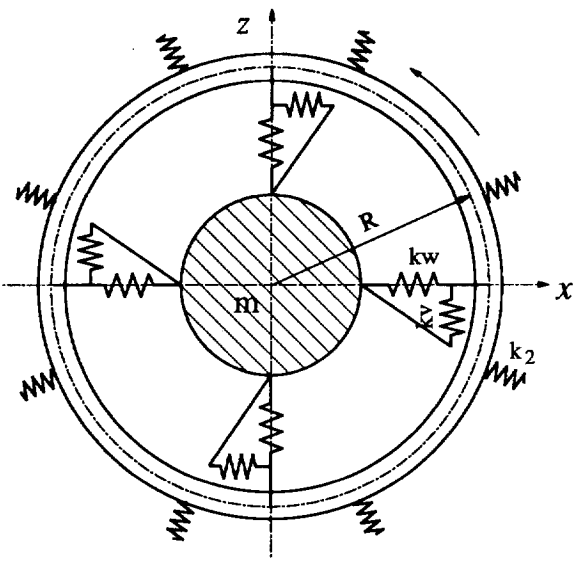

Figure 5.1: The modified tire ring model

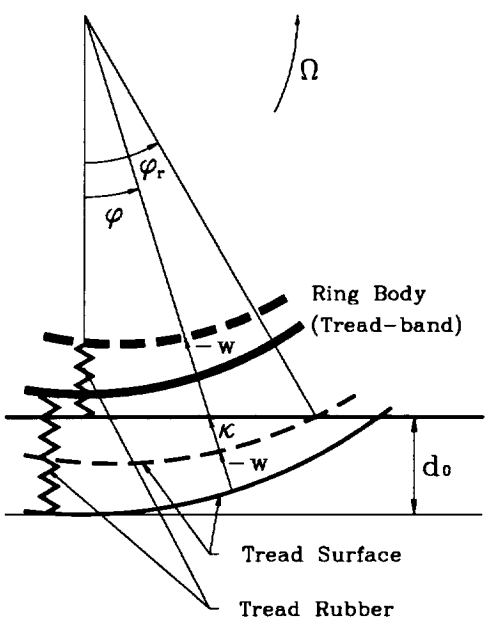

Figure 5.2: The tread geometry

the treadband will cause a change of locations of the secondary springs with respect to their original locations. This change of central angle is rather small, and therefore is neglected in the above equation.

The contact pressure in the radial direction is thus

$$q(\phi) = k_2 \cdot \kappa(\phi) = k_2 \left[w(\phi) + d_0 - \bar{R}(1 - \cos\phi) \right] \tag{5.2}$$

in which k_2 is the stiffness of the secondary radial springs (tread rubber). Equation (5.2) defines another relation between the radial displacement of the treadband and the contact pressure, which is derived from the geometrical relation between the radial displacement of the treadband and the deformation of the tread rubber.

In the following sections, the tire responses to concentrated forces acting on the treadband are analyzed first. Later, the tire responses to concentrated forces are integrated along the contact length for an arbitrary distribution of the contact forces so that the total responses of the tire to the distributed forces are obtained. Further, by utilizing the additional relation between the contact pressure and the treadband displacement, the tire-road rolling contact problem is solved for known contact length. Finally, algorithms are developed for real tire-road contact problems in which the known variable is either the tire deflection or the vertical axle force.

5.3 Tire Responses to Concentrated Line Forces

To study the tire-road rolling contact problem, the translational DOFs of the wheel are constrained and the wheel is only allowed to rotate at a constant speed Ω, i.e., $x = z = \theta_r = 0$. The transformed equations of motion in the rotating coordinate system (see Chapter 4) are thus simplified as

$$\begin{bmatrix} m_n & 0 \\ 0 & m_n \end{bmatrix} \begin{Bmatrix} \ddot{a}_n \\ \ddot{b}_n \end{Bmatrix} + \begin{bmatrix} c_n & g_n \\ -g_n & c_n \end{bmatrix} \begin{Bmatrix} \dot{a}_n \\ \dot{b}_n \end{Bmatrix} + \begin{bmatrix} k_n & 0 \\ 0 & k_n \end{bmatrix} \begin{Bmatrix} a_n \\ b_n \end{Bmatrix} = \begin{Bmatrix} \xi_n \\ \eta_n \end{Bmatrix} \tag{5.3}$$

Suppose that the tire is in contact with the road in a very small area, then we can describe the concentrated line forces acting on the tire as follows:

$$q_w(\theta, t) = -Q_w \delta\left(\theta - (\phi_0 - \Omega t)\right) \tag{5.4a}$$

$$q_v(\theta, t) = Q_v \delta(\theta - (\phi_0 - \Omega t)) \tag{5.4b}$$

here ϕ_0 is the stationary angular coordinate of the tire-road contact area; Q_w and Q_v are the magnitudes of radial and tangential external forces acting at the small contact area, respectively; and $\delta(\theta - (\phi_0 - \Omega t))$ is Dirac delta function. Note Q_w and Q_v have the same unit as q_w and q_v (N/m). When tire is rolling steadily on a perfectly flat road, Q_w and Q_v can be considered to be constant. Substituting q_w, q_v into the expressions of ξ_n and η_n (see Chapter 4, page 55), we have

$$\xi_0 = \frac{1}{2\pi} Q_v \tag{5.5a}$$

$$\xi_n = \frac{1}{\pi} [Q_v \cos n(\phi_0 - \Omega t) - n Q_w \sin n(\phi_0 - \Omega t)] \tag{5.5b}$$

$$\eta_n = \frac{1}{\pi} [Q_v \sin n(\phi_0 - \Omega t) + n Q_w \cos n(\phi_0 - \Omega t)] \tag{5.5c}$$

Usually, the tangential force Q_v is in some way related to the normal force (radial contact force Q_w) and to the relative displacements between the tread elements and the road in the contact patch. For the sake of simplicity, we assume here that the following simple relation exists between Q_v and Q_w:

$$Q_v = \mu \cdot Q_w$$

in which μ is a non-dimensional variable which describes the tangential force acting on the tire.

With the introduction of the above relation, we may now rewrite Equation (5.5) as follows:

$$\xi_0 = \frac{\mu}{2\pi} \cdot Q_w \tag{5.6a}$$

$$\xi_n = -\frac{1}{\pi} \sqrt{\mu^2 + n^2} \sin n(\phi_0 - \Omega t + \psi_n) \cdot Q_w \tag{5.6b}$$

$$\eta_n = \frac{1}{\pi} \sqrt{\mu^2 + n^2} \cos n(\phi_0 - \Omega t + \psi_n) \cdot Q_w \tag{5.6c}$$

in which $n\psi_n = \tan^{-1}(-\mu/n)$, $n = 1, 2, 3, \ldots$.

Equation (5.3) can now readily be solved for a_n and b_n. The tangential displacement of the tire treadband under concentrated contact forces is finally obtained:

$$v(\phi) = \sum_{n=0}^{\infty} A_n \sin n(\phi_0 - \phi + \psi_n + \gamma_n) \tag{5.7}$$

in which

$$A_n = -\frac{\sqrt{\mu^2+n^2}}{\pi}\frac{Q_w}{\sqrt{\left[k_n - m_n(n\Omega)^2 - g_n(n\Omega)\right]^2 + \left[c_n(n\Omega)\right]^2}}$$

$$n\gamma_n = \tan^{-1}\left(\frac{c_n(n\Omega)}{k_n - m_n(n\Omega)^2 - g_n(n\Omega)}\right)$$

The corresponding radial displacement of the model tire is

$$w(\phi) = \sum_{n=0}^{\infty} nA_n \cos n(\phi_0 - \phi + \psi_n + \gamma_n) \tag{5.8}$$

Figure 5.3 shows the relation between the displacement amplitude A_n (may be considered as the Fourier coefficients of the displacement response) and the order number n of the Fourier series. It can be seen that A_n decreases very quickly as n increases. The model parameters for this calculation are taken from [15].

5.4 Finite Contact Between the Tire and the Flat Road Surface

For a freely rolling tire, we may assume that the forces act on the tire in the contact patch only in the radial direction. The tire response to a constant concentrated load Q_w at $\phi = \phi_0$ can be rewritten as

$$w(\phi) = \sum_{n=0}^{\infty} \left[A'_n \cos n(\phi_0 - \phi + \gamma_n) \cdot Q_w\right] \tag{5.9}$$

in which

$$A'_n = -\frac{n^2}{\pi}\frac{1}{\sqrt{\left[k_n - m_n(n\Omega)^2 - g_n(n\Omega)\right]^2 + \left[c_n(n\Omega)\right]^2}}$$

We now consider the case in which the tire is in finite contact with the road. The contact area extends from angular coordinate ϕ_f at the front

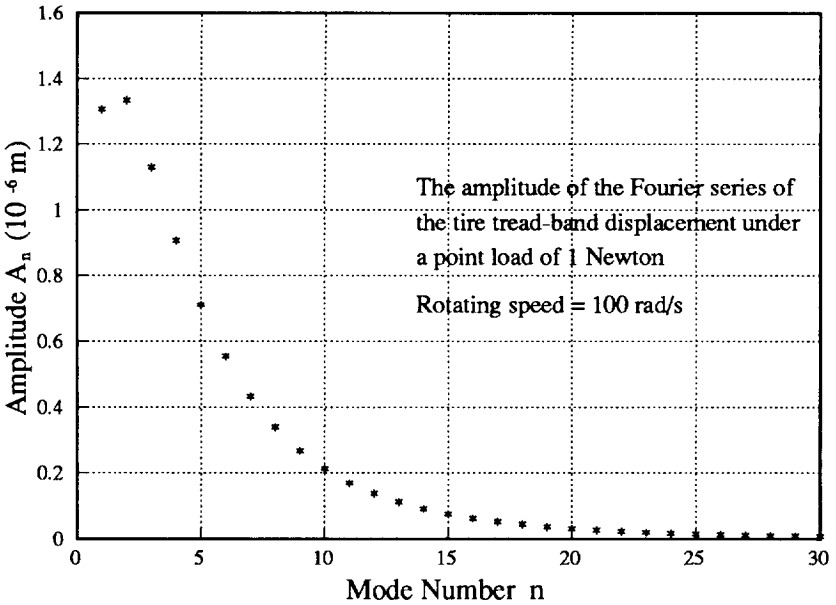

Figure 5.3: Amplitude-mode number relation

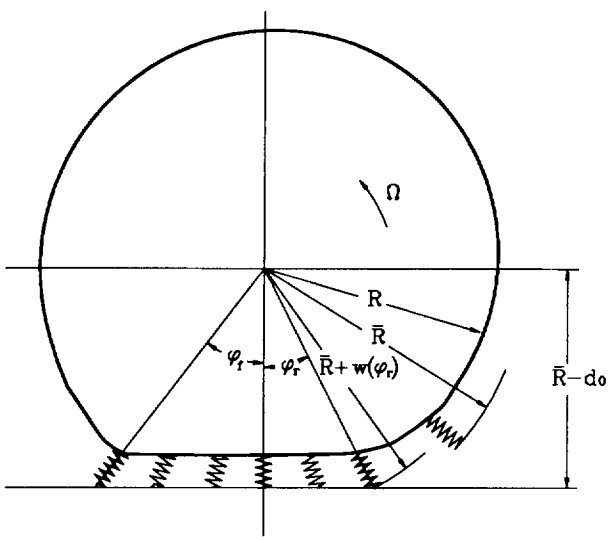

Figure 5.4: The tire-road contact

edge of the contact patch to ϕ_r at the rear edge (see Figure 5.4). Suppose that the contact force acting on the tire is a distributed radial force $q(\phi_0)$ $(\phi_f \leq \phi_0 \leq \phi_r)$, the total displacement of the tire treadband in radial direction due to $q(\phi)$ is thus

$$w(\phi) = \int_{\phi_f}^{\phi_r} \sum_{n=0}^{\infty} [A'_n \cos n\,(\phi_0 - \phi + \gamma_n) \cdot q(\phi_0)\, d\phi_0]$$
$$= \sum_{n=0}^{\infty} A'_n [\alpha_n \cos n\,(\phi - \gamma_n) + \beta_n \sin n\,(\phi - \gamma_n)] \qquad (5.10)$$

in which

$$\alpha_n = \int_{\phi_f}^{\phi_r} q(\phi) \cdot \cos(n\phi) d\phi \qquad (5.11a)$$

$$\beta_n = \int_{\phi_f}^{\phi_r} q(\phi) \cdot \sin(n\phi) d\phi \qquad (5.11b)$$

Equation (5.10) describes the relation between the radial displacement of the tire and the contact force $q(\phi)$, which is derived from the governing equations of the tire ring model. Note that up until now the distribution of the contact force $q(\phi)$ is arbitrary and no conditions concerning the tire-road contact have yet been imposed.

For a rolling tire which is in contact with a flat road, the contact force and the radial displacement of the treadband has to satisfy yet another equation, i.e., Equation (5.2). With Equations (5.2), (5.10) and (5.11), and assuming that only the first N modes make significant contributions to the tire deformation (which is true, as we saw from Figure 5.3), the following linear algebra equations are obtained:

$$\begin{bmatrix} A & B \\ C & D \end{bmatrix} \begin{Bmatrix} \alpha \\ \beta \end{Bmatrix} = \begin{Bmatrix} E \\ F \end{Bmatrix} \qquad (5.12)$$

here $\alpha = \{\alpha_1, ..., \alpha_i, ..., \alpha_N\}^T$; $\beta = \{\beta_1, ..., \beta_i, ..., \beta_N\}^T$. A, B, C, D are $N \times N$ matrices, E, F are $N \times 1$ column vectors whose elements are solely the functions of tire-road contact angles ϕ_f, ϕ_r and tire geometry.

$$a_{ij} = A'_j \left[-\cos j\,(\phi_r - \gamma_j) \frac{\sin i\phi_r - \sin i\phi_f}{i} \right.$$

$$+\frac{\sin((i-j)\phi_r+j\gamma_j)-\sin((i-j)\phi_f+j\gamma_j)}{2(i-j)}$$

$$+\frac{\sin((i+j)\phi_r-j\gamma_j)-\sin((i+j)\phi_f-j\gamma_j)}{2(i+j)}\Bigg] \qquad \text{for } i\neq j$$

$$a_{ij}=A'_j\left[-\cos j(\phi_r-\gamma_j)\frac{\sin i\phi_r-\sin i\phi_f}{i}+\cos j\gamma_j\frac{\phi_r-\phi_f}{2}\right.$$

$$\left.+\frac{\sin((i+j)\phi_r-j\gamma_j)-\sin((i+j)\phi_f-j\gamma_j)}{2(i+j)}\right]-\frac{1}{k_2} \qquad \text{for } i=j$$

$$b_{ij}=A'_j\left[-\sin j(\phi_r-\gamma_j)\frac{\sin i\phi_r-\sin i\phi_f}{i}\right.$$

$$+\frac{\cos((i-j)\phi_r+j\gamma_j)-\cos((i-j)\phi_f+j\gamma_j)}{2(i-j)}$$

$$\left.-\frac{\cos((i+j)\phi_r-j\gamma_j)-\cos((i+j)\phi_f-j\gamma_j)}{2(i+j)}\right] \qquad \text{for } i\neq j$$

$$b_{ij}=A'_j\left[-\sin j(\phi_r-\gamma_j)\frac{\sin i\phi_r-\sin i\phi_f}{i}-\sin j\gamma_j\frac{\phi_r-\phi_f}{2}\right.$$

$$\left.-\frac{\cos((i+j)\phi_r-j\gamma_j)-\cos((i+j)\phi_f-j\gamma_j)}{2(i+j)}\right] \qquad \text{for } i=j$$

$$c_{ij}=A'_j\left[\cos j(\phi_r-\gamma_j)\frac{\cos i\phi_r-\cos i\phi_f}{i}\right.$$

$$-\frac{\cos((i-j)\phi_r+j\gamma_j)-\cos((i-j)\phi_f+j\gamma_j)}{2(i-j)}$$

$$\left.-\frac{\cos((i+j)\phi_r-j\gamma_j)-\cos((i+j)\phi_f-j\gamma_j)}{2(i+j)}\right] \qquad \text{for } i\neq j$$

$$c_{ij}=A'_j\left[\cos j(\phi_r-\gamma_j)\frac{\cos i\phi_r-\cos i\phi_f}{i}+\sin j\gamma_j\frac{\phi_r-\phi_f}{2}\right.$$

$$\left.-\frac{\cos((i+j)\phi_r-j\gamma_j)-\cos((i+j)\phi_f-j\gamma_j)}{2(i+j)}\right] \qquad \text{for } i=j$$

$$d_{ij}=A'_j\left[\sin j(\phi_r-\gamma_j)\frac{\cos i\phi_r-\cos i\phi_f}{i}\right.$$

$$+\frac{\sin((i-j)\phi_r+j\gamma_j)-\sin((i-j)\phi_f+j\gamma_j)}{2(i-j)}$$

$$\left.-\frac{\sin((i+j)\phi_r-j\gamma_j)-\sin((i+j)\phi_f-j\gamma_j)}{2(i+j)}\right] \qquad \text{for } i\neq j$$

$$d_{ij}=A'_j\left[\sin j(\phi_r-\gamma_j)\frac{\cos i\phi_r-\cos i\phi_f}{i}+\cos j\gamma_j\frac{\phi_r-\phi_f}{2}\right.$$

$$- \frac{\sin((i+j)\phi_r - j\gamma_j) - \sin((i+j)\phi_f - j\gamma_j)}{2(i+j)}\Bigg] - \frac{1}{k_2} \qquad \text{for } i = j$$

$$e_i = -\bar{R}\left[-\cos\phi_r \frac{\sin i\phi_r - \sin i\phi_f}{i} + \frac{\sin(i-1)\phi_r - \sin(i-1)\phi_f}{2(i-1)}\right.$$
$$\left. + \frac{\sin(i+1)\phi_r - \sin(i+1)\phi_f}{2(i+1)}\right] \qquad \text{for } i \neq 1$$

$$e_i = -\bar{R}\left[-\cos\phi_r \frac{\sin i\phi_r - \sin i\phi_f}{i} + \frac{\phi_r - \phi_f}{2}\right.$$
$$\left. + \frac{\sin(i+1)\phi_r - \sin(i+1)\phi_f}{2(i+1)}\right] \qquad \text{for } i = 1$$

$$f_i = \bar{R}\left[-\cos\phi_r \frac{\cos i\phi_r - \cos i\phi_f}{i} + \frac{\cos(i-1)\phi_r - \cos(i-1)\phi_f}{2(i-1)}\right.$$
$$\left. + \frac{\cos(i+1)\phi_r - \cos(i+1)\phi_f}{2(i+1)}\right] \qquad \text{for } i \neq 1$$

$$f_i = \bar{R}\left[-\cos\phi_r \frac{\cos i\phi_r - \cos i\phi_f}{i}\right.$$
$$\left. + \frac{\cos(i+1)\phi_r - \cos(i+1)\phi_f}{2(i+1)}\right] \qquad \text{for } i = 1$$

Equation (5.12) can easily be solved for α and β. Therefore the tire tread-band displacements and tire-road contact force can be determined for a given ϕ_r, ϕ_f.

At the two ends of the contact area, the secondary radial spring should have zero deformation. Therefore, the following relation between the overall tire deflection d_0 and ϕ_r are obtained:

$$d_0 = \bar{R}(1 - \cos\phi_r) - w(\phi_r) \tag{5.13}$$

This relation was used in deriving Equation (5.12). In the case that the known quantity is the tire deflection d_0 instead of the contact angles, an iteration procedure is necessary, which will be explained in Section 5.5.

In deriving Equation (5.12), we assumed that the force in the tire-road contact area acts only in the radial direction. This assumption implies that the tire-road interface must supply horizontal force in addition to the vertical contact pressure so that the resulting force is always directed toward the center of the wheel. This is not exactly true, of course. However, for a freely

rolling tire, the friction force in the tire-road interface has a more or less sinusoidal distribution along the contact length and is directed toward the center of the contact patch, as was shown by Akasaka [1]. Therefore, this assumption should be quite close to the real situation of a freely rolling tire.

5.5 Constraint Conditions and Special Considerations

In the previous section when we derived the equations which formulated the tire-flat road contact problem, Equation (5.1), which represents the geometric relation between the treadband displacement and the tread rubber deformation in the contact area, was used as it is. However, for the true contact problem, the tread rubber cannot be stretched nor can it be compressed into zero or negative thickness. That is to say the tread rubber deformation must be positive and smaller than the rubber thickness. This statement can be expressed in formulae:

$$0 \leq \kappa = w + d_0 - \bar{R}(1 - \cos\phi) < \tau \qquad \text{for } \phi_f \leq \phi \leq \phi_r \tag{5.14}$$

The condition represented by Equation (5.14) is typical to contact mechanics. It is very difficult, if not impossible, to implement this condition. But numerical examples show that this condition is rarely violated.

When deriving Equation (5.12), we also assumed that the rubber deformation vanishes at the front and rear edges of the contact area. This implies the condition described by the following equation:

$$w(\phi_r) + \bar{R}\cos\phi_r = w(\phi_f) + \bar{R}\cos\phi_f \tag{5.15}$$

However, if the front and rear contact angles are both given at the same time, this condition may be violated. For non-rotating tires, the tire-road contact is symmetric with respect to the vertical axis passing the wheel center. If the central angle ϕ of the contact point on the vertical axis is designated to be zero and we choose $\phi_f = -\phi_r$, Equation (5.15) will be automatically satisfied. However, for the rolling contact between the tire and the road, since the damping within the treadband and sidewall tends to shift the location of the maximum radial deformation of the treadband backwards, the treadband displacement is not symmetric any more with respect to the vertical axis. The front contact angle ϕ_f will become larger while the rear contact angle

ϕ_r becomes smaller. Therefore an iterative procedure is necessary so that once one of the contact angles is known, the contact problem can be solved while Equation (5.15) is satisfied. The iterative procedure for this purpose is described later in this section.

Another factor which needs to be taken into account is that, usually, for the tire-road contact, the known quantity is the static tire load in the vertical direction or the overall tire deflection d_0, instead of the contact angles. The total forces in the contact area are

$$F_z = R \int_{\phi_f}^{\phi_r} q(\phi) \cos\phi \, d\phi = R\alpha_1 \tag{5.16a}$$

$$F_x = -R \int_{\phi_f}^{\phi_r} q(\phi) \sin\phi \, d\phi = -R\beta_1 \tag{5.16b}$$

If the known quantity is the overall tire deflection d_0, the contact angle ϕ_r has to satisfy Equation (5.13).

An iterative procedure is therefore needed in order to solve the tire-road contact problem whose known quantity is the vertical load or the tire deflection, which is discussed later in this section.

A computer program has been developed to solve the tire-flat road rolling contact problem using the method developed in the above sections. The condition described in Equation (5.14) is not incorporated into the program, but the condition check is performed. If condition (5.14) is violated, a warning sign is given. However our numerical calculation shows that this condition is rarely violated.

In case the known variable is the tire deflection or the tire vertical load instead of the rear contact angle, another iterative procedure based on the secant method is incorporated into the program. The initial value of the rear contact angle ϕ_r is estimated as follows:

If the tire deflection d_0 is known, then

$$\phi_r = \arctan\left(\frac{\sqrt{(2\bar{R} - d_0)\, d_0}}{\bar{R} - d_0}\right) \tag{5.17}$$

If the tire vertical load F_z is known, then

$$\phi_r = \arcsin\left(\frac{F_z}{p_0 b \bar{R}}\right) \tag{5.18}$$

The iterative procedure finds the correct value ϕ_r which satisfies either Equation (5.16) or (5.13).

To ensure Equation (5.15) is satisfied, we adopted the following procedure: first the rear contact angle is given (if the known quantity is the vertical load or tire deflection, then the rear contact angle itself is determined by another iterative procedure, as was described earlier), and then an initial value of the front contact angle is estimated as follows

$$\phi_f = -(\phi_r + \gamma_1) \tag{5.19}$$

in which γ_1 is the phase shift of the first order component of the treadband displacement in space, see Section (5.3). A simple iterative procedure based on the false position method is used to find the right ϕ_f value satisfying condition (5.15).

5.6 Convergence of the Method

The convergence of the method developed in the above section is examined in two aspects: the convergence of the treadband displacements and the convergence of the contact pressure. Figure 5.5 demonstrates the radial displacements of a tire treadband calculated using different numbers of modes (N) for two different tire deflection values. It shows clearly that the tire treadband displacement converges very quickly with the increase of the number of included modes N. For the different numbers of modes included in the calculation, the numerical results are almost identical. Actually, the rapid convergence of tire treadband displacement is expected, considering the rapid decrease of the amplitude A_n with mode number n (Figure 5.3).

Figure 5.6 shows the calculated contact pressure distributions of two different tire deflection values with the inclusion of different numbers of modes. It is seen that the convergence of the contact pressure distribution is somewhat slower than that of the treadband displacement. In order to get reliable

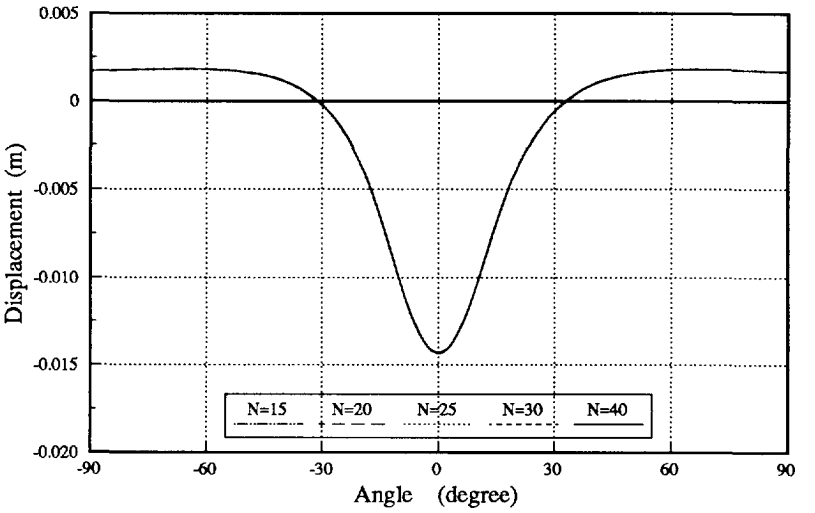

(a) $d_0 = 0.015$ m

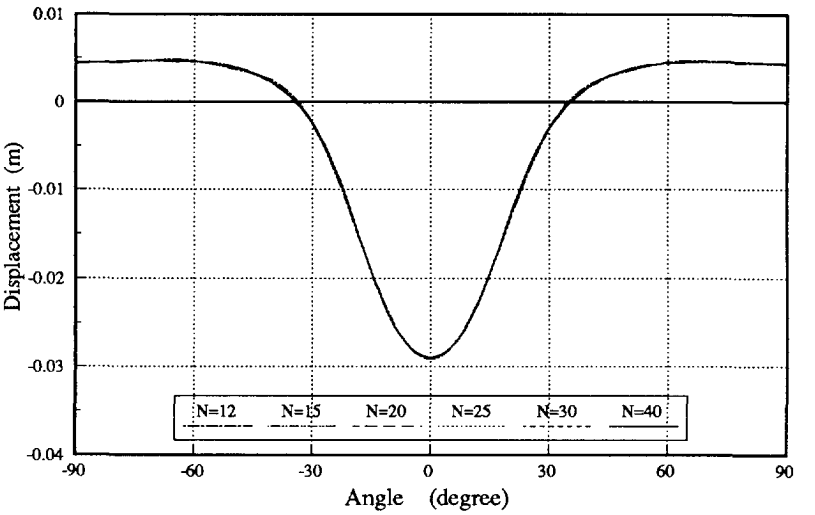

(b) $d_0 = 0.03$ m

Figure 5.5: The convergence of radial displacement of a tire treadband (Ω = 100 rad/s; damping coefficient $\lambda = 0.05$)

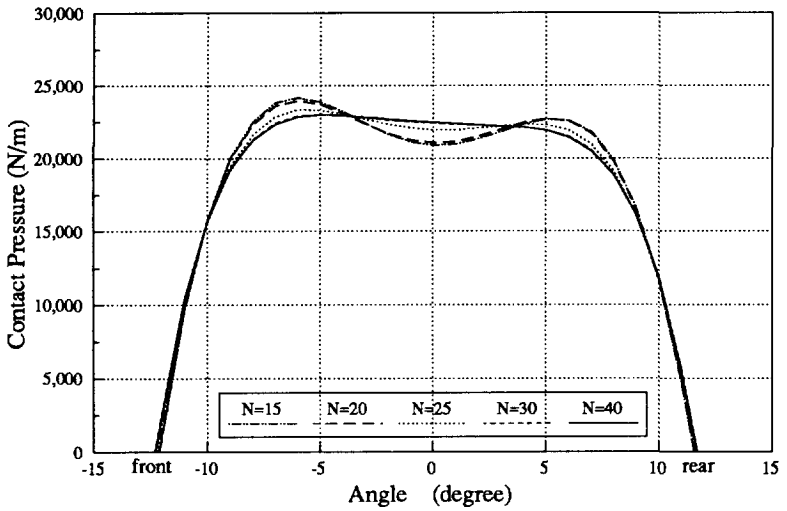

(a) $d_0 = 0.015$ m

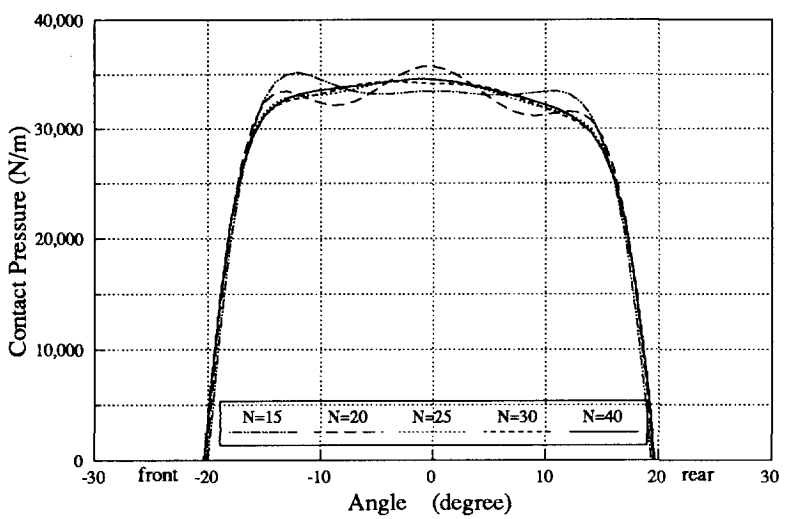

(b) $d_0 = 0.03$ m

Figure 5.6: The convergence of contact pressure distributions ($\Omega = 100$ rad/s; damping coefficient $\lambda = 0.05$)

results for the contact pressure distribution, thirty or more modes should be included, as Figure 5.6 shows.

The difference of convergence speeds between the displacement and contact pressure is due to the large value of the spring stiffness of the tread rubber used in the calculation. Examining Equation (5.2) we can see that the contact pressure actually converges at the same speed as the displacement in relative terms. But due to the large value of the rubber spring stiffness k_2, the absolute cutoff error in the displacement is enlarged in the contact pressure. It should be noted that including too many modes in the calculation will not necessarily improve the accuracy of the contact pressure and displacement results. If the magnitude A'_k of mode k is smaller than the precision the computer and its software can provide, there is no sense in including the kth and higher order modes.

5.7 Numerical Results and Discussions

In this section, the numerical results of the tire-flat road rolling contact are presented, analyzed and compared with the experimental results whenever available. In Section 5.7.1 and 5.7.2, numerical examples for a particular case of tire-road rolling contact—static contact ($\Omega = 0$)—are presented and the general pattern of the tire-road contact pressure distributions are discussed. One of the numerical results is compared with the experimental results documented in literature. In Section 5.7.1 and 5.7.2, the model parameters used for the calculation are quoted from papers by Yamagishi and Jenkins [99, 50]. The numerical examples given from Section 5.7.3 to Section 5.7.5 are calculated with model parameters quoted from Reference [15] by Böhm.

5.7.1 Comparison of a numerical result with a test result from literature

Figure 5.7 shows a numerical example for the static contact between a tire and a flat road. The line marked with Modal Expansion Method is the calculated contact pressure using the method developed in the previous sec-

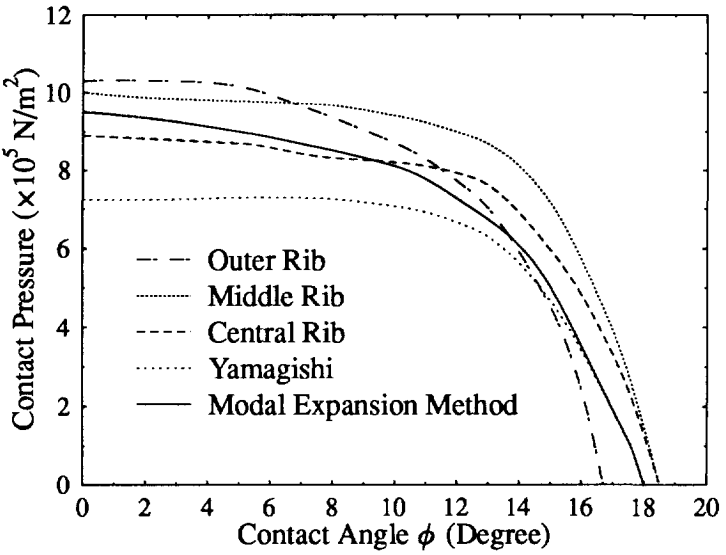

Figure 5.7: The contact pressure as measured and calculated by Yamagishi [99] and with the modal expansion method

tions. The lines marked with Outer Rib, Middle Rib and Central Rib are test results measured by Yamagishi [99]. The line marked with Yamagishi is the calculated result from Yamagishi's paper. The model parameters used here for the calculation are the same as the ones given in [99]. From this numerical example, it can be seen that the method developed in this chapter gives a better prediction for the contact force than Yamagishi's method does.

5.7.2 General patterns of the contact pressure distribution

As was mentioned in the introduction, experimental results often show that the contact pressure distribution along the contact length has a concave shape at large vertical load. But the example in the previous section does not show such a contact pressure distribution pattern. So the question one asks is whether it is due to the inability of the model and the method or due to the model parameters used. In order to check this, another set of parameters is used, which are quoted from Reference [50]. Figure 5.8(a) shows the numerical results for three different inflation pressures (thus three

different radial stiffnesses) with tire deflection $d_0 = 0.04$ m. The curves clearly have a concave shape and, the smaller the inflation pressure of the tire (thus smaller radial spring stiffness), the deeper the concavity of the pressure distribution curve. Figure 5.8(b) is another calculation result for the same set of model parameters but with a smaller tire deflection $d_0 = 0.02$ m (thus a smaller vertical load). It shows that at small vertical load, the contact pressure distribution does not have a concave shape any more. These two numerical examples show that the shape of the contact pressure distribution depends not only on the vertical load of the tire but also on the tire structure, especially the stiffness of the tire sidewall. The numerical results correspond well with the contact pressure distributions observed in tests for both small and large tire deflections.

5.7.3 Influence of tire rotating speed on the tire-road contact

The rotating speed of a tire influences the tire-flat road contact in that the distribution of contact pressure and the contact length of the tire-road interface change in a certain way with the rotating speed. With the tire model and the algorithm developed in the previous sections, we are able to investigate those influences numerically. Figure 5.9 shows the contact pressure distributions at various tire rotating speeds and with different damping coefficient λ (see Section 4.3). When the tire is standing still, i.e. $\Omega = 0$, the contact pressure distribution is symmetric with respect to the vertical axis passing the tire-wheel center. When the tire is rotating, it is seen that at the front part of the tire-road interface (where tire tread elements come into contact with the road) the contact pressure increases, and at the rear part of the interface (where the tire tread elements leave the road surface) the contact pressure decreases. The contact pressure distribution becomes asymmetric. With the increase of the tire rotating speed, the asymmetric nature of contact pressure becomes more obvious. Figure 5.9 also shows that the larger the tire internal damping, the more influence the tire rotating speed has on the contact pressure distribution. If the damping coefficient equals to zero, then the contact pressure distribution is always symmetric with respect to the vertical axis at any speed. When the damping coefficient increases, the contact pressure distribution becomes more asymmetric when the tire rotates. Therefore high speed combined with large internal damping will give rise to more severe asymmetric distribution of the tire-road contact

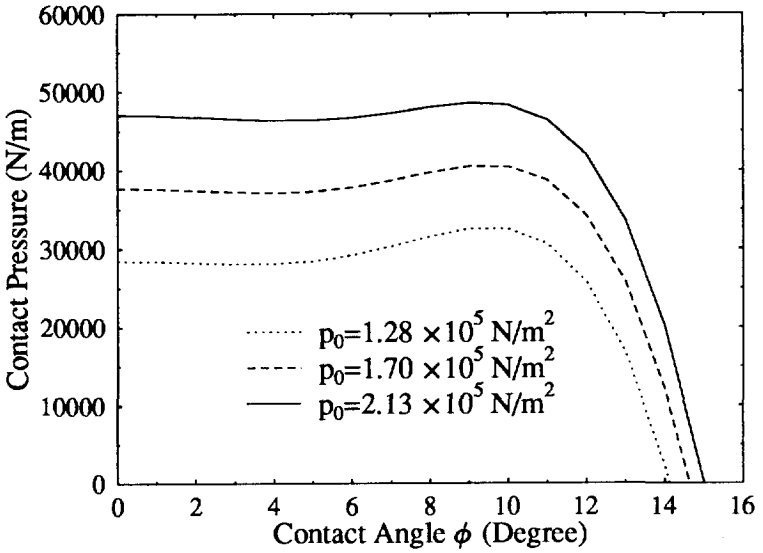

(a) $d_0 = 0.04$ m

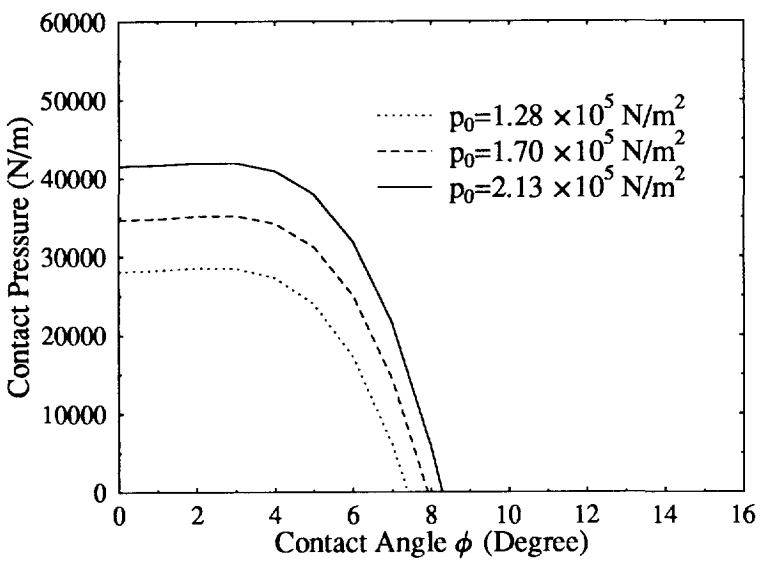

(b) $d_0 = 0.02$ m

Figure 5.8: The pressure distribution patterns of tire-flat road contact (R = 0.3 m, b = 0.14 m, τ = 0.014 m, $k_v = 0$ N/m^2)

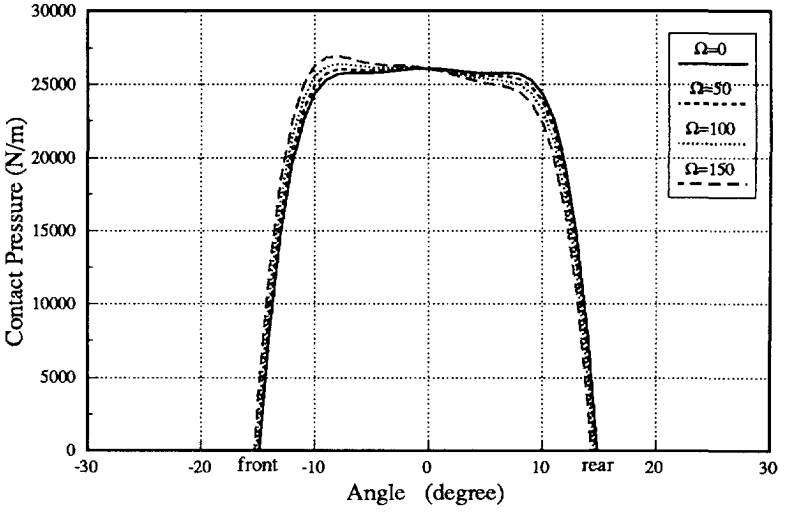

(a) $\lambda = 0.05$

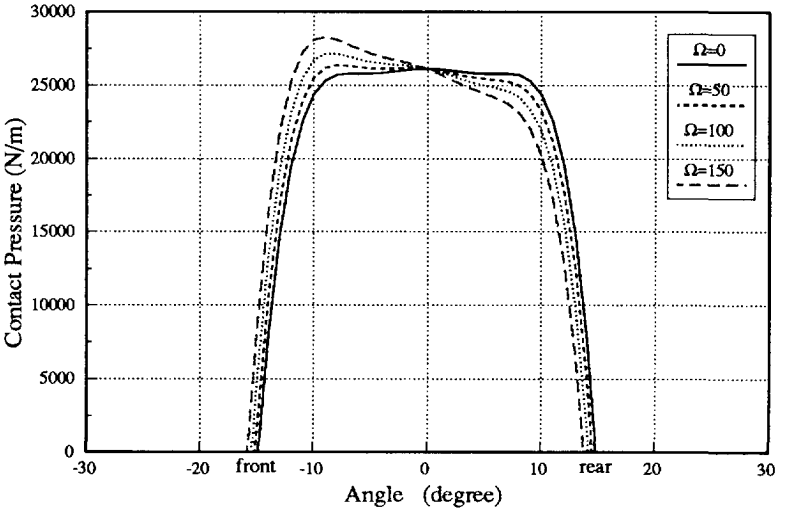

(b) $\lambda = 0.10$

Figure 5.9: The influence of tire rotating speed on the contact pressure distribution ($d_0 = 0.02$ m) (*cont.*)

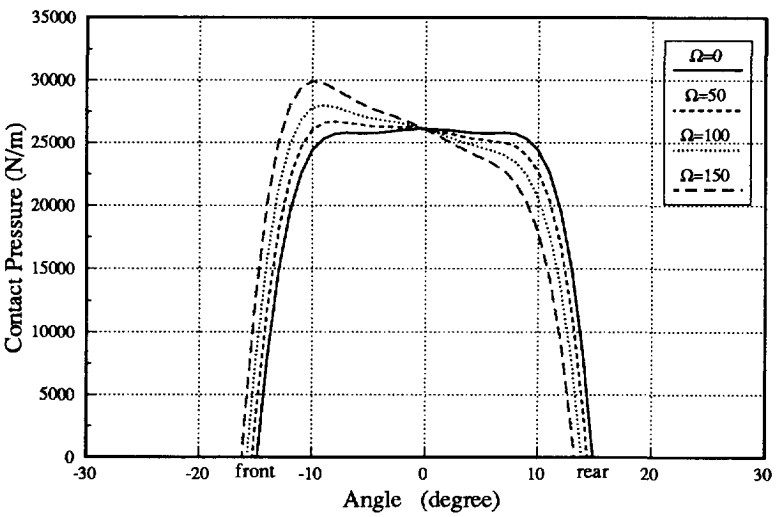

(c) $\lambda = 0.15$

Figure 5.9 (*cont.*): The influence of tire rotating speed on the contact pressure distribution ($d_0 = 0.02$ m)

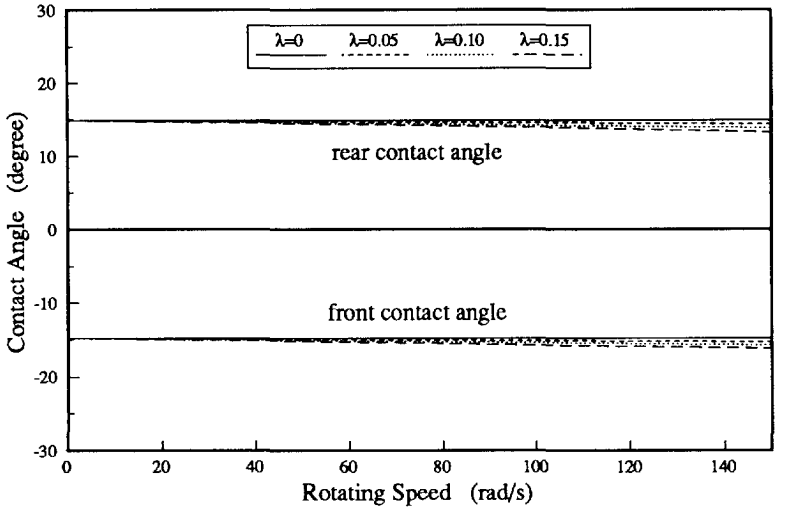

Figure 5.10: The influence of tire rotating speed on the contact angles (d_0 = 0.02 m)

pressure. Figure 5.10 shows the changes of the tire-road contact area with the rotating speed Ω. Four different values of damping coefficient are used. It is observed that the rotating speed has little influence on the tire-road contact length. But when the rotating speed increases, the whole contact area between the tire and the road shifts slightly to the front. That is to say, if we divide the contact area into two parts at the point directly beneath the wheel-center, the front part of the contact area increases with the rotating speed while the rear part decreases by approximately the same amount. Again, the forward shifting of the contact area due to rotating speed is related to the tire internal damping. The larger the tire internal damping, the more obvious the forward shifting of the contact area.

5.7.4 Relation between the vertical force and the tire deflection

Figure 5.11 shows an example of the relation between the axle force in the vertical direction and the tire deflection. It can be seen clearly that the vertical force–tire deflection is non-linear. However, it should be noted that this non-linear force–deflection relation is obtained from the linear tire model.

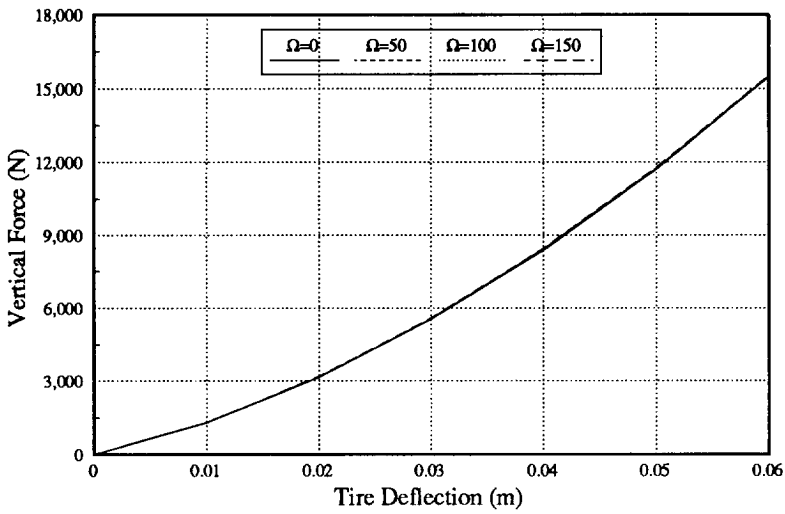

Figure 5.11: The relation between vertical axle force and tire deflection ($\lambda = 0.10$)

This is important because it proves that a non-linear vertical force–deflection relation does not necessarily mean the tire itself is a non-linear system.

5.7.5 Relation between the contact length and the tire deflection

Figure 5.12 is one of the numerical results showing that the front and rear contact angles change with the tire deflection. The relation between the contact angles and the deflection is almost linear. That is to say the tire-road contact length increases almost linearly with the tire deflection.

5.8 Conclusions

In this chapter, a new method to study the tire-flat road contact problem was developed. This new method differs from conventional ones in that the tire is treated as one entity instead of being divided into different regions. The convergence of the algorithm associated with this new method was examined.

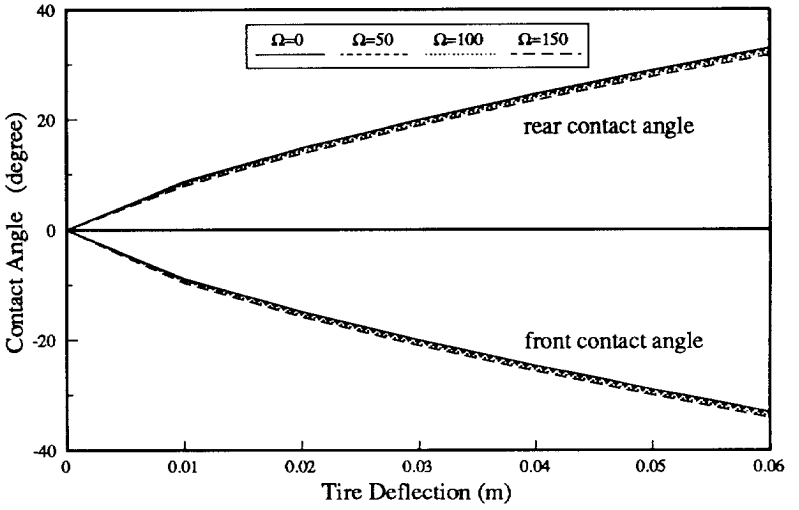

Figure 5.12: The relation between the contact angles and tire deflection ($\lambda = 0.10$)

The numerical result for a static tire was compared with one experimental result available in literature, which showed that the new method gives quite an accurate prediction of the tire-road contact pressure distribution. It was also shown that the new method developed here is able to reproduce different types of contact pressure distributions. The influences of different variables on the tire-road contact were studied numerically using this new method. It showed that the non-linear relation between tire vertical load and tire deflection can be obtained using this linear tire model. The numerical study also showed that the tire model and the new method are able to predict the changes in contact pressure distribution, contact length, as well as the tire-wheel axle forces with the tire rotating speed, tire deflection and other variables.

Chapter 6

Frequency Response Functions of a Free Tire-Wheel System

In this chapter, we will derive the frequency response functions of the free tire-wheel system. Tire contact with the road is not introduced at this stage, so the compliances of the tread elements are not considered here. The tire treadband is assumed to be in-extensible, thus the in-extensible ring model is used. With regard to the problem of vibration transmission, the frequency response functions between the wheel-axle and a point on the tire treadband are of most interest.

6.1 External Forces and Displacements

6.1.1 External forces

We assume there are five external forces acting on the tire-wheel system: force $f_x(t)$ acting at the wheel center in the longitudinal direction; force $f_z(t)$ acting at the wheel center in the vertical direction; torque $T(t)$ acting on the wheel; and forces $p_w(t)$ and $p_v(t)$ acting at a point on the tire treadband in the radial and tangential directions, respectively. The forces q_w and q_v then

can be expressed as:

$$q_w(\phi,t) = \frac{p_w(t)}{R}\delta(\phi - (2i\pi + \phi_0)) \tag{6.1a}$$

$$q_v(\phi,t) = \frac{p_v(t)}{R}\delta(\phi - (2i\pi + \phi_0)) \tag{6.1b}$$

where $i = 0,1,2,3,...$; ϕ_0 defines the location of the force acting point. It should be noted here that $p_w(t)$, $p_v(t)$ are now point forces with the unit of Newton. And it is also worth mentioning that although $p_w(t)$, $p_v(t)$ are point forces, which by themselves cannot be expanded into Fourier series, q_w, q_v are periodic functions in terms of variable ϕ, where ϕ is defined in the domain of infinity. Therefore q_w, q_v can indeed be expanded into Fourier series.

Substituting Equation (6.1) into Equation (4.6) (with the primes omitted), we have

$$\xi_0 = \frac{1}{2\pi R}p_v \tag{6.2a}$$

$$\xi_n = \frac{1}{\pi R}(p_v \cos n\phi_0 + p_w n \sin n\phi_0) \tag{6.2b}$$

$$\eta_n = \frac{1}{\pi R}(p_v \sin n\phi_0 - p_w n \cos n\phi_0) \tag{6.2c}$$

Therefore the relations between the generalized forces and physical forces are established, which can be written in matrix form as follows

$$\mathbf{f}_n = \mathbf{T}_{fn}\mathbf{f} \tag{6.3}$$

in which $\mathbf{f} = \{p_v, p_w, T, f_x, f_z\}^T$ and

$$\mathbf{T}_{fn} = \frac{1}{2\pi R}\begin{bmatrix} 1 & 0 & 0 & 0 & 0 \\ 0 & 0 & 0 & 0 & 0 \\ 0 & 0 & 1 & 0 & 0 \end{bmatrix}, \qquad \text{for } n = 0 \tag{6.4a}$$

$$\mathbf{T}_{fn} = \frac{1}{\pi R}\begin{bmatrix} \cos n\phi_0 & n\sin n\phi_0 & 0 & 0 & 0 \\ \sin n\phi_0 & -n\cos n\phi_0 & 0 & 0 & 0 \\ 0 & 0 & 0 & 1 & 0 \\ 0 & 0 & 0 & 0 & 1 \end{bmatrix}, \qquad \text{for } n = 1 \tag{6.4b}$$

$$\mathbf{T}_{fn} = \frac{1}{\pi R}\begin{bmatrix} \cos n\phi_0 & n\sin n\phi_0 & 0 & 0 & 0 \\ \sin n\phi_0 & -n\cos n\phi_0 & 0 & 0 & 0 \end{bmatrix}, \qquad \text{for } n \neq 0,1 \tag{6.4c}$$

6.1.2 Displacements

Utilizing Equation (4.4), we can easily write the relations between the physical displacements and the generalized displacements of the system:

$$\mathbf{u} = \sum_{n=0}^{+\infty} \mathbf{T}_{dn}\mathbf{u}_n \tag{6.5}$$

in which $\mathbf{u} = \{v, w, \theta_r, x, z\}^T$ and

$$\mathbf{T}_{dn} = \begin{bmatrix} \cos n\phi & \sin n\phi & 0 \\ n\sin n\phi & -n\cos n\phi & 0 \\ 0 & 0 & 1 \\ 0 & 0 & 0 \\ 0 & 0 & 0 \end{bmatrix}, \qquad \text{for } n = 0 \tag{6.6a}$$

$$\mathbf{T}_{dn} = \begin{bmatrix} \cos n\phi & \sin n\phi & 0 & 0 \\ n\sin n\phi & -n\cos n\phi & 0 & 0 \\ 0 & 0 & 0 & 0 \\ 0 & 0 & 1 & 0 \\ 0 & 0 & 0 & 1 \end{bmatrix}, \qquad \text{for } n = 1 \tag{6.6b}$$

$$\mathbf{T}_{dn} = \begin{bmatrix} \cos n\phi & \sin n\phi \\ n\sin n\phi & -n\cos n\phi \\ 0 & 0 \\ 0 & 0 \\ 0 & 0 \end{bmatrix}, \qquad \text{for } n \neq 0, 1 \tag{6.6c}$$

6.2 Transfer Functions between Generalized Displacements and Forces

Applying Laplace transform to the transformed equations of motion (Equation (4.8)), we have

$$\mathbf{U}_n(s) = \mathbf{T}_{mn}\mathbf{F}_n(s) \tag{6.7}$$

in which

$$\mathbf{T}_{mn} = \left[\mathbf{M}_n s^2 + \mathbf{G}_n s + \mathbf{K}_n\right]^{-1} \tag{6.8}$$

$\mathbf{T}_{mn}$ is a 3×3 matrix when $n=0$; 4×4 when $n=1$ and 2×2 when $n\neq0,1$.

When $n=0$, the elements of matrix $\mathbf{T}_{mn}$ are

$$t_{m0}^{11}=\frac{m_r s^2+c_r s+k_r}{(m_0 s^2+c_0 s+k_0)(m_r s^2+c_r s+k_r)-k_{0r}^2}$$
$$t_{m0}^{12}=t_{m0}^{21}=0$$
$$t_{m0}^{13}=\frac{-k_{0r}}{(m_0 s^2+c_0 s+k_0)(m_r s^2+c_r s+k_r)-k_{0r}^2}$$
$$t_{m0}^{22}=\frac{1}{m_0 s^2+c_0 s+k_0}$$
$$t_{m0}^{23}=t_{m0}^{32}=0$$
$$t_{m0}^{31}=t_{m0}^{13}$$
$$t_{m0}^{33}=\frac{m_0 s^2+c_0 s+k_0}{(m_0 s^2+c_0 s+k_0)(m_r s^2+c_r s+k_r)-k_{0r}^2}$$

When $n=1$, the elements of matrix $\mathbf{T}_{mn}$ are

$$t_{m1}^{11}=\frac{m_a s^2+c_a s+k_a}{(m_1 s^2+c_1 s+k_1)(m_a s^2+c_a s+k_a)-k_1^2}$$
$$t_{m1}^{12}=t_{m1}^{21}=t_{m1}^{13}=t_{m1}^{31}=t_{m1}^{24}=t_{m1}^{42}=t_{m1}^{34}=t_{m1}^{43}=t_{m1}^{43}=0$$
$$t_{m1}^{14}=\frac{k_1}{(m_1 s^2+c_1 s+k_1)(m_a s^2+c_a s+k_a)-k_1^2}$$
$$t_{m1}^{33}=\frac{m_1 s^2+c_1 s+k_1}{(m_1 s^2+c_1 s+k_1)(m_a s^2+c_a s+k_a)-k_1^2}$$
$$t_{m1}^{22}=t_{m1}^{11}$$
$$t_{m1}^{44}=t_{m1}^{33}$$
$$t_{m1}^{41}=t_{m1}^{14}$$
$$t_{m1}^{23}=t_{m1}^{32}=-t_{m1}^{14}$$

When $n\neq0,1$, the elements of matrix $\mathbf{T}_{mn}$ are

$$t_{mn}^{11}=\frac{m_n s^2+c_n s+k_n}{(m_n s^2+c_n s+k_n)^2+(g_n s)^2}$$
$$t_{mn}^{12}=\frac{-g_n s}{(m_n s^2+c_n s+k_n)^2+(g_n s)^2}$$

$$t_{mn}^{21} = -t_{mn}^{12}$$
$$t_{mn}^{22} = t_{mn}^{11}$$

6.3 Transfer Functions of the Free Tire-Wheel System

With the equations derived in the previous sections, we are now ready to obtain the transfer functions of the free tire-wheel system between any two points in the system. Substituting Equations (6.3), (6.7) into Equation (6.5), we have

$$\mathbf{U}(s) = \mathbf{T}\,\mathbf{F}(s) \tag{6.9}$$

where $\mathbf{T}$ is a 5×5 transfer function matrix. $\mathbf{U}(s)$ and $\mathbf{F}(s)$ are the Laplace transform of the physical displacement $\mathbf{u}$ and force $\mathbf{f}$ respectively.

$$\mathbf{T} = \sum_{n=0}^{+\infty} [\mathbf{T}_{dn}\mathbf{T}_{mn}\mathbf{T}_{fn}] \tag{6.10}$$

The individual elements of the matrix $\mathbf{T}$ represent the transfer functions between any two points on the tire treadband in either tangential or radial directions and between a point on the tire treadband and the wheel. Substituting $\mathbf{T}_{dn}$, $\mathbf{T}_{mn}$ and $\mathbf{T}_{fn}$ into Equation (6.10), these transfer functions can be obtained.

The tangential displacement response on treadband at ϕ to tangential force excitation on the treadband at ϕ_0:

$$T_{11} = \frac{1}{\pi R}\left\{0.5t_{m0}^{11} + \sum_{n=0}^{+\infty}\left[t_{mn}^{11}\cos n(\phi-\phi_0) - t_{mn}^{12}\sin n(\phi-\phi_0)\right]\right\} \tag{6.11a}$$

The tangential displacement response on the treadband at ϕ to radial force excitation on the treadband at ϕ_0:

$$T_{12} = -\frac{1}{\pi R}\sum_{n=1}^{+\infty}\left[n\left(t_{mn}^{11}\sin n(\phi-\phi_0) + t_{mn}^{12}\cos n(\phi-\phi_0)\right)\right] \tag{6.11b}$$

The tangential displacement response on treadband at ϕ to torque excitation on the wheel:

$$T_{13} = \frac{1}{2\pi R}t_{m0}^{13} \tag{6.11c}$$

The tangential displacement response on the treadband at ϕ to longitudinal force excitation at the wheel center:

$$T_{14} = -\frac{1}{\pi R} t_{m1}^{14} \sin \phi \tag{6.11d}$$

The tangential displacement response on the treadband at ϕ to vertical force excitation at the wheel center:

$$T_{15} = \frac{1}{\pi R} t_{m1}^{14} \cos \phi \tag{6.11e}$$

The radial displacement response on the treadband at ϕ to tangential force excitation on the treadband at ϕ_0:

$$T_{21} = \frac{1}{\pi R} \sum_{n=1}^{+\infty} \left[n \left(t_{mn}^{11} \sin n(\phi - \phi_0) + t_{mn}^{12} \cos n(\phi - \phi_0) \right) \right] \tag{6.11f}$$

The radial displacement response on the treadband at ϕ to radial force excitation on the treadband at ϕ_0:

$$T_{22} = \frac{1}{\pi R} \sum_{n=1}^{+\infty} \left[n^2 \left(t_{mn}^{11} \cos n(\phi - \phi_0) - t_{mn}^{12} \sin n(\phi - \phi_0) \right) \right] \tag{6.11g}$$

The radial displacement response on the treadband at ϕ to torque excitation on the wheel:

$$T_{23} = 0 \tag{6.11h}$$

The radial displacement response on the treadband at ϕ to longitudinal force excitation at the wheel center:

$$T_{24} = \frac{1}{\pi R} t_{m1}^{14} \cos \phi \tag{6.11i}$$

The radial displacement response on the treadband at ϕ to vertical force excitation at the wheel center:

$$T_{25} = \frac{1}{\pi R} t_{m1}^{14} \sin \phi \tag{6.11j}$$

The dynamic angular displacement response of the wheel to tangential force excitation on the treadband at ϕ_0:

$$T_{31} = \frac{1}{2\pi R} t_{m0}^{13} \tag{6.11k}$$

The dynamic angular displacement response of the wheel to radial force excitation on the treadband at ϕ_0:

$$T_{32} = 0 \tag{6.11l}$$

The dynamic angular displacement response of the wheel to torque excitation on the wheel:

$$T_{33} = \frac{1}{2\pi R} t_{m0}^{33} \tag{6.11m}$$

The dynamic angular displacement response of the wheel to longitudinal force excitation at the wheel center:

$$T_{34} = 0 \tag{6.11n}$$

The dynamic angular displacement response of the wheel to vertical force excitation at the wheel center:

$$T_{35} = 0 \tag{6.11o}$$

The longitudinal displacement response at the wheel center to tangential force excitation on the treadband at ϕ_0:

$$T_{41} = -\frac{1}{\pi R} t_{m1}^{14} \sin \phi_0 \tag{6.11p}$$

The longitudinal displacement response at the wheel center to radial force excitation on the treadband at ϕ_0:

$$T_{42} = \frac{1}{\pi R} t_{m1}^{14} \cos \phi_0 \tag{6.11q}$$

The longitudinal displacement response at the wheel center to torque excitation at the wheel:

$$T_{43} = 0 \tag{6.11r}$$

The longitudinal displacement response at the wheel center to longitudinal force excitation at the wheel center:

$$T_{44} = \frac{1}{\pi R} t_{m1}^{33} \tag{6.11s}$$

The longitudinal displacement response at the wheel center to vertical force excitation at the wheel center:

$$T_{45} = 0 \tag{6.11t}$$

The vertical displacement response at the wheel center to tangential force excitation on the treadband at ϕ_0:

$$T_{51} = \frac{1}{\pi R} t_{m1}^{14} \cos \phi_0 \tag{6.11u}$$

The vertical displacement response at the wheel center to radial force excitation on the treadband at ϕ_0:

$$T_{52} = \frac{1}{\pi R} t_{m1}^{14} \sin \phi_0 \tag{6.11v}$$

The vertical displacement response at the wheel center to torque excitation on the wheel:

$$T_{53} = 0 \tag{6.11w}$$

The vertical displacement response at the wheel center to longitudinal force excitation at the wheel center:

$$T_{54} = 0 \tag{6.11x}$$

The vertical displacement response at the wheel center to vertical force excitation at the wheel center:

$$T_{55} = \frac{1}{\pi R} t_{m1}^{33} \tag{6.11y}$$

With matrix **T**, the transfer function between any two points in the tire-wheel system is defined. However, it should be noted here that **T** is not a transfer function matrix in the conventional sense since Equation (6.9) does not represent a discrete system. Instead, it represents a continuous system and has *infinite numbers of DOFs* (the continuous variable ϕ plus the three DOFs of the wheel). The first two rows of the matrix **T** can be considered as the Laplace transforms of the dynamic influence functions of the ring structure. Of course we can consider ϕ not as an independent variable but as a parameter defining a point on the tire treadband and have a transfer function matrix concerning three locations on the system: points on the treadband at ϕ and ϕ_0, and the wheel center. Such a transfer function matrix can easily be obtained from matrix **T** when necessary.

It can be seen from the above equations that the torque excitation on the wheel will not cause any radial displacement of the treadband and any displacement of the wheel center ($T_{23} = T_{43} = T_{53} = 0$). This is understandable

since the torque will only excite the rotational motion of the tire-wheel system; and the displacement of the treadband and the displacement of the wheel center are decoupled from the rotational motion. Inversely, excitations at the wheel center in the vertical and longitudinal directions and at the treadband in the radial direction will not cause rotational vibration of the tire-wheel system ($T_{32} = T_{34} = T_{35} = 0$).

6.4 Transfer Functions between the Contact Patch and the Wheel

As we mentioned earlier, one of the main objectives of this study is to investigate the vibrational transmission properties of the tire from the ground to the axle. Therefore, among all the transfer functions of the tire-wheel system, our primary interest lies in those transfer functions between the wheel and the tire-road contact patch. As the first step, we assume the tire-road contact patch is small so that point contact between the tire and road can be assumed. Figure 6.1 illustrates a tire-wheel system with forces acting at the tire-road contact point G and at the wheel center (point O). The forces and displacements shown in the figure are positive.

With respect to the coordinate system shown in Figure 6.1, let $\phi = \phi_0 = -90°$ in matrix $\mathbf{T}$, then we obtain the transfer function matrix between the wheel (point O) and the ground contact point (point G).

$$\begin{Bmatrix} V \\ W \\ \Theta_r \\ X \\ Z \end{Bmatrix} = \begin{bmatrix} H_{11} & H_{12} & H_{13} & H_{14} & 0 \\ H_{21} & H_{22} & 0 & 0 & H_{25} \\ H_{31} & 0 & H_{33} & 0 & 0 \\ H_{41} & 0 & 0 & H_{44} & 0 \\ 0 & H_{52} & 0 & 0 & H_{55} \end{bmatrix} \begin{Bmatrix} P_v \\ P_w \\ T \\ F_x \\ F_z \end{Bmatrix} \tag{6.12}$$

in which

$$H_{11} = \frac{1}{\pi R}\left[0.5t_{m0}^{11} + \sum_{n=1}^{+\infty} t_{mn}^{11}\right] \tag{6.13a}$$

$$H_{12} = -\frac{1}{\pi R}\sum_{n=1}^{+\infty}\left[nt_{mn}^{12}\right] \tag{6.13b}$$

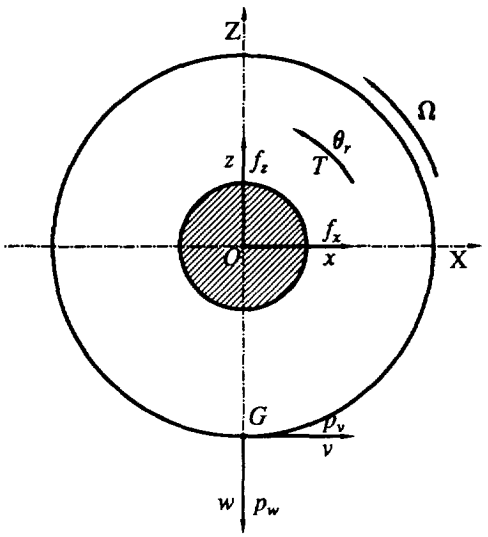

Figure 6.1: Forces and displacements on the wheel and at the tire-road contact point ($\phi = \phi_0 = -90°$)

$$H_{13} = \frac{1}{2\pi R} t^{13}_{m0} \tag{6.13c}$$

$$H_{14} = \frac{1}{\pi R} t^{14}_{m1} \tag{6.13d}$$

$$H_{21} = -H_{12} \tag{6.13e}$$

$$H_{22} = \frac{1}{\pi R} \sum_{n=1}^{+\infty} \left[n^2 t^{11}_{mn} \right] \tag{6.13f}$$

$$H_{25} = -\frac{1}{\pi R} t^{14}_{m1} \tag{6.13g}$$

$$H_{31} = \frac{1}{2\pi R} t^{13}_{m0} = H_{13} \tag{6.13h}$$

$$H_{33} = \frac{1}{2\pi R} t^{33}_{m0} \tag{6.13i}$$

$$H_{41} = \frac{1}{\pi R} t^{14}_{m1} = H_{14} \tag{6.13j}$$

$$H_{44} = \frac{1}{\pi R} t^{33}_{m1} \tag{6.13k}$$

$$H_{52} = -\frac{1}{\pi R} t^{14}_{m1} = H_{25} \tag{6.13l}$$

$$H_{55} = \frac{1}{\pi R} t_{m1}^{33} \tag{6.13m}$$

6.5 General Characteristics of the Vibration Transmission between the Contact Patch and the Wheel

The above transfer functions apply to the rotating tire-wheel system. The transfer function matrix is in general asymmetric, as we have already seen. The tangential displacement response to radial force excitation is not equal to the radial displacement response to the same force excitation in the tangential direction. In other words, the reciprocity law does not apply to the rotating tire-wheel system in general. However, if the rotating speed is equal to zero, i.e., the tire-wheel system is in the non-rotating state, H_{12} and H_{21} become zero and the transfer function matrix $\mathbf{H}$ is symmetric. Therefore, the reciprocity law applies to the non-rotating tire-wheel system.

Examining the expressions of H_{12} and H_{21}, it is found that the radial displacement response of the treadband to tangential force excitation at the same point (or the tangential displacement response to radial force excitation) are purely due to the coriolis effect of the rotating system, and its magnitude is linearly proportional to the rotating speed of the system. The two transfer function H_{12} and H_{21} have the same magnitude but opposite signs.

The wheel motion in the vertical direction is decoupled from that in the longitudinal direction. This is to say that the force excitation acting on the wheel center in the vertical direction will not cause any response in the longitudinal direction and vice versa ($H_{45} = H_{54} = 0$). It is also observed that the transfer function between the vertical displacement of the wheel and the vertical force at the wheel is equal to the transfer function between the longitudinal displacement of the wheel and the longitudinal force excitation ($H_{44} = H_{55}$). This is understandable, because the free tire-wheel system is isotropic with respect to the center of the wheel, i.e., the vibrational behavior of a point on the system at any central angle is the same as that of another point at another central angle, due to the periodic property of the system.

Another characteristic of the vibration transmission between the wheel and

the ground contact point is that the cross point transfer function between the wheel and the ground contact point in the vertical direction equals that in the longitudinal direction in magnitude but has opposite signs ($H_{52} = -H_{41}$). The underlying reason for this may not be obvious at first glance. However, if we recall the analysis on the vibration modes and natural frequencies of the system in Chapter 3, we know that the translational DOFs of the wheel affect only the first order natural frequencies and modes of the entire system, and that for the first order modes, the tire treadband (the ring) is moving as a rigid body on the tire sidewall (the radial and tangential springs). As a result, the cross point transfer functions contain only the first order natural modes of the system, which is the same whether it is in the vertical direction or in the longitudinal direction. The difference in sign of the two transfer functions is due to the definitions of positive directions of the forces and displacements (see Figure 6.1).

Considering the skew symmetric elements $H_{12} = -H_{21}$ and the symmetry of the other off-diagonal elements as well as the axisymmetry of the tire-wheel structure, only seven transfer functions are needed to specify the vibration transmission between the two points (O and G in Figure 6.1).

6.6 Numerical Examples and Analysis

Figure 6.2 shows the transfer functions of the free tire-wheel system in the non-rotating state. The transfer functions are shown here in terms of their magnitudes in logarithmic scale. The driving point transfer function H_{12} is not shown in Figure 6.2 because for the non-rotating tire-wheel system, H_{12} is equal to zero across the frequency spectrum.

As expected, the driving point transfer functions on the treadband, i.e., the tire-road contact point, have multiple peaks due to the high order vibration modes of the treadband. The cross point transfer functions between the wheel and the road contact point and the driving point transfer functions at the wheel have only one resonant peak respectively. The reason for this is again due to the periodic properties of the tire treadband motion in terms of the central angle. We know from Chapter 3 that the mode shapes of the tire treadband vibration are sinusoidal. The high frequency components

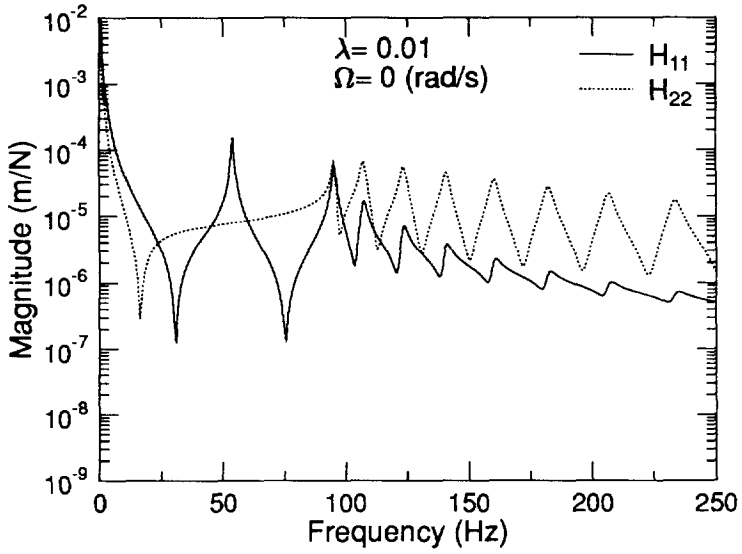

(a)

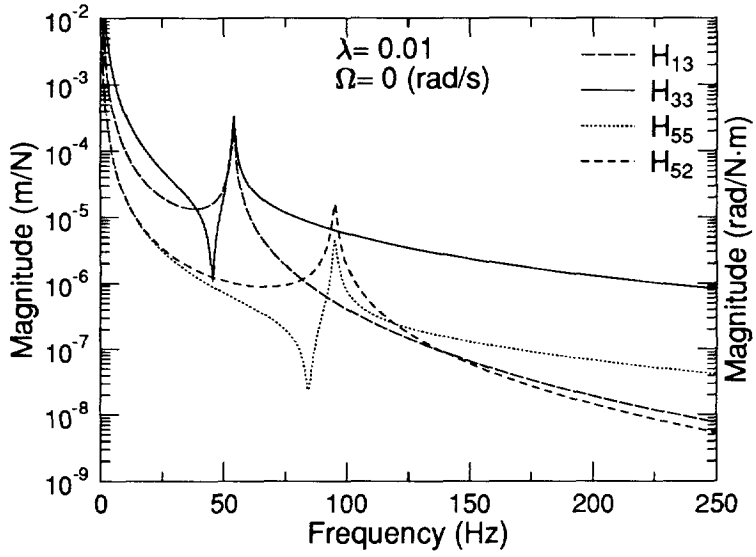

(b)

Figure 6.2: The transfer functions of a free, non-rotating tire-wheel system

of the excitation forces acting on the tire treadband will excite the high frequency modes ($n \geq 2$) of the tire-wheel system. However, the $n \geq 2$ vibration modes of the treadband will not be transmitted to the wheel due to their axisymmetric property. Only the first order mode component of the treadband vibration will cause the translational motion of the wheel and the zeroth order mode component will cause the rotational motion of the wheel.

Figure 6.3 shows the transfer functions for a free, rotating tire-wheel system. Comparing it with Figure 6.2, we can see that there are many more resonant frequencies for the rotating tire-wheel system than for the non-rotating system, especially in the high frequency range. This is caused by the effect of the coriolis acceleration of the tire treadband. Another point to be noted is the longitudinal response of tire tread band to vertical force excitation at point G (H_{12}). For the non-rotating tire-wheel system, H_{12} is zero. But for the rotating system, H_{12} is not zero, caused also by the coriolis effect.

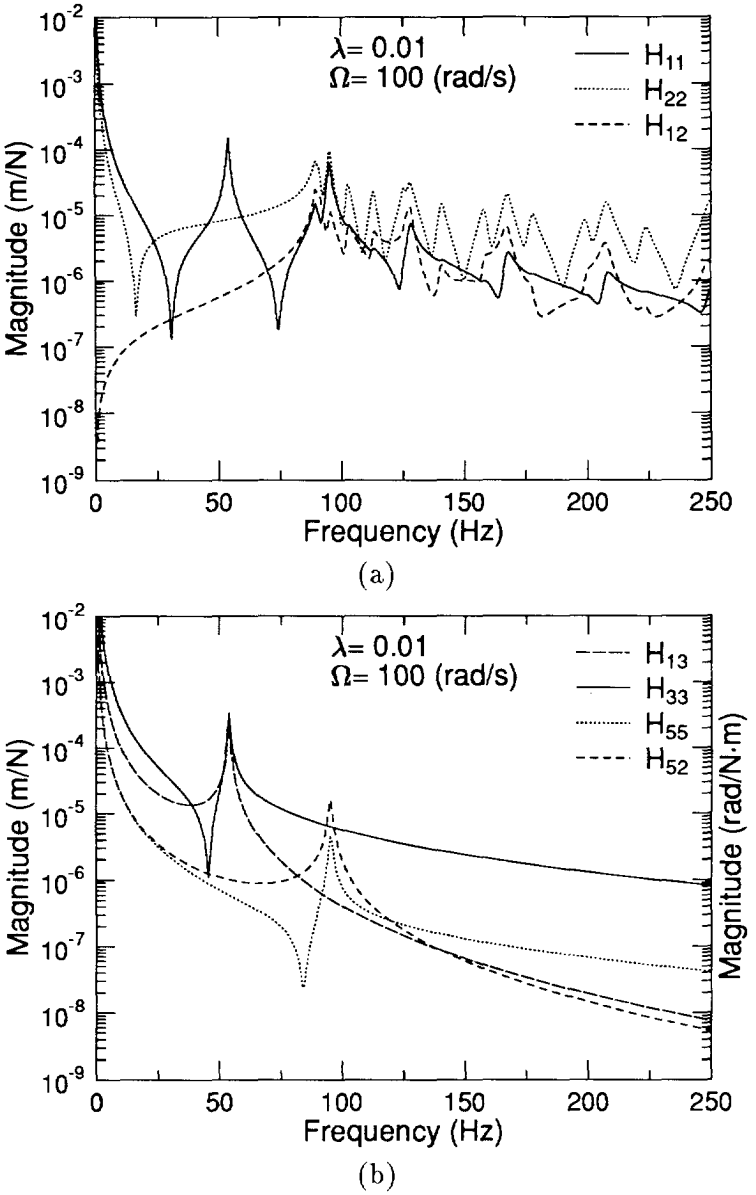

Figure 6.3: The transfer functions of a free, rotating tire-wheel system

Chapter 7

Vibration Transmission of Tires under Various Boundary Conditions

7.1 Introduction

The vibration transmission properties of tires have an important influence on the ride and comfort characteristics of vehicles. Testing and evaluation of the vibration characteristics of tires are generally performed on different types of indoor test facilities where test conditions can be controlled and monitored. However, different types of laboratory tests usually lead to different results which cannot be directly compared with one another. It is well known that the boundary conditions and constraints imposed at the axle and the tire-road contact patch can differ greatly in laboratory tests. It is of practical interest to examine the influences of boundary conditions on tire vibration properties, and, more importantly, to establish the relations between the vibration transmission properties of tires under different boundary conditions.

Richards et al. [81] found by both experiments and FEM analysis that tire resonant frequencies are highly dependent on the boundary conditions at

the axle and the contact patch. However, to the author's knowledge, few studies have so far explored the underlying relations between the vibration properties of tires under different boundary conditions. Soedel [88] developed a method to calculate vibration modes of tires with ground contact from the eigenvalues of non-contacting tires. Huang and Su [47] extended Soedel's work by including tire rotation in the analysis. However, their study dealt only with conditions where the axles as well as the tire-road contact patches are fixed. It is not directly applicable to the study of the vibration transmission of tires.

In this chapter, an analysis is made to investigate the influences of boundary conditions on the vibration transmission properties of tires based on a basic set of transfer functions of an unconstrained tire-wheel system. First the different configurations of tires on roads and in laboratory tests are described. The boundary conditions and constraints of tires under those configurations are then formulated. By making use of the transfer functions of the free tire-wheel system, the transfer functions of tires under different boundary conditions are obtained. Numerical results of the most important transfer functions are presented and analyzed.

7.2 The Differences between Rotating and Rolling of a Tire-Wheel System

A tire-wheel system rolling on the road surface differs from a rotating tire-wheel system in two aspects: 1) the tire is preloaded by a vertical static load. Therefore the tire is in contact with the road in a finite area instead of at one single point; and the dynamic behavior of the tire changes to a certain extent; and 2) due to the friction existing at the tire-road interface, extra constraints are imposed on the tire-wheel system.

7.2.1 The influence of the static vertical load

Consider a tire-wheel system loaded against the road surface by a constant vertical load. The application of the static load has two effects: a) the preload to the tire-wheel system changes the system properties to some ex-

tent; and b) the contact patch extends over a finite region. The first effect can be taken into account by modifying the model parameters and the vibration transfer functions defined in the previous chapters. Richards et al. [81] have shown that it is possible to establish a free tire-wheel model including the effect of the static vertical load.

The second effect of the static load is more difficult to deal with. Because of the finite contact the force or motion inputs to the system are at an infinite number of points in the contact patch, instead of at a single point. In addition, the inputs (or constraints) act at the contact patch of the tire not only in the vertical but also in the longitudinal direction. The analysis here is restricted to the case of point contact between the tire and the road. The input (or constraint) complexity due to the finite contact is not considered.

7.2.2 The effect of the friction between the tire and the road

For a free, rotating tire-wheel system, the forces acting on the wheel and acting at a point on the treadband are independent of each other. However, this is not the case for a tire-wheel system rolling on the road. Due to the friction between the tire and the road, the force acting on the wheel axle in the longitudinal direction or torque acting on the wheel will generate a longitudinal force in the tire-road contact patch. Therefore extra constraint is imposed on the tire in the contact patch. If the friction coefficient is sufficiently large, the tread elements in the contact patch will have no motion in the longitudinal direction. Neglecting the compliance of the tread elements, this boundary condition in the contact patch can be described as follows:

$$V = 0 \tag{7.1}$$

7.3 Typical Boundary Conditions of Tire-Wheel Systems

In addition to the aspects mentioned in the previous section, the tire-wheel systems on vehicles or in laboratory tests are frequently subjected to specific constraints. In this section, the constraints of several tire-wheel system

configurations, which are often seen in laboratory tests as well as on vehicles on the road, are formulated in terms of mathematical boundary conditions.

The boundary conditions of tire-wheel systems in various laboratory tests and on moving vehicles can be classified into two categories: constraints at the tire-road contact patch and constraints at the tire-wheel axle. When the excitation is applied to the system at the tire-road contact patch, it is usually defined as displacement input. Three cases of different boundary conditions and input variables are discussed in this section.

7.3.1 Case I

For a vehicle on the road, the excitation caused by the irregularities of the road surface may be viewed as displacement inputs at the tire-road contact patch. The most important transfer function to describe the vibration transmission of the tire-wheel system on a moving vehicle is:

$$H_{\alpha 1} = \frac{Z}{W} \tag{7.2}$$

where Z and W are the Laplace transforms of the vertical displacement response of the wheel and the vertical displacement excitation on the tire treadband due to the road profile.

Another transfer function which is of interest is

$$H_{\alpha 2} = \frac{X}{W} \tag{7.3}$$

The only constraint on the tire-wheel system in this case is the constraint described by Equation (7.1).

Vibration transmission tests of tires are often performed with a vibrating platform. The tire is usually mounted on a laboratory suspension system or on a vehicle. External dynamic force or displacement is applied by the vibrator in the vertical direction to the tire through the contact patch. The axle motion in the vertical direction (sometimes also in the longitudinal direction) is measured. The ratio of the axle motion to the dynamic displacement (force) at the contact patch is used to define the vibration transmission properties of tires. Such tests are reported by Potts et al. [77], among others.

The tire-wheel system in this type of laboratory test can be considered as a special case of the tire-wheel system we just described with the angular speed of the system equal to zero ($\Omega = 0$).

7.3.2 Case II

Cleat tests are widely used to determine the vibration transmission properties of tires. During a cleat test, a tire is pressed against a moving surface (a rotating drum) with the help of a test rig and the wheel. The axle of the system are usually fixed in space. The response variables are the longitudinal and vertical forces at the axle and the angular speed changes of the wheel during the passage of the tire over the cleat. The input (excitation) to the system is the vertical displacement in the contact patch generated by the cleat.

If the wheel is fixed, the boundary conditions for the longitudinal and vertical displacements of the wheel axle are

$$X = 0, \quad Z = 0 \tag{7.4}$$

The transfer function which is of most importance for the vibration transmission of the tire-wheel system in this case is:

$$H_{\beta 1} = \frac{F_z}{W} \tag{7.5}$$

Other transfer functions of interest are

$$H_{\beta 2} = \frac{F_x}{W} \tag{7.6}$$

$$H_{\beta 3} = \frac{\Theta_r}{W} \tag{7.7}$$

7.3.3 Case III

For the tire configurations described in the previous two subsections, the excitations are all applied to the tire-wheel system in the contact patch. There is another type of laboratory test in which the external excitation

to the tire-wheel system is applied at the wheel axle. The Goodyear *Tire Modal Test Rig* [80] and the tire mobility measurements described by Mills and Dunn [67] are two examples. In this type of test, the tire-wheel system is preloaded against a moving surface (usually a rotating drum) by some loading mechanism. The axle is free to move at least in the vertical direction (sometimes axle motion in the longitudinal direction too is allowed, such as in the Goodyear tire modal tests). External forces are applied at the axle of the tire in the vertical (and/or longitudinal) direction by electromagnetic vibrators. The driving point receptances or mobilities are usually obtained from this type of test.

Since the tire-wheel system in this case is rolling on a smooth surface, no motion of the tire treadband in the contact patch is allowed in the vertical direction. Therefore, the boundary condition for this type of test can be described by:

$$W = 0 \tag{7.8}$$

In addition, the tire-wheel system in this case is also subjected to the constraint described in Equation (7.1).

The most important transfer function is

$$H_{\gamma 1} = \frac{Z}{F_z} \tag{7.9}$$

Other transfer functions of interest are

$$H_{\gamma 2} = \frac{X}{F_z}, \qquad H_{\gamma 3} = \frac{X}{F_x}$$

The boundary conditions for the tire-wheel system configurations discussed in this section are listed in Table 7.1 together with the input and output variables usually used to describe the vibration transmissions of the systems.

Table 7.1: The boundary conditions of tires in laboratory tests & on moving vehicles

Tire config.	Constraints	Inputs	Outputs
Case I	$v = 0$	w	x, z
Case II	$v = 0, x = 0, z = 0$	w	f_x, f_z, θ_r
Case III	$v = 0, w = 0$	f_x, f_z	x, z

7.4 Transfer Functions of Tire-Wheel Systems under Various Boundary Conditions

7.4.1 The method

The *modal synthesis method* (sometimes called *receptance method*) is used to obtain the transfer functions of the tire-wheel system under various boundary conditions. Soedel [88] applied this method to obtain the natural frequencies and modes of tires with ground contact from the eigenvalues of non-contacting tires.

According to the modal synthesis theory, the DOFs of a substructure (component) can be divided into two categories: boundary DOFs and remainder DOFs. The boundary DOFs of a component are those connected with adjacent components. Therefore a system represented by the transfer function matrix equation can be partitioned according to boundary and remainder DOFs:

$$\begin{Bmatrix} X_r \\ X_b \end{Bmatrix} = \begin{bmatrix} [H]_{rr} & [H]_{rb} \\ [H]_{br} & [H]_{bb} \end{bmatrix} \begin{Bmatrix} F_r \\ F_b \end{Bmatrix} \tag{7.10}$$

in which X_r, X_b and F_r, F_b are the Laplace transforms of the displacements and forces at the remainder and boundary DOFs, respectively.

At the boundary DOFs, the forces and displacements must satisfy the compatibility conditions between the concerned components. By enforcing the compatibility conditions, the transfer function matrix of the complete system can be obtained.

Take as an example the tire-wheel system with a fixed axle. In this case, the boundary DOFs of the tire-wheel substructure are the longtudinal and vertical motion of the wheel. The displacements x, z of the wheel have to satisfy the compatibility conditions $x = z = 0$ since the axle is fixed. Imposing this condition on Equation (6.12), we have

$$\begin{Bmatrix} F_x \\ F_z \end{Bmatrix} = - \begin{bmatrix} H_{44} & H_{45} \\ H_{54} & H_{55} \end{bmatrix}^{-1} \begin{bmatrix} H_{41} & H_{42} & H_{43} \\ H_{51} & H_{52} & H_{53} \end{bmatrix} \begin{Bmatrix} P_v \\ P_w \\ T \end{Bmatrix} \tag{7.11}$$

Substituting Equation (7.11) back into Equation (6.12), a 3×3 transfer function matrix is obtained which describes the vibration properties of the tire-wheel system with a fixed axle:

$$\begin{Bmatrix} V \\ W \\ \Theta_r \end{Bmatrix} = \begin{bmatrix} H_{11} - \frac{H_{14}^2}{H_{44}} & H_{12} & H_{13} \\ H_{21} & H_{22} - \frac{H_{25}^2}{H_{55}} & 0 \\ H_{31} & 0 & H_{33} \end{bmatrix} \begin{Bmatrix} P_v \\ P_w \\ T \end{Bmatrix} \tag{7.12}$$

The natural frequencies and modes determined by the above equation are in general different from those of the free tire-wheel system. Equation (7.11) describes the force transmission between the tire-road contact patch and the fixed axle of the tire-wheel system.

The same technique is used to obtain transfer functions with displacements as input variables.

7.4.2 The vibration transmission under various boundary conditions

Using the method described above, the transfer functions of a tire-wheel system with various boundary conditions in each of the three cases discussed in the previous section are derived from those of a free tire-wheel system based on the point contact assumption.

Case I

In this case, the boundary condition is the zeroth longitudinal displacement at the tire-road contact point ($V = 0$). The most important input variable to be considered is the vertical displacement W prescribed by the road profile. Therefore W and V are the boundary DOFs in this case. From Equation (6.12), the following equation is obtained:

$$\begin{Bmatrix} P_v \\ P_w \\ \Theta_r \\ X \\ Z \end{Bmatrix} = \begin{bmatrix} [H]_{bb}^{-1} & -[H]_{bb}^{-1}[H]_{br} \\ [H]_{rb}[H]_{bb}^{-1} & [H]_{rr} - [H]_{rb}[H]_{bb}^{-1}[H]_{br} \end{bmatrix} \begin{Bmatrix} V \\ W \\ T \\ F_x \\ F_z \end{Bmatrix} \tag{7.13}$$

in which $V = 0$ and W is an input variable determined by the road profile or the excitator in a laboratory test.

$$[H]_{bb} = \begin{bmatrix} H_{11} & H_{12} \\ H_{21} & H_{22} \end{bmatrix}$$

$$[H]_{br} = \begin{bmatrix} H_{13} & H_{14} & 0 \\ 0 & 0 & H_{25} \end{bmatrix}$$

$$[H]_{rb} = \begin{bmatrix} H_{31} & 0 \\ H_{41} & 0 \\ 0 & H_{52} \end{bmatrix}$$

$$[H]_{rr} = \begin{bmatrix} H_{33} & 0 & 0 \\ 0 & H_{44} & 0 \\ 0 & 0 & H_{55} \end{bmatrix}$$

Equation (7.13 can be rewritten as follows:

$$\begin{Bmatrix} P_v \\ P_w \\ \Theta_r \\ X \\ Z \end{Bmatrix} = \begin{bmatrix} \alpha_{11} & \alpha_{12} & \cdots & \alpha_{15} \\ \vdots & \vdots & \ddots & \vdots \\ \alpha_{51} & \alpha_{52} & \cdots & \alpha_{55} \end{bmatrix} \begin{Bmatrix} V \\ W \\ T \\ F_x \\ F_z \end{Bmatrix} \tag{7.14}$$

Actually the first column of the transfer function matrix in the above equation is irrelevant here since $V = 0$ in this case.

The transfer functions of interest are thus obtained:

$$H_{\alpha 1} = \frac{Z}{W} = \alpha_{52} = \frac{H_{52}H_{11}}{H_{11}H_{22} - H_{12}H_{21}} \tag{7.15}$$

$$H_{\alpha 2} = \frac{X}{W} = \alpha_{42} = -\frac{H_{41}H_{12}}{H_{11}H_{22} - H_{12}H_{21}} \tag{7.16}$$

Case II

In this case, in addition to the boundary condition $V = 0$, the tire-wheel system is also subjected to extra constraints at the wheel axle, i.e. $X = Z = 0$. By applying this condition directly to Equation (7.14), the most important transfer functions describing the vibration transmission of tires in cleat tests are obtained:

$$H_{\beta 1} = \frac{F_z}{W} = \frac{\alpha_{54}\alpha_{42} - \alpha_{44}\alpha_{52}}{\alpha_{44}\alpha_{55} - \alpha_{45}\alpha_{54}} \tag{7.17}$$

$$H_{\beta 2} = \frac{F_x}{W} = \frac{\alpha_{45}\alpha_{52} - \alpha_{55}\alpha_{42}}{\alpha_{44}\alpha_{55} - \alpha_{45}\alpha_{54}} \tag{7.18}$$

$$H_{\beta 3} = \frac{\Theta_r}{W} = \alpha_{32} + \alpha_{34}H_{\beta 2} + \alpha_{35}H_{\beta 1} \tag{7.19}$$

Case III

In this case, the boundary conditions ($V = W = 0$) can be applied directly to Equation (6.12). The vibration transmission functions of tire-wheel systems thus obtained are:

$$H_{\gamma 1} = \frac{Z}{F_z} = H_{55} - \frac{H_{52}H_{11}H_{25}}{H_{11}H_{22} - H_{12}H_{21}} \tag{7.20}$$

$$H_{\gamma 2} = \frac{X}{F_z} = \frac{H_{41}H_{12}H_{25}}{H_{11}H_{22} - H_{12}H_{21}} \tag{7.21}$$

$$H_{\gamma 3} = \frac{X}{F_x} = H_{44} - \frac{H_{41}H_{22}H_{14}}{H_{11}H_{22} - H_{12}H_{21}} \tag{7.22}$$

7.5 Numerical Examples and Discussions

Figure 7.1 shows the transfer functions of a non-rotating tire-wheel system under different boundary conditions. For the system in the non-rotating state, the transfer functions $H_{\alpha 2}, H_{\beta 2}, H_{\beta 3}, H_{\gamma 2}$ are all equal to zero, which means excitations in the vertical direction will not generate any responses in the longitudinal direction and vice versa. Since the transfer function $H_{12} = 0$ for the non-rotating system, the constraint $V = 0$ at the contact patch has no effect on the transfer functions concerning the vertical vibration of the system.

Comparing Figure 7.1 with Figure 6.2 we can see that all the resonant vibration peaks (except for the first one in $H_{\beta 1}$ and the second one in $H_{\gamma 1}$) of the transfer functions in the vertical direction of the constrained tire-wheel system correspond to the *antiresonant* frequencies of the transfer function H_{22} of the corresponding free tire-wheel system. This is in agreement with the experimental findings reported by Potts [77]. The second resonant peak in $H_{\gamma 1}$ is the combined result of the resonance of the transfer function H_{55} and the antiresonance of the transfer function H_{22} of the free system. These two frequencies are very close to each other (see Figure 6.2); therefore only one peak, instead of two separate ones, is visible in $H_{\gamma 1}$.

The resonant peaks of the transfer function $H_{\gamma 3}$ correspond to the antiresonances of the transfer function H_{11} of the free system, which are different from the antiresonances of H_{22}.

We originally expected that the transfer functions under different boundary conditions would exhibit different resonant frequencies. However, the numerical results show that except for the two lowest ones, the transfer functions reach resonant peaks at the same frequencies. This is due to the fact that among the three transfer functions shown here, the first two ($H_{\alpha 1}, H_{\beta 1}$) are defined as axle responses versus vertical displacement input W at the contact point G. The corresponding homogeneous system with W defined as the input variable is that of $W = 0$, which is exactly the boundary condition of the tire-wheel system in Case III ($H_{\gamma 1}$). This also explains why good agreement was found between Soedel's analytical results [88] and the test results of Potts [77], even though the boundary conditions considered were different. However, because the axle was fixed in his analysis, Soedel

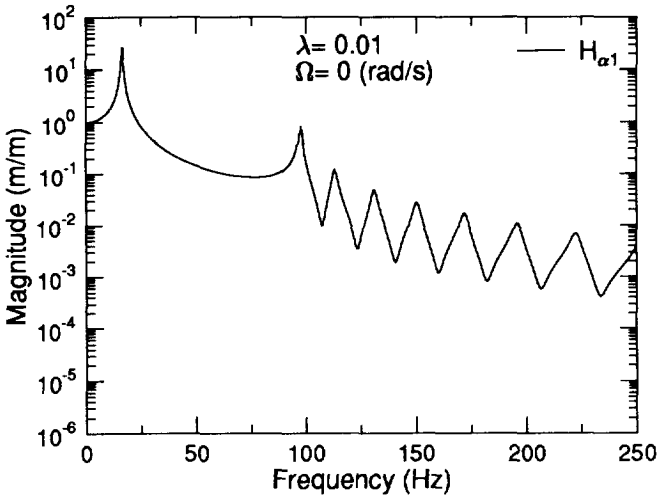

(a) Case I

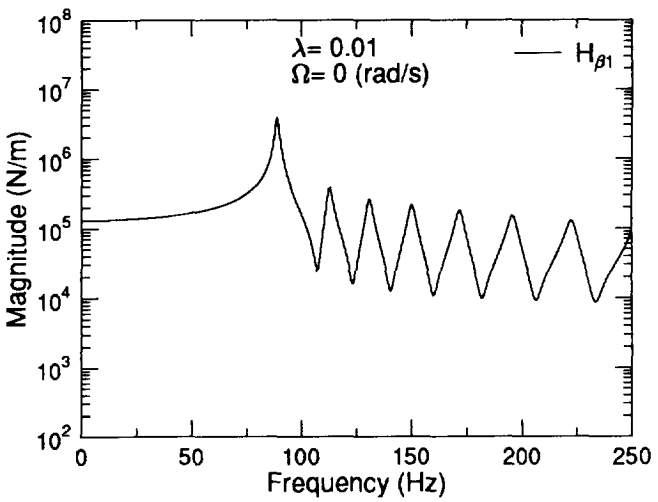

(b) Case II

Figure 7.1: The transfer functions of the non-rotating tire-wheel system under various boundary conditions ($\Omega = 0$) (*cont.*)

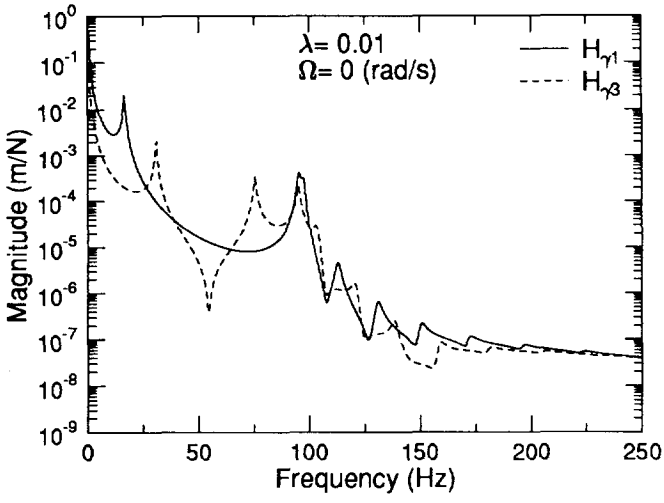

(c) Case III

Figure 7.1 (*cont.*): The transfer functions of the non-rotating tire-wheel system under various boundary conditions ($\Omega = 0$)

did not find the lowest resonant frequency found by Potts. In addition, a discrepancy in the second resonant frequency remains between his analytical and Potts' experimental results.

Comparing $H_{\beta 1}$ with the other three transfer functions in Figure 7.1, we can see that the lowest resonant peak which appears in the other transfer functions is missing from $H_{\beta 1}$; and the second resonant peak (the first for $H_{\beta 1}$) is located at a different frequency for $H_{\beta 1}$ than that for the others. This is because for $H_{\beta 1}$ the wheel axis is fixed and the influence of the wheel mass is thus eliminated from the transfer function. Therefore, in order to get a complete picture of the vibration transmission of tires, it is important to include the DOFs of the wheel mass into the theoretical analysis or laboratory tests on tire vibrations.

The first resonant frequency (typically of the order of 15–20 Hz) corresponds to the mode where the wheel vibrates on the sidewall springs while the tread-band is constrained at the contact point. This resonant frequency is of importance to vehicle dynamics simulations, where the tire is often modeled as a simple spring.

Figure 7.2 shows the transfer functions of the rotating tire-wheel system under constraints. It differs from the non-rotating case in that the resonant peaks of transfer functions in Figure 7.2 do not correspond to the anti-resonances of the free system in general. Instead the resonances correspond to the frequencies at which $H_{11}H_{22} - H_{12}H_{21} = 0$ in Figure 7.2(a), 7.2(c) and $\alpha_{44}\alpha_{55} - \alpha_{45}\alpha_{54} = 0$ in Figure 7.2(b).

7.6 Conclusions and Recommendations

- The vibration transmission properties of a tire-wheel system can be described completely by a set of transfer functions of the free system, from which the vibration properties of tire-wheel systems under various boundary conditions can be derived.

- It is important to include the wheel DOFs into the analyses or tests of tires in order to obtain a complete picture of the vibration transmission properties of tires.

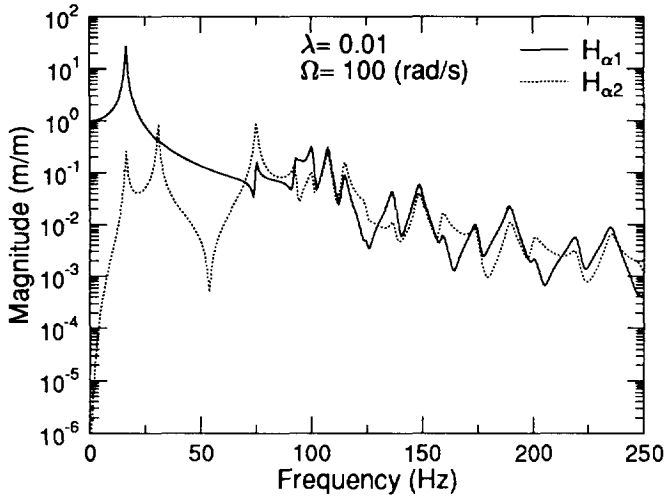

(a) Case I

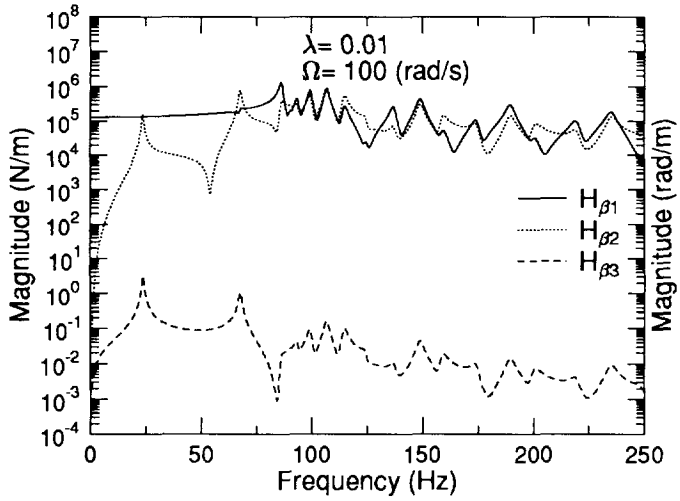

(b) Case II

Figure 7.2: The transfer functions of the rotating tire-wheel system under various boundary conditions ($\Omega = 100$ rad/s) (*cont.*)

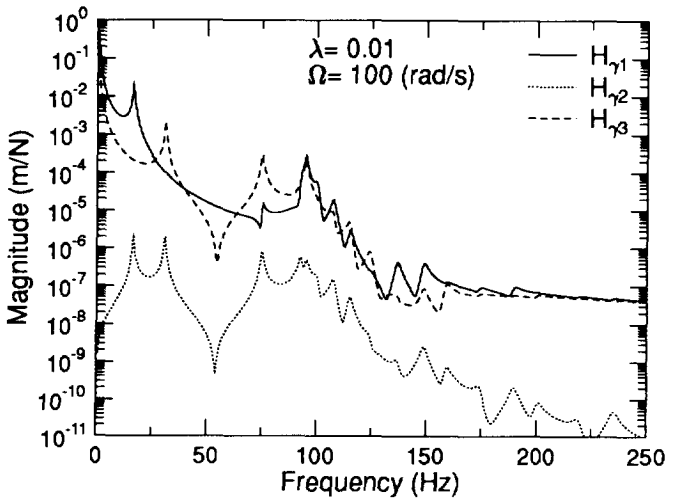

(c) Case III

Figure 7.2 (*cont.*): The transfer functions of the rotating tire-wheel system under various boundary conditions (Ω = 100 rad/s)

- The constraints at the contact point and the axle will affect the vibration properties of a tire-wheel system. However, when the vibration transmission properties of tires are presented in transfer functions under different conditions, they may have the same resonant peaks. Therefore, care should be taken in interpreting and utilizing the results from various vibration tests of tires under different boundary conditions.

- The factor of finite contact should be taken into consideration when dealing with constraints in the longitudinal direction in the contact patch.

- For more realistic f_x to w responses, an extensible ring model (the effective rolling radius r_{eft} not constant) may be needed; and the longitudinal slips and compliance of the tread should be taken into account. In addition, a finite contact length will improve the results at short wavelengths of road profiles.

Chapter 8

Parameter Estimation and Model Validation

The ring model developed in this thesis is an approximation of the real tire. The parameters involved in the ring model are not the exact parameters of a tire. Therefore an accurate estimation of these parameters must be carried out in order for the ring model to best represent a tire. Also, since the model is an approximation of the real tire, it needs to be validated against experimental results.

8.1 Parameter Estimation Methods

The model parameters can be divided into three categories: geometric parameters, stiffness parameters and inertial parameters. The geometric parameters include: the radius R, the width b, the thickness h of the ring, and the thickness τ of the secondary spring. The stiffness parameters include: the stiffness of radial and tangential springs k_w, k_v; the stiffness of the secondary radial spring k_2; and the bending stiffness of the ring EI. The inertial parameters are the density of the ring ρ, the mass of the wheel m and the moment of inertia of the wheel I_r.

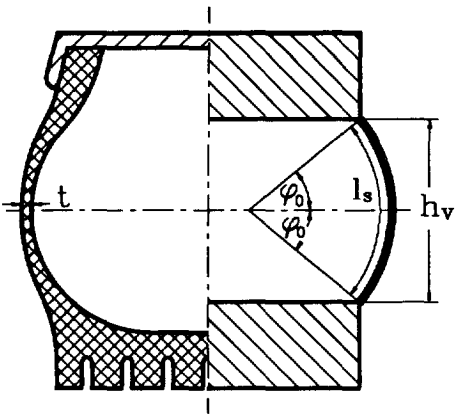

Figure 8.1: Cross section of a tire

The geometric parameters of a tire ring model, the density, and the wheel mass are usually measured or obtained directly according to the tire geometry and materials. Most of the efforts concerning the parameter estimation are concentrated on the stiffness parameters.

Böhm [15] estimated the parameters in his tire ring model largely by means of theoretical analysis. The stiffness of the radial spring was estimated by the following equation by Rotta:

$$k_w = \frac{\cos\phi_0 + \phi_0 \sin\phi_0}{\sin\phi_0 - \phi_0 \cos\phi_0} p_0 \tag{8.1a}$$

The stiffness of the tangential spring was estimated by

$$k_v = \frac{G_r t}{l_s} + p_0 \cot\phi_0 \tag{8.1b}$$

in which p_0 is the tire inflation pressure; ϕ_0 is half of the angle which the tire sidewall arc covers; l_s is the length of the tire sidewall arc; t is the thickness of the tire sidewall; and G_r is the shear modulus of rubber material which surrounds the high modulus cords.

The bending stiffness was calculated by the following equation:

$$EI = \frac{3d^2EA + E_r b t^3}{12} \tag{8.1c}$$

in which E_r is the elastic modulus of the rubber base; d is the thickness of each individual layer of the tire tread belt (the tire consisted of three layers); EA is the membrane stiffness of the ring, which in turn was estimated by

$$EA = E_r \frac{3db}{1-\nu_r^2}\left[1 - \frac{2\nu_r}{\tan^2\beta} + \frac{1}{\tan^4\beta}\right] \tag{8.1d}$$

where ν_r is Poisson's ratio of rubber material; β is the crown angle of tire tread-belt plies. The second term in Equation (8.1c) accounts for the bending stiffness of the rubber layer under the tread-belt plies.

Potts et al. estimated the parameters of their tire model by experimental means [77]. By measuring the natural frequencies of a non-rotating tire and utilizing the characteristic equation of their tire model, they were able to obtain the stiffness parameters.

In a recently published paper, Huang et al. used the following formula to estimate the stiffnesses of radial and tangential springs of a tire ring model [47]:

$$k_w = 2p_0 \frac{1}{\tan\phi_0} \tag{8.2a}$$

$$k_v = 2p_0 \frac{l_s \cos\phi_0}{\phi_0 h_v [1 - h_v/(4R)]} \tag{8.2b}$$

in which R is the radius of the tire treadband.

The bending stiffness of the ring was determined by measuring the natural frequency of the second order mode of the tire belt. By substituting the second order natural frequency and the geometric parameters of the tire belt into the natural frequency equation of a simple ring (a ring without an elastic foundation), the bending stiffness was obtained.

In this chapter, we will estimate the stiffness parameters of the model from the results of tire dynamic tests.

8.2 Tire Tests and Parameter Estimation

8.2.1 Theoretical background

In Chapter 3, the natural frequencies of a tire were obtained from the ring model. Under the in-extensibility assumption, the natural frequencies of a non-rotating tire are:

$$\omega_n = \left\{ \frac{1}{\rho A (1+n^2)} \left[\left[\frac{EI}{R^4} \left(1-n^2\right) - \frac{p_0 b}{R} \right] n^2 \left(1-n^2\right) + k_v + k_w n^2 \right] \right\}^{\frac{1}{2}} \tag{8.3}$$

in which $n = 0, 1, ..., +\infty$ for the tire with a fixed wheel ($x = z = \theta_r = 0$).

The geometric parameters and mass density of the model can be estimated directly from the tire structure. The only parameters which need to be determined from measurements are the bending stiffness EI and the radial and tangential spring stiffness k_w, k_v. If three natural frequencies of the tire are known, then the stiffness parameters can be obtained from the above equation.

8.2.2 Tire tests

Dynamic tests are performed on a Pirelli P4 175/70R13 tire, for the purposes of both parameter estimation and model validation. The tire tests are carried out in two different configurations: one with the tire mounted on a fixed wheel, the other with the entire tire-wheel system suspended in the air so that the wheel can move freely in either rotational or translational direction. In the latter case, two different wheels are used: one is a heavy steel wheel; the other is a light alloy wheel. Both wheels do not have any resonant frequency under 250 Hz in the radial and tangential directions. The tire is inflated to $2 \times 10^5 \mathrm{N/m^2}$ (two bars) for the tests.

The tire is excited by an impulse force generated by a hammer hitting the tire tread surface. The acceleration responses in both radial and tangential directions at different locations along the tire circumference are measured. In this way the mode shapes and natural frequencies are obtained. For details

Table 8.1: Natural frequencies ω_n of a Pirelli P4 175/70R13 tire with and without wheel DOFs ($\Omega = 0$)

n	without Wheel DOFs (Hz)	with Wheel DOFs (Hz)	
		heavy wheel	light wheel
0	69	97	143
1	89	97	124
2	112	112	112
3	134	134	134
4	159	159	159
5	186	186	186
6	216	216	216

of the tire modal tests, please refer to Reference [84].

From the tire tests, natural frequencies and mode shapes up to the sixth order are obtained. The measured natural frequencies are listed in Table 8.1.

8.2.3 Parameter estimation

The geometric parameters and inertial parameters are estimated directly according to the tire structure. They are listed in Table 8.2. The zeroth, fifth and sixth order natural frequencies measured under the fixed wheel configuration are used for the estimation of the three stiffness parameters. By utilizing Equation (8.3), the stiffness parameters are obtained, as listed in Table 8.3.

8.3 Validation of the Model

The tire model developed in this thesis is validated from the following three aspects:

Table 8.2: Geometric and inertial parameters for a Pirelli P4 175/70R13 tire

Parameter	Unit	Value
radius R	m	0.280
width b	m	0.130
density ρA	kg/m	2.500
total mass of the tire m_t	kg	6.900
mass of the heavy steel wheel m	kg	24.900
moment of inertia of the steel wheel I_r	kg·m^2	0.319
mass of the light alloy wheel m	kg	3.550
moment of inertia of the alloy wheel I_r	kg·m^2	0.045

Table 8.3: Stiffness parameters for a Pirelli P4 175/70R13 tire ($p_0 = 2 \times 10^5 \mathrm{N/m^2}$)

Parameter	Unit	Value
bending stiffness EI	N·m^2	1.571
radial spring stiffness k_w	N/m^2	1.156×10^6
tangential spring stiffness k_v	N/m^2	4.699×10^5

Table 8.4: Natural frequencies of the Pirelli tire with a fixed wheel as measured in tests and calculated from the model

n	measured (Hz)	calculated (Hz)	error %
0	69	—	—
1	89	90.8	2.02
2	112	112.3	0.27
3	134	134.0	0.00
4	159	158.6	0.25
5	186	—	—
6	216	—	—

- The natural frequencies of the tire with a fixed wheel;
- The frequencies of the free tire-wheel system;
- The mode shapes of the tire.

Table 8.4 lists the measured and calculated natural frequencies of the Pirelli tire with a fixed wheel. The error percentage of the natural frequencies calculated from the tire model is also shown in the table. Since the natural frequencies of the zeroth, fifth and sixth order modes were used to obtain the model parameters, there are no theoretical natural frequencies available for these modes. It can be seen that the tire model gives a very good prediction of the natural frequencies of the tire. Figure 8.2 shows graphically the measured and calculated natural frequencies of the tire with a fixed wheel.

Comparing the experimental results of the tire with a fixed wheel and a free wheel in Table 8.1, we find that only the zeroth and first order natural frequencies are different for these two different configurations, while the other natural frequencies remain the same in these two cases. Also, in the free wheel case, different natural frequencies of the zeroth and first order are obtained when different wheels are used. These experimental findings prove the analytical conclusions in Chapter 3.

The zeroth and first order natural frequencies of the free tire-wheel system are also calculated from the tire model using the parameters obtained in

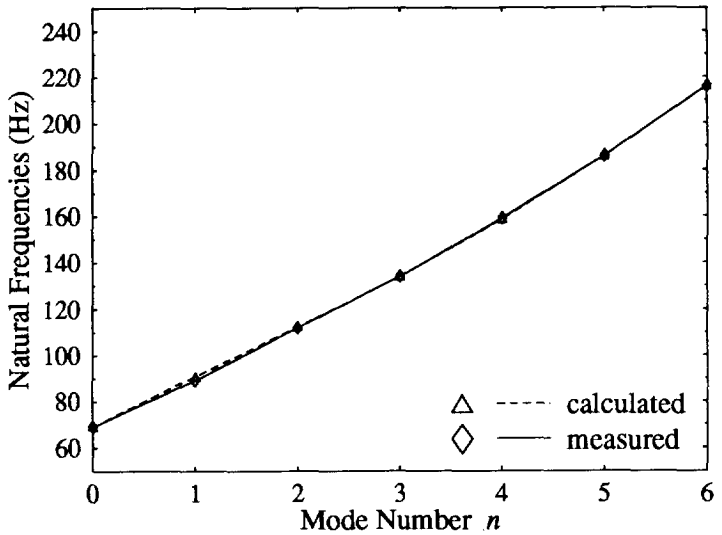

Figure 8.2: The comparison of theoretical and experimental natural frequencies of the Pirelli tire with a fixed wheel

the previous section. The theoretical results are listed together with the experimental ones in Table 8.5 for both the heavy and light wheels.

It is observed that for the tire with a heavy steel wheel, the calculated natural frequencies are quite close to the measured ones. However, in the case of the light wheel, a large discrepancy exists between the theoretical and experimental results.

Table 8.5: The zeroth and first order natural frequencies of the free tire-wheel system as measured in tests and calculated from the model

	n	measured (Hz)	calculated (Hz)	error %
heavy wheel	0	97	99.6	2.68
	1	97	98.4	1.44
light wheel	0	143	202.2	40.40
	1	124	135.8	9.52

Table 8.6: The zeroth and first order natural frequencies of the free tire-wheel system calculated using the modified wheel parameters

	n	frequency (Hz)	error %
heavy wheel	0	95.1	1.96
	1	97.8	0.82
light wheel	0	140.6	1.68
	1	119.3	3.79

This disagreement between the theoretical and experimental results is due to the fact that in calculating the natural frequencies, only the mass and moment of inertia of the wheel itself are used. However, for the free tire-wheel system, part of the tire sidewall (especially the beads) will move together with the wheel; thus its mass and moment of inertia should be taken into account in the model. The mass m and moment of inertia I_r of the model therefore should be modified to accommodate the sidewall effect. The following simple relations can be used for this purpose.

$$I_r' = I_r + (m_t - 2\pi R\rho A)R_r^2 \tag{8.4}$$

$$m' = m + (m_t - 2\pi R\rho A) \tag{8.5}$$

in which m_t is the total mass of the tire; R_r is the radius of the wheel.

The natural frequencies calculated from the tire model using the modified wheel parameters are listed in Table 8.6. It can be seen that the theoretical results now agree very well with the experimental ones for both the heavy and light wheels. In the case of the heavy wheel, this modification in wheel parameters did not change the results very much, since the sidewall effect is very small compared with the heavy wheel itself. However, in the case of the light wheel, the mass of part of the sidewall moving together with the wheel is quite substantial considering the light wheel mass; thus modifying m and I_r in the model leads to a dramatic improvement of the theoretical results.

The mode shapes obtained from the dynamic tests of the tire with a fixed wheel are shown in Figure 8.3. It is obvious that the results agree very well with the theoretical ones in Chapter 3.

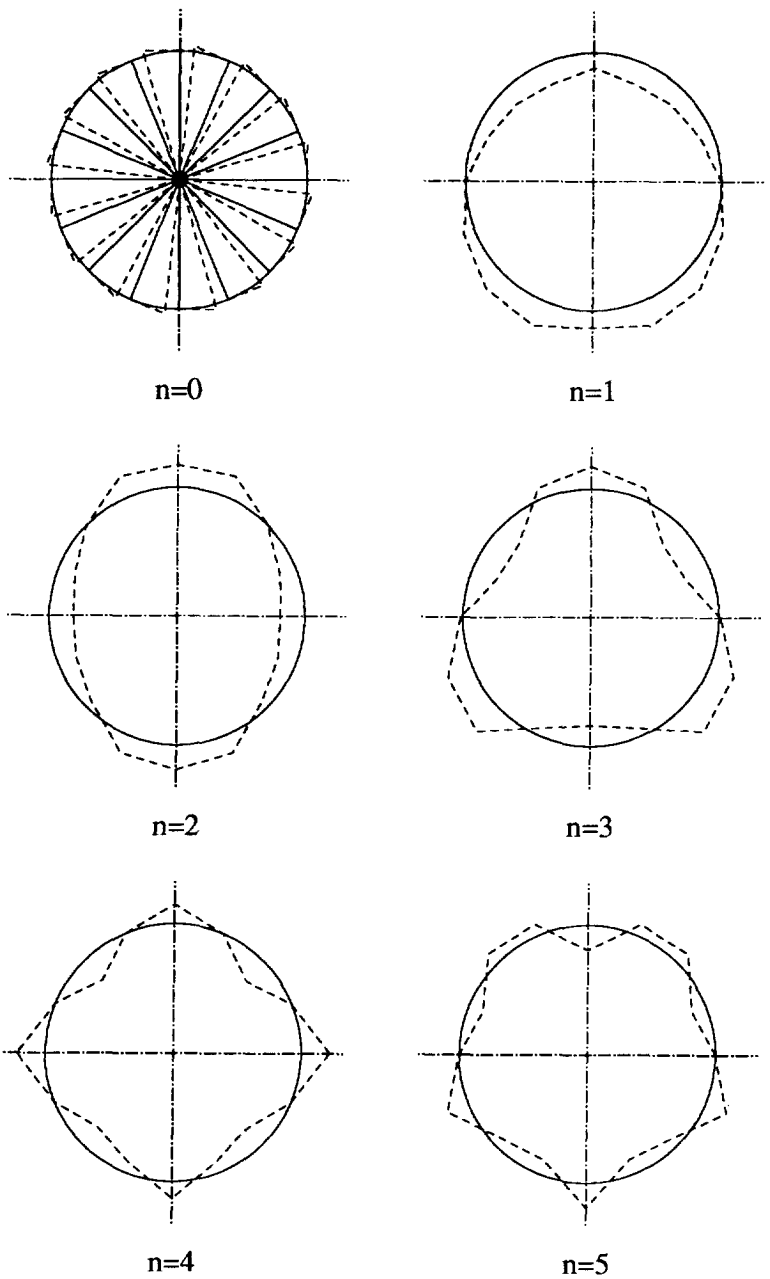

Figure 8.3: The measured mode shapes of the Pirelli tire with a fixed wheel

8.4 Conclusions

In this chapter, the model parameters of a Pirelli tire have been obtained. The stiffness parameters were estimated from three natural frequencies measured from tire modal tests with a fixed wheel. The natural frequencies calculated from the tire model using the estimated parameters were compared with the experimental results, which showed good agreement between the model and test results. Also, the theoretical analysis on the influences of the wheel DOFs in Chapter 3 has been verified by the dynamic tests of the tire with both a fixed wheel and a free wheel. It has been shown that for a free tire-wheel system, modification on the mass and moment of inertia of the wheel in the model is necessary when the wheel is light in order to take into account the contribution of the sidewall mass. Finally, the measured mode shapes of the tire were presented. Again, the measured mode shapes agreed very well with the theoretical mode shapes.

Chapter 9

Conclusions and Recommendations

9.1 Contributions of This Thesis

In this thesis, a tire ring model has been developed which is suitable for the study of the in-plane dynamics of tires. The equations of motion of the tire model have been derived. It has been demonstrated that the model is capable of dealing with all three aspects of the in-plane dynamics of tires, namely, the treadband vibration, the rolling contact with the road, and the vibration transmission from the road surface to the wheel axle. It has also been shown in this thesis that with the use of the modal expansion method, the application of the model can be greatly simplified. With the wheel axle free to move in the vertical, longitudinal as well as rotational directions in the wheel plane, the model can be readily applied to study the vibration transmission from the road to the vehicle.

The vibrational properties of the tire model have been studied in detail in Chapter 3. It has been found that the extensional stiffness of the ring, i.e., the tire treadband, mainly influences the vibration modes at very high frequencies. For many practical problems of tire in-plane dynamics, the ring can be assumed to be in-extensible. It has also been found that the sidewall

stiffness (thus the inflation pressure) has a profound influence on the natural frequencies of tires.

Because of rotation, the vibration modes of a tire are complex. The space and time coordinates thus cannot be decoupled from each other in the conventional way in the real domain. Therefore the concept of time dependent modes [44] can be adopted for such rotating systems. Another effect of the tire rotation is the so-called *bifurcation* (doubling) of natural frequencies of modes of the same order.

The DOFs of the wheel axle influence only the zeroth and first order vibration modes of the tire-wheel system. In other words, the difference in natural frequencies of a tire with a fixed and free wheel is limited only to the zeroth and first order modes. The natural frequencies of higher order modes are identical in these two cases. This theoretical finding has been confirmed by laboratory tests of tires.

In Chapter 5 the ring model has been applied to the study of the rolling contact problem between the tire and the flat road. Secondary radial springs representing the tire tread elements were added to the tire model in order to take into account the compliance of the tread elements in the contact patch. Based on the modified ring model and the modal expansion method, a new approach has been developed for the study of the contact problem. This approach differs from conventional ones in that the tire is treated as one entity instead of being divided into different regions, thus eliminating the need to solve the equations of motion for different regions and to apply continuity conditions at the boundaries of these regions. The numerical results have shown that the new method can be used successfully to predict the contact pressure distribution in the tire-road contact patch. Using this tire model and the new method, different characteristic shapes of contact pressure distribution have been predicted for tires under different inflation pressure and vertical static loads. The results showed qualitative agreement with measurements reported in the literature.

The ring model has also been used to study the vibration transmission properties of tires. The transfer functions between any two points of a free tire-wheel system have been derived. It has been found that due to the coriolis forces, the transfer function matrix between the wheel and the contact point on the treadband is in general asymmetric for a free, rotating tire-

wheel system. Due to the periodic nature of the mode shapes of the tire, resonance occurs only at the frequency of either the zeroth or the first order natural mode in each of the transfer functions related to the wheel motion. This finding provides theoretical ground for further simplification of the tire model aimed at the study of vibration transmissions in the low and medium frequency range.

In Chapter 7, different configurations of tire-wheel systems on vehicles and in laboratory tests have been discussed and the corresponding mathematical expressions of the boundary conditions were formulated. The appropriate boundary conditions are then applied to the free tire-wheel system. The transfer functions of the tire-wheel system under various boundary conditions were thus obtained from the transfer functions of the corresponding free system. Hence the vibration transmission properties of a tire-wheel system can be described completely by a basic set of transfer functions of the free system. It is therefore important to include the wheel DOFs into the analyses or tests of tires in order to obtain a complete picture of the vibration transmission properties of tires.

The tire ring model has been validated by experimental modal analysis carried out on a test tire. Good agreement has been found between the analytical and experimental results of the natural frequencies and mode shapes. The experimental results of the tire with a fixed wheel and with free wheels of different weights confirm the predictions of the theoretical analysis in Chapter 3 concerning the influences of the wheel DOFs on the natural frequencies of the tire-wheel system.

9.2 Recommendations for Further Research

There are many issues deserving further investigation on the subject of this thesis. Having said that, we would like to point out only a few of them which deserve special attention.

The tire model developed in this thesis considers the sidewall as radial and tangential springs with linear stiffness characteristics. In reality, the stiffness of the tire sidewall is non-linear [69]. This non-linearity of tire sidewall

stiffnesses does not normally pose a major problem for the study of small vibration where the amplitudes of the tire deformation are usually small and can be linearized. However, differentiation should be made between a tire with a static preload and one without preload. Due to the non-linearity, the static preload on the tire will change the values of the sidewall stiffnesses, although the linear model will still be valid. Therefore, efforts should be made to determine the influences of preloads on the tire dynamic characteristics.

In dealing with the tire-road contact problem, only the freely rolling tire is studied in this thesis. The method developed in Chapter 5 can be extended so that it can also be used for the contact problems of a braking or driving tire. Two issues have to be addressed in order to achieve that. First a tire-road interface model has to be developed to determine the relationship between the longitudinal force and the displacement of the tread element in the contact area. For this purpose the brush-type model may be used. Secondly the compatibility conditions between the tire and the road should also include that for the tangential displacement of the tire tread element, unlike the present case which considers the radial displacement only. Also, the non-linear characteristics of the sidewall stiffnesses may be needed for large tire deformation.

The study of the vibration transmission between the contact patch and the wheel axle could be extended to consider finite contact between the tire and the road. As a first step, the case of a single continuous region of contact may be considered. The tire can be considered to be in contact with the road at several points where the road irregularity generates displacement inputs to the tire. The transfer functions obtained in Section 6.3 are valid and can be used for this extension. More complicated situations such as multiple contact patches between the tire and the road can be considered at a later stage. By considering the finite contact between the tire and the road, more realistic boundary conditions at the contact patch can also be applied, especially in the longitudinal direction.

Ideally, a universal tire-road interface model should be established. This interface model should be common to tires of all types and sizes and can have arbitrary road profile as input. Two steps must be taken in order to establish such an interface model. First the geometric relations have to be established between the road profile, the tire-wheel motion and the

treadband displacements in the contact area. Secondly, relations between the force at the interface and the relative displacements have to be obtained. The tire-road interface model can then be combined or integrated with the tire ring model to calculate the complete dynamic properties of a wheel-tire-road system. The compliance of tire tread elements can be taken into account in the interface model.

9.3 Concluding Remarks

The studies reported in this thesis attempt to gain a better understanding of the in-plane dynamics of tires. The approach taken here is to study separately the basic properties of tire-wheel systems and the interaction between the tire and the road. The compelling reasons for taking this approach are: 1). A tire operates under different road conditions; and 2). Different tires may be operating on the same road. By separating the tire and the tire-road interface, a tire model can be used with several different interface models and a tire-road interface model can be used for different tires. In this way, the modeling of the vehicle-tire-road system can be greatly simplified. This thesis is the first effort in this direction. Much remains to be done.

Bibliography

[1] Akasaka, T., Katoh, M., Nihei, S., and Hiraiwa, M., Two-dimensional contact pressure distribution of a radial tire, *Tire Science and Technology, TSTCA*, 18(2):80–103, 1990.

[2] Allaei, D., Soedel, W., and Yang, T. Y., Natural frequencies and modes of rings that deviate from perfect axisymmetry, *Journal of Sound and Vibration*, 111(1):9–27, 1986.

[3] Ames, W. F., Waves in tires, *Textile Research Journal*, 40:498–507, 1970.

[4] Bachrach, B. I. and Rivin, E., Pneumatic damping of vehicle tires to improve ride quality, SAE Paper No. 840746, 1984.

[5] Badalamenti, J. M. and Doyle, Jr., G. R., Radial-interradial spring tire models, *Journal of Vibration, Acoustics, Stress, and Reliability in Design*, 110(1):70–75, 1988.

[6] Bandel, P. and Monguzzi, C., Simulation model of the dynamic behavior of a tire running over an obstacle, *Tire Science and Technology, TSTCA*, 16(2):62–77, 1988.

[7] Barkwell, L. and Lancaster, P., Overdamped and gyroscopic vibrating systems, *Journal of Applied Mechanics*, 59:176–181, 1992.

[8] Barone, M. R., Impact vibrations of rolling tires, SAE Paper No. 770612, 1977.

[9] Barson, C. W., Gough, V. E., Hutchinson, J. C., and James, D. H., Tyre and vehicle vibration, in *Proceedings of Institution of Mechanical Engineers*, volume 179 (Part 2A), pp. 213–237, 1964–1965.

[10] Barson, C. W., James, D. H., and Morcombe, A. W., Some aspects of tyre and vehicle vibration testing, in *Proceedings of Institution of Mechanical Engineers*, volume 182 (Part 3B), pp. 32–42, 1967–1968.

[11] Barson, C. W. and Dodd, A. M., Vibrational characteristics of tyres, in *Vibration and Noise in Motor Vehicles*, Automobile Division of the Institution of Mechanical Engineers, 1972.

[12] Bert, C. W. and Chen, T. L. C., On vibration of a thick flexible ring rotating at high speed, *Journal of Sound and Vibration*, 61(4):517–530, 1978.

[13] Bickford, W. B. and Reddy, E. S., On the in-plane vibrations of rotating rings, *Journal of Sound and Vibration*, 101(1):13–22, 1985.

[14] Bickford, W. B. and Maganty, S. P., On the out-of-plane vibrations of thick rotating rings, *Journal of Sound and Vibration*, 110(1):121–127, 1986.

[15] Böhm, F., Mechanik des Gürtelreifens, *Ingenieur Archiv*, 35:82–101, 1966.

[16] Böhm, F., Zur Statik und Dynamik des Gürtelreifens, *Automobiltechnische Zeitschrift*, 69(8):255–261, 1967.

[17] Böhm, F., Models for the radial tire for high frequency rolling contact, in *The Dynamics of Vehicles on Roads and on Tracks, Proceedings of the 11th IAVSD symposium*, pp. 72–83, Kingston, Canada, 1989.

[18] Böhm, F., Dynamic behavior of radial tires, Private communication, 1992.

[19] Captain, K. M., Boghani, A. B., and Wormley, D. N., Analytical tire models for dynamic vehicle simulation, *Vehicle System Dynamics*, 8(1):1–32, 1979.

[20] Chang, Y. B., Yang, T. Y., and Soedel, W., Dynamic analysis of a radial tire by finite elements and modal expansion, *Journal of Sound and Vibration*, 96(1):1–11, 1984.

[21] Chiesa, A., Oberto, L., and Tamburini, L., Transmission of tyre vibrations, *Automobile Engineer*, pp. 520–530, 1964.

[22] Chiesa, A., Vibrational performance differences between tires with cross-biased plies and radial plies, SAE Paper No. 990B, 1965.

[23] Clark, S. K., The rolling tire under load, SAE Paper No. 650493, 1965.

[24] Clark, S. K., *Mechanics of Pneumatic Tires*, National Bureau of Standards, Monograph 122, Washington, D. C., 1971.

[25] Davis, D. C., A radial-spring terrain-enveloping tire model, *Vehicle System Dynamics*, 4(1):55–69, 1975.

[26] DeEskinazi, J., Soedel, W., and Yang, T. Y., Contact of an inflated toroidal membrane with a flat surface as an approach to the tire deflection problem, *Tire Science and Technology, TSTCA*, 3(1):43–61, 1975.

[27] Deneuvy, A. C., Modal analysis of a pneumatic tyre and dynamic simulation by a substructuring method, in *Proceedings of the 7th International Modal Analysis Conference*, Vol. II, Las Vegas, Nevada, 1989.

[28] Dodge, R. N., The dynamic stiffness of a pneumatic tire model, SAE Paper No. 650491, 1965.

[29] Dovstam, K. and Nilsson, N., Influence from coriolis and centripetal accelerations on in-service tire vibrations, Technical Report 6.371.01, IFM Akustikbyran AB, 1981.

[30] Dunn, J. W. and Mills, B., An instrumentation system for the analysis of the forced vibration characteristics of stationary and rolling tyres, in *Proceedings of the Dynamic Testing Symposium*, The Society of Enviromental Engineers, London, 1971.

[31] Dunn, J. W. and Olatunbosun, O. A., A new electro-hydraulic triaxial tyre test facility for low-frequency rolling tyre dynamics, *International Journal of Vehicle Design*, 9(2):242–251, 1988.

[32] Dunn, J. W. and Olatunbosun, O. A., Linear and non-linear modelling of vehicle rolling tyre low frequency dynamic behaviour, in *The Dynamics of Vehicles on Roads and on Tracks, Proceedings of the 11th IAVSD symposium*, pp. 179–189, Kingston, Canada, 1989.

[33] Endo, M., Hatamura, K., Sakata, M., and Taniguchi, O., Flexural vibration of a thin rotating ring, *Journal of Sound and Vibration*, 92(2):261–272, 1984.

[34] Ewins, D. J., *Modal Testing: Theory and Practice*, Research Studies Press LTD., 1984.

[35] Fiala, E. and Willumeit, H. -P., Radiale Schwingungen von Gürtel-Radialreifen, *Automobiltechnische Zeitschrift*, 68(2):33–38, 1966.

[36] Gong, S., Tire ring models—literature review, Technical Report 89.3.VT.2662, Vehicle Research Laboratory, Faculty of Mechanical Engineering and Marine Technology, Delft University of Technology, 1989.

[37] Gong, S., A comparison of vibrational properties of various tire ring models, Technical Report 89.3.VT.2663, Vehicle Research Laboratory, Faculty of Mechanical Engineering and Marine Technology, Delft University of Technology, 1989.

[38] Gong, S., The development of a ring model for the study of tire in-plane dynamics, Technical Report MEMT 20 (ISBN 90-370-0062-2), Faculty of Mechanical Engineering and Marine Technology, Delft University of Technology, 1992.

[39] Gong, S., Rolling contact between a tire and a flat road, Technical Report, Vehicle Research Laboratory, Faculty of Mechanical Engineering and Marine Technology, Delft University of Technology, 1992.

[40] Gong, S., Savkoor, A. R., and Pacejka, H. B., The influence of boundary conditions on the vibration transmission properties of tires, SAE Paper No. 931280, 1993.

[41] Hawkings, D. L., A generalized analysis of the vibration of circular rings, *Journal of Sound and Vibration*, 54(1):67–74, 1977.

[42] Hirano, M. and Akasaka, T., Natural frequencies of the bias tire, *Tire Science and Technology, TSTCA*, 4(2):86–114, 1976.

[43] Hooker, R. J., A model for the radial dynamic behaviour of pneumatic tyres, *International Journal of Vehicle Design*, 1(4):361–372, 1980.

[44] Huang, S. C. and Soedel, W., Effects of coriolis acceleration on the free and forced in-plane vibrations of rotating rings on elastic foundation, *Journal of Sound and Vibration*, 115(2):253–274, 1987.

[45] Huang, S. C. and Soedel, W., Response of rotating rings to harmonic and periodic loading and comparison with the inverted problem, *Journal of Sound and Vibration*, 118(2):253–270, 1987.

[46] Huang, S. C., The vibration of rolling tyres in ground contact, *International Journal of Vehicle Design*, 13(1):78–95, 1992.

[47] Huang, S. C. and Su, C. K., In-plane dynamics of tires on the road based on an experimentally verified rolling ring model, *Vehicle System Dynamics*, 21(4):247–267, 1992.

[48] Hunckler, C. J., Yang, T. Y., and Soedel, W., A geometrically nonlinear shell finite element for tire vibration analysis, *Computers and Structures*, 17(2):217–225, 1983.

[49] Irie, T., Yamada, G., and Koizumi, H., The steady state out-of-plane response of an internally damped ring supported by springs in some bays, *Journal of Sound and Vibration*, 81(2):187–197, 1982.

[50] Jenkins, J. T., The circumferential contact problem for the belted radial passenger car tire, *Vehicle System Dynamics*, 11:325–343, 1982.

[51] Kao, B., Riesner, M., and Surulinarayanasami, P., Modal analysis of a tire and wheel and its application for vehicle ride evaluation, SAE Paper No. 860826, 1986.

[52] Kao, B. G., Kuo, E. Y., Adelberg, M. L., et al., A new tire model for vehicle NVH analysis, SAE Paper No. 870424, 1987.

[53] Kilner, J. R., Pneumatic tire model for aircraft simulation, *Journal of Aircraft*, 19(10):851–857, 1982.

[54] Klamp, W. K. and Milligan, W. J., Performance characteristics—radial ply tires, SAE Paper No. 670471, 1967.

[55] Kobiki, Y., Kinoshita, A., and Yamada, H., Analysis of interior booming noise caused by tyre and powertrain-suspension system vibration, *International Journal of Vehicle Design*, 11(3):303–313, 1990.

[56] Koutny, F., A method for computing the radial deformation characteristics of belted tires, *Tire Science and Technology, TSTCA*, 4(3):190–212, 1976.

[57] Koutny, F., Air volume energy method in theory of tyres, *International Polymer Science and Technology*, 5(8):101–105, 1978.

[58] Koutny, F., Load-deflection curves for radial tyres, *Applied Mathematical Modelling*, 5:422–427, 1981.

[59] Kung, L. E., Soedel, W., Yang, T. Y., and Charek, L. T., Natural frequencies and mode shapes of an automotive tire with interpretation and classification using 3-d computer graphics, *Journal of Sound and Vibration*, 102(3):329–346, 1985.

[60] Kung, L. E., Soedel, W., and Yang, T. Y., Free vibration of a pneumatic tire-wheel unit using a ring on an elastic foundation and a finite element model, *Journal of Sound and Vibration*, 107(2):181–194, 1986.

[61] Kung, L. E., Soedel, W., and Yang, T. Y., On the dynamic response at the wheel axle of a pneumatic tire, *Journal of Sound and Vibration*, 107(2):195–213, 1987.

[62] Kung, L. E., Soedel, W., and Yang, T. Y., On the vibration transmission of a rolling tire on a suspension system due to periodic tread excitation, *Journal of Sound and Vibration*, 115(1):37–63, 1987.

[63] Lippmann, S. A. and Nanny, J. D., A quantitative analysis of the enveloping forces of passenger tires, SAE Paper No. 670174, 1967.

[64] Lippmann, S. A., Effects of tire structure and operating conditions on the distribution of stress between the tread and the road, in M. G. Pottinger and T. J. Yager, editors, *The Tire Pavement Interface, ASTP STP 929*, American Society for Testing and Materials, Philadelphia, 1986.

[65] Meirovitch, L., A new method of solution of the eigenvalue problem for gyroscopic systems, *AIAA Journal*, 12(10):1337–1342, 1974.

[66] Meirovitch, L., A modal analysis for the response of linear gyroscopic systems, *Journal of Applied Mechanics*, 42:446–450, 1975.

[67] Mills, B. and Dunn, J. W., The mechanical mobility of rolling tires, in *Vibration and Noise in Motor Vehicles*, Automobile Division of the Institution of Mechanical Engineers, 1972.

[68] Olatunbosun, O. A. and Dunn, J. W., Generalized representation of the low frequency radial dynamic parameters of rolling tyres, *International Journal of Vehicle Design*, 12(5/6):513–524, 1991.

[69] Pacejka, H. B., Analysis of tire properties, in S. K. Clark, editor, *Mechanics of Pneumatic Tires*, Chapter 9, U. S. Goverment Printing Office, Washington, D. C., 1981.

[70] Pacejka, H. B., *Modelling of the Pneumatic Tyre and Its Impact on Vehicle Dynamic Behaviour*, Lecture Note, Delft University of Technology, Delft, 1988.

[71] Padovan, J., On viscoelasticity and standing waves in tires, *Tire Science and Technology, TSTCA*, 4(4):233–246, 1976.

[72] Padovan, J., On standing waves in tires, *Tire Science and Technology, TSTCA*, 5(2):83–101, 1977.

[73] Pottinger, M. G., Thomas, R. A., and Naghshineh, K., Stiffness properties of agricultural tires, in *Proceedings of the International Conference on Soil Dynamics*, American Society for Testing and Materials, Auburn, AL, 1985.

[74] Pottinger, M. G., Marshall, K. D., Lawther, J. M., and Thrasher, D. B., A review of tire/pavement interaction induced noise and vibration, in M. G. Pottinger and T. J. Yager, editors, *The Tire Pavement Interface, ASTP STP 929*, American Society for Testing and Materials, Philadelphia, 1986.

[75] Potts, G. R., Application of holography to the study of tire vibration, *Tire Science and Technology, TSTCA*, 1(3):255–266, 1973.

[76] Potts, G. R. and Csora, T. T., Tire vibration studies: The state of the art, *Tire Science and Technology, TSTCA*, 3(3):196–210, 1975.

[77] Potts, G. R., Bell, C. A., Charek, L. T., and Roy, T. K., Tire vibrations, *Tire Science and Technology, TSTCA*, 5(4):202–225, 1977.

[78] Rasmussen, R. E. and Cortese, A. D., Dynamic spring rate performance of rolling tires, SAE Paper No. 680408, 1968.

[79] Reddy, E. S. and Bickford, W. B., On the in-plane vibrations of rotating rings with equi-spaced spokes, *Journal of Sound and Vibration*, 103(4):533–544, 1985.

[80] Richards, T. R., Brown, J. E., Hohman, R. L., and Sundaram, S. V., Modal analysis of tires relevant to vehicle system dynamics, 3rd International Modal Analysis Conference, 1985.

[81] Richards, T. R., Charek, L. T., and Scavuzzo, R. W., The effect of spindle & patch boundary conditions on tire vibration modes, SAE Paper No. 860243, 1986.

[82] Rosenberg, R. M., *Analytical Dynamics of Discrete Systems*, Plenum Press, New York, 1977.

[83] Saigal, S., Yang, T. Y., Kim, H. W., and Soedel, W., Free vibrations of a tire as a toroidal membrane, *Journal of Sound and Vibration*, 107(1):71–82, 1984.

[84] Savkoor, A. R. and Fejes, I., Experimental modal analysis of in-plane and anti-plane vibration of pneumatic tyres, Technical Report 93.3.VT.4201, Vehicle Research Laboratory, Faculty of Mechanical Engineering and Marine Technology, Delft University of Technology, 1993.

[85] Scavuzzo, R. W., Richards, T. R., and Charek, L. T., Tire vibration modes and effects on vehicle ride quality, *Tire Science and Technology, TSTCA*, 21(1):23–39, 1993.

[86] Soedel, W., On the dynamic response of rolling tires according to thin shell approximations, *Journal of Sound and Vibration*, 41(2):233–246, 1975.

[87] Soedel, W., A new frequency formula for closed circular cylindrical shells for a large variety of boundary conditions, *Journal of Sound and Vibration*, 70(3):309–317, 1980.

[88] Soedel, W. and Prasad, M. G., Calculation of natural frequencies and modes of tires in road contact utilizing eigenvalues of the axisymmetric non-contacting tire, *Journal of Sound and Vibration*, 70(4):573–584, 1980.

[89] Soedel, W., *Vibrations of Shells and Plates*, Marcel Dekker, Inc., New York, 1981.

[90] Springer, H., Ecker, H., and Slibar, A., A new analytical model to investigate transient rolling conditions of a steel-belted tire, in *The*

Dynamics of Vehicles on Roads and on Tracks, Proceedings of the 10th IAVSD Symposium, Prague, Czechoslovakia, 1987.

[91] Sundaram, S. V., Hohman, R. L., and Richards, T. R., Vibration modes of a tire using MSC/NASTRAN, MSC/NASTRAN User's Conference, 1985.

[92] Takahashi, F., Watanabe, G., Nakada, M., et al., Tyre/suspension system modelling for investigation of road noise characteristics, *International Journal of Vehicle Design*, 8(4–6):588–597, 1987.

[93] Tielking, J. T., Plane vibration characteristics of a pneumatic tire model, SAE Paper No. 650492, 1965.

[94] Timoshenko, S. and Young, D. H., *Advanced Dynamics*, McGraw-Hill Book Company, Inc., New York, 1948.

[95] Ushijima, T. and Takayama, M., Modal analysis of tire and system simulation, SAE Paper No. 880585, 1988.

[96] Vinesse, E., Tyre vibration testing: From modal analysis to dispersion relations, in *Proceedings of the 18th ISATA Conference*, Florence, Italy, 1988.

[97] Vinesse, E. and Nicollet, H., Surface waves on the rotating tyre: An application of functional analysis, *Journal of Sound and Vibration*, 126(1):85–96, 1988.

[98] Vinesse, E., Three problems of tire vibration: A unifying approach, in *Proceedings of the International Symposium on Advanced Vehicle Control*, Yokohama, Japan, 1992.

[99] Yamagishi, K. and Jenkins, J. T., The circumferential contact problem for the belted radial tire, *Journal of Applied Mechanics*, 47:513–518, 1980.

[100] Yamagishi, K. and Jenkins, J. T., Singular perturbation solutions of the circumferential contact problem for the belted radial truck and bus tire, *Journal of Applied Mechanics*, 47:519–524, 1980.

[101] Zegelaar, P. W. A., Gong, S., and Pacejka, H. B., Tyre models for the study of in-plane dynamics, in *The Dynamics of Vehicles on Roads and on Tracks, Proceedings of the 13th IAVSD Symposium*, Chengdu, China, 1993.

[102] Zorowski, C. F., Mathematical prediction of dynamic tire behavior, *Tire Science and Technology, TSTCA*, 1(1):99–117, 1973.

[103] Zu, J. W.-Z. and Han, R. P. S., Natural frequencies and normal modes of a spinning Timoshenko beam with general boundary conditions, *Journal of Applied Mechanics*, 59:S197–S204, 1992.

Appendix A

Strain-Displacement Relations

Figure A.1 shows the locations of two neighboring points on the ring before deformation (**A** and **B**) and after deformation (**A'** and **B'**) in a polar coordinate system. The location of point **A** before deformation is defined by a set of polar coordinates (θ, r); the location of point **B** is thus defined by $(\theta + d\theta, r + dr)$.

The infinitesimal distance between points **A** and **B** is

$$(ds)^2 = (d\theta)^2 + (dr)^2 + O(3) \tag{A.1}$$

After the ring deformation, point **A** moves a distance of W and V in the radial and tangential directions respectively to **A'**, and point **B** moves to **B'**. The location of **A'** is defined by $(\theta + \zeta_\theta, r + \zeta_r)$. That is

$$\mathbf{A}(\theta, r) \xrightarrow{W,V} \mathbf{A}'(\theta + \zeta_\theta, r + \zeta_r)$$
$$\mathbf{B}(\theta + d\theta, r + dr) \longrightarrow \mathbf{B}'(\theta + \zeta_\theta + d\theta + d\zeta_\theta, r + \zeta_r + dr + d\zeta_r)$$

It can be seen from Figure A.1 that

$$\zeta_\theta = \sin \zeta_\theta + O(3) = \frac{V}{r + W} + O(3) \tag{A.2a}$$

$$\zeta_r = \sqrt{(r + W)^2 + V^2} - r = W + O(2) \tag{A.2b}$$

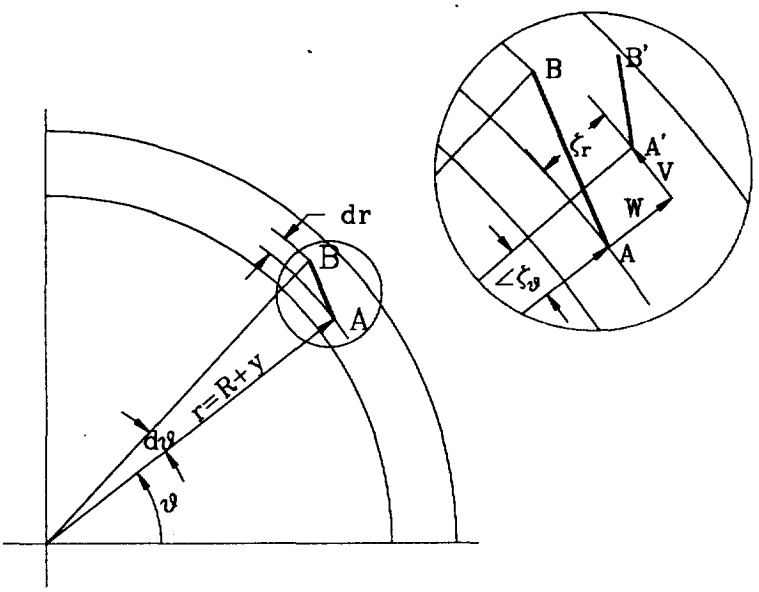

Figure A.1: The locations of two neighboring points before and after ring deformation

The infinitesimal distance between the two points after the ring deformation is

$$(ds')^2 = (r + \zeta_r)^2 (d\theta + d\zeta_\theta)^2 + (dr + d\zeta_r)^2 + O(3) \tag{A.3}$$

in which

$$d\zeta_\theta = \frac{\partial \zeta_\theta}{\partial \theta} d\theta + \frac{\partial \zeta_\theta}{\partial r} dr \tag{A.4a}$$

$$d\zeta_r = \frac{\partial \zeta_r}{\partial \theta} d\theta + \frac{\partial \zeta_r}{\partial r} dr \tag{A.4b}$$

Substituting Equation (A.4) into Equation (A.3) yields

$$(ds')^2 = G_{\theta\theta} (d\theta)^2 + 2G_{r\theta}\, d\theta\, dr + G_{rr} (dr)^2 \tag{A.5}$$

in which

$$G_{\theta\theta} = (r + \zeta_r)^2 \left(1 + \frac{\partial \zeta_\theta}{\partial \theta}\right)^2 + \left(\frac{\partial \zeta_r}{\partial \theta}\right)^2 \tag{A.6a}$$

$$G_{r\theta} = (r + \zeta_r)^2 \left(1 + \frac{\partial \zeta_\theta}{\partial \theta}\right) \frac{\partial \zeta_\theta}{\partial r} + \frac{\partial \zeta_r}{\partial \theta} \left(1 + \frac{\partial \zeta_r}{\partial r}\right) \tag{A.6b}$$

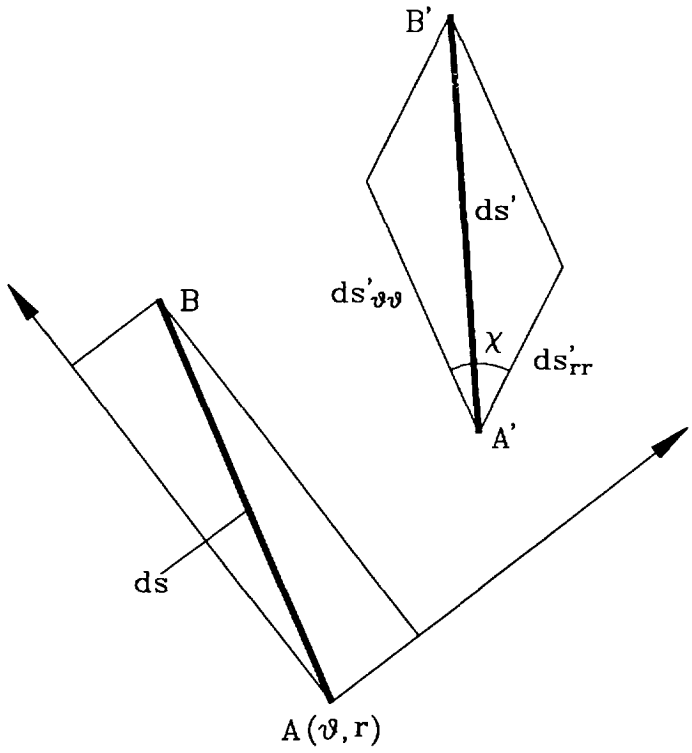

Figure A.2: An element of the ring before and after deformation

$$G_{rr} = (r + \zeta_r)^2 \left(\frac{\partial \zeta_\theta}{\partial r}\right)^2 + \left(1 + \frac{\partial \zeta_r}{\partial r}\right)^2 \tag{A.6c}$$

Now we consider an infinitesimal element of the ring shown in Figure A.2. The points **A** and **B** constitute one diagonal of the element. Before deformation, the point **A** is located at $(\theta,\, r)$ and **B** at $(\theta + d\theta,\, r + dr)$. Note that a local Cartesian coordinate system is used in Figure A.2 with its origin at point $\mathbf{A}(\theta, r)$. After deformation, points **A** and **B** move to $\mathbf{A}'$ and $\mathbf{B}'$ respectively. Utilizing Equation (A.5) we can write the distance between **A** and **B** after deformation as

$$(ds')^2 = G_{\theta\theta}\,(d\theta)^2 + 2G_{r\theta}\,d\theta\,dr + G_{rr}\,(dr)^2 \tag{A.7}$$

The normal strains can be readily written as

$$\epsilon_\theta = \frac{ds'_{\theta\theta} - rd\theta}{rd\theta} \tag{A.8a}$$

$$\epsilon_r = \frac{ds'_{rr} - dr}{dr} \tag{A.8b}$$

The shear strain is defined as the angular change of the infinitesimal element

$$\epsilon_{r\theta} = \frac{\pi}{2} - \chi \tag{A.8c}$$

According to the cosine law, the following equation can be written:

$$(ds')^2 = (ds'_{\theta\theta})^2 + 2\cos\chi\, ds'_{\theta\theta}\, ds'_{rr} + (ds'_{rr})^2 \tag{A.9}$$

It is easy to show that

$$(ds'_{\theta\theta})^2 = G_{\theta\theta}\,(d\theta)^2$$
$$(ds'_{rr})^2 = G_{rr}\,(dr)^2$$

Comparing Equation (A.9) with Equation (A.7), we have

$$\epsilon_\theta = \frac{\sqrt{G_{\theta\theta}}}{r} - 1 \tag{A.10a}$$

$$\epsilon_r = \sqrt{G_{rr}} - 1 \tag{A.10b}$$

$$\epsilon_{r\theta} \approx \sin(\epsilon_{r\theta}) = \cos\chi = \frac{G_{r\theta}}{\sqrt{G_{\theta\theta}G_{rr}}} \tag{A.10c}$$

According to Equation (A.2)

$$\frac{\partial\zeta_\theta}{\partial\theta} = \frac{1}{r+W}\frac{\partial V}{\partial\theta} - \frac{V}{(r+W)^2}\frac{\partial W}{\partial\theta} + O(3) \tag{A.11a}$$

$$\frac{\partial\zeta_\theta}{\partial r} = \frac{1}{r+W}\frac{\partial V}{\partial r} - \frac{V}{(r+W)^2}\left(1 + \frac{\partial W}{\partial r}\right) + O(3) \tag{A.11b}$$

$$\frac{\partial\zeta_r}{\partial\theta} = \frac{\partial W}{\partial\theta} + O(2) \tag{A.11c}$$

$$\frac{\partial\zeta_r}{\partial r} = \frac{\partial W}{\partial r} + O(2) \tag{A.11d}$$

Substituting the above equations into Equation (A.6) results in

$$G_{\theta\theta} = r^2 + 2r\left(W + \frac{\partial V}{\partial \theta}\right) + \left(W + \frac{\partial V}{\partial \theta}\right)^2 + \left(V - \frac{\partial W}{\partial \theta}\right)^2 + O(3) \tag{A.12a}$$

$$G_{rr} = 1 + 2\frac{\partial W}{\partial r} + O(2) \tag{A.12b}$$

$$G_{r\theta} = r\frac{\partial V}{\partial \theta} - V + \frac{\partial W}{\partial \theta} + O(2) \tag{A.12c}$$

Substituting Equations (A.12) into Equation (A.10), under the condition that the ring deformation is small, we get

$$\epsilon_\theta = \frac{1}{r}\left(W + \frac{\partial V}{\partial \theta}\right) + \frac{1}{2r^2}\left(V - \frac{\partial W}{\partial \theta}\right)^2 + O(3) \tag{A.13a}$$

$$\epsilon_r = \frac{\partial W}{\partial r} + O(2) \tag{A.13b}$$

$$\epsilon_{r\theta} = \frac{\partial V}{\partial r} + \frac{1}{r}\left(\frac{\partial W}{\partial \theta} - V\right) + O(2) \tag{A.13c}$$

If the ring is thin, then the Bernoulli-Euler assumption can be used. According to this assumption, the plane cross-sections of the ring remain plane and normal to the middle surface after deformation, and the in-plane shear strain is very small and can be negelected. The only significant strain is therefore the one in the tangential direction.

The radial displacement W can be approximated by that of the middle surface and the tangential displacement varies linearly across the ring thickness. The radial and tangential displacements W, V can thus be expressed as

$$W \approx w \tag{A.14a}$$

$$V(\theta, y, t) = v(\theta, t) + y \cdot \beta(\theta, t) \tag{A.14b}$$

in which β is the rotation angle of the ring cross-section and y is the distance from the middle surface (see Figure A.1); w, v are the displacements of the middle surface in the radial and tangential directions, respectively.

The strain-displacement relations can thus be rewritten as

$$\epsilon_\theta = \frac{1}{R+y}\left(w + \frac{\partial v}{\partial \theta} + y\frac{\partial \beta}{\partial \theta}\right) + \frac{1}{2(R+y)^2}\left(\frac{\partial w}{\partial \theta} - v - y\beta\right)^2 \tag{A.15a}$$

$$\epsilon_{r\theta} = \frac{1}{R+y}\left(\frac{\partial w}{\partial \theta} - v + R\beta\right) \tag{A.15b}$$

Since the ring is thin, which means that the mean radius of the ring is much larger than the ring thickness ($R >> h$), $R + y$ in the strain-displacement relations can be replaced by R. With shear strain $\epsilon_{r\theta}$ being set to zero we have

$$\beta = \frac{1}{R}\left(v - \frac{\partial w}{\partial \theta}\right)$$

Replacing β in Equation (A.15) with the above relation and neglecting the second order terms related to β and y, we get

$$\epsilon_\theta = \frac{1}{R}\left(w + \frac{\partial v}{\partial \theta}\right) + \frac{y}{R^2}\left(\frac{\partial v}{\partial \theta} - \frac{\partial^2 w}{\partial \theta^2}\right) + \frac{1}{2R^2}\left(\frac{\partial w}{\partial \theta} - v\right)^2 \tag{A.16}$$

Appendix B

Prestress in the Ring Due to Rotation and Inflation Pressure

When the tire is rotating at high speed and inflated by internal pressure, the tire treadband is subjected to *prestress*, which exists in the treadband before the tire deformation caused by external excitations such as road contact. Figure B.1 shows an element of the rotating ring under equilibrium. The ring element is subjected to four forces: inflation pressure $p_0 b R d\theta$, centrifugal force $\rho A R^2 \Omega^2 d\theta$, initial spring force $k_w w_0 R d\theta$, and the pretension force S_0 ($S_0 = \sigma_\theta^0 A$). It is assumed that the thickness/radius ratio of the ring is sufficiently small so that the radial prestress is negligible.

The equilibrium equation of the ring element in the radial direction can be written as follows:

$$2S_0 \sin(d\theta/2) = p_0 b R d\theta + \rho A R^2 \Omega^2 d\theta - k_w w_0 R d\theta \qquad \text{(B.1)}$$

in which w_0 is the initial displacement of the ring element in the radial direction; $\sin(d\theta/2)$ can be approximated by $d\theta/2$. Due to w_0, the ring element is expanded in the the circumferential direction by a length of $w_0 d\theta$. The following equation can be obtained according to Hooke's law:

$$\sigma_\theta^0 = E\frac{w_0}{R} \qquad \text{(B.2)}$$

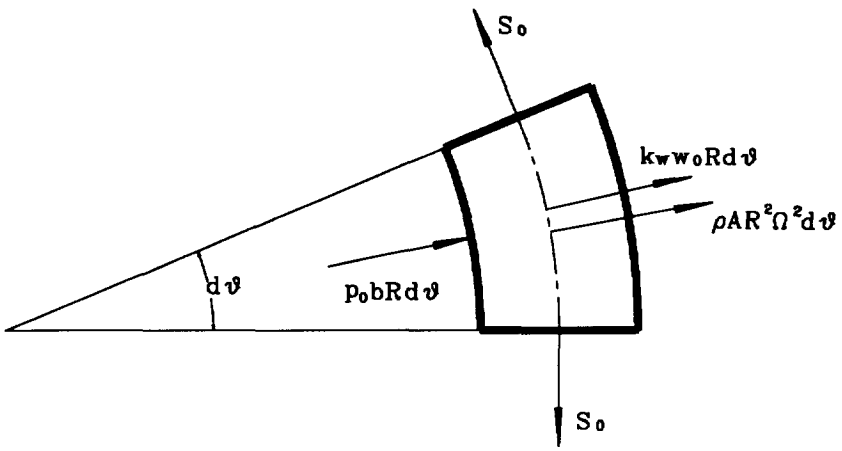

Figure B.1: The equilibrium of a ring element

Combining Equations (B.1) and (B.2) to eliminate w_0, the following equation is obtained

$$\sigma_\theta^0 A = \frac{p_0 bR + \rho AR^2\Omega^2}{1 + k_w R^2/(EA)} \tag{B.3}$$

Usually, the extensional stiffness of the tire treadband is very high. Therefore the pretension force in the treadband can be approximated by the following equation:

$$\sigma_\theta^0 A = p_0 bR + \rho AR^2\Omega^2 \tag{B.4}$$

Summary

The in-plane dynamics of tires deals with the forces and motion in the plane of rotation of the wheel. Three aspects of tire in-plane dynamics can be identified: the rolling contact between the tire and the road surface; the transmission of forces and motion from the contact patch to the wheel axle; and the vibration of the tire treadband. The main objective of the investigation reported in this thesis is to develop a tire model which is suitable to study all three aspects of the in-plane dynamics of tires in both low and high frequency ranges. Emphasis is placed on the analyses of the dynamic properties of the model and its application to the three aforementioned problems.

The work can be divided into three parts: theoretical modeling and analysis; applications; and parameter estimation and experimental validation. The tire model developed in this thesis consists of a circular ring supported on an elastic foundation. In this model, the wheel has the freedom to move in the translational as well as rotational directions in the wheel plane. This makes the model suitable for the study of all three aspects of tire in-plane dynamics. The equations of motion are derived using Hamilton's principle. A simplified set of the equations is obtained by assuming the ring to be inextensible. The simplified equations are used for the study of the vibration transmission and the rolling contact problem of the tire and the road.

The natural frequencies and modes are obtained for the ring model without the *in-extensibility assumption*. The influences of model parameters on the dynamic properties of the tire model are analyzed in detail. The validity of the in-extensibility assumption is thus examined. Furthermore, with the use of the *modal expansion method*, the equations of motion are transformed into ordinary differential equations based on mixed modal and physical coordinates. Two sets of the transformed equations are derived, one in the

rotating coordinate system, the other in the non-rotating coordinate system. Depending on the problem at hand, one of the two sets is preferred.

The model is used to study two dynamic problems of tires: the rolling contact between a tire and a flat road; and the vibration transmission from the ground to the wheel axle via the tire. For the rolling contact problem, the model is modified to take into account the compliance of the tire tread elements in the radial direction. A new approach based on the modified tire model and modal expansion method is developed to solve the problem. With this new approach, the tire deformation and contact pressure can be solved simultaneously for an assumed length of contact. This simplifies the iteration needed to ultimately obtain the contact length for a prescribed overall tire deformation or static load. The new method is implemented into a computer program. Numerical results are compared with experimental ones from literature. Using this new method, different patterns of contact pressure distribution are predicted for tires with different inflation pressures and vertical loads.

The vibration transmission problem is studied in the context of point contact assumption. The transfer functions of a free tire-wheel system are first derived from the tire model. These transfer functions determine the dynamic displacement responses of the system to force excitations. Later the boundary conditions typical to tires in service and in laboratory tests are discussed and formulated. The mathematical expressions of these boundary conditions are determined. By applying these conditions to the free tire-wheel system, the vibration transmission properties of a tire-wheel system under various boundary conditions are obtained. Transfer functions under these conditions are derived using the *modal synthesis method.* Numerical results are presented and discussed.

The tire model is finally validated by experimental modal analysis of a test tire. Laboratory tests are conducted to establish the modal shapes and natural frequencies of the test tire. The tests are carried out for two different configurations of the tire: one with the wheel rim fixed in space and one with the tire-wheel system suspended freely in the air. Three of the measured natural frequencies of the tire with a fixed wheel are used to estimate the stiffness parameters of the model. The other measured natural frequencies and mode shapes are compared with the calculated ones from the model. Good agreement is found between the experimental and theoretical results.

Samenvatting

De dynamica van de autoband in het wielvlak heeft betrekking op de krachten en bewegingen in het rotatievlak van het wiel. Drie aspecten met betrekking tot de dynamica in dit wielvlak kunnen worden onderscheiden: het contact tussen rollend wiel en wegdek; de overdracht van krachten en bewegingen vanuit het contactvlak van de band naar de wielas; en de trillingen van de gordel van de band. Het hoofddoel van het onderzoek, zoals beschreven in deze dissertatie, heeft betrekking op het ontwikkelen van een bandmodel dat geschikt is om alle drie aspecten van de banddynamica in zowel het lage als het hoge frequentiebereik te bestuderen. De nadruk ligt op de analyse van de dynamische eigenschappen van het bandmodel en de toepassing van het model op de drie eerder vermelde aspecten.

De studie kan in drie delen worden opgesplitst: theoretische modellering en analyse; toepassingen; en parameter schatting en experimentele validatie. Het bandmodel dat in dit proefschrift ontwikkeld en beschreven is, bestaat uit een cirkelvormige ring die ten opzichte van de velg afgesteund is op een elastische bedding. Het wiel heeft drie vrijheidsgraden van beweging in translatie- en rotatierichtingen in het wielvlak. Deze vrijheidsgraden zijn voldoende om alle drie aspecten van de dynamica in het wielvlak te beschrijven. De bewegingsvergelijkingen zijn afgeleid met behulp van het principe van Hamilton. De bewegingsvergelijkingen kunnen vereenvoudigd worden als aangenomen wordt dat de cirkelvormige ring in omtreksrichting onvervormbaar is. De vereenvoudigde bewegingsvergelijkingen zijn gebruikt voor het onderzoek naar de trillingsoverdracht en de studie met betrekking tot het contact van een rollende band op een wegdek.

De eigenfrequenties en trilvormen zijn uitgerekend voor een bandmodel geba-

seerd op een samendrukbare ring. De invloed van de modelparameters op de dynamische eigenschappen van het bandmodel zijn gedetailleerd onderzocht. De geldigheid van de veronderstelling dat de ring in omtreksrichting onsamendrukbaar is, is nagegaan. Bovendien zijn de bewegingsvergelijkingen met behulp van een modale decompositiemethode getransformeerd naar een verzameling van gewone differentiaalvergelijkingen welke gebaseerd zijn op een combinatie van modale en fysische coordinaten. Twee verzamelingen van getransformeerde vergelijkingen zijn afgeleid: in het roterende coordinatensysteem, en in het vast coordinatensysteem. Er wordt een keuze gemaakt tussen beide mogelijkheden afhankelijk van het probleem dat onderzocht wordt.

Het bandmodel wordt gebruikt om twee aspecten van de banddynamica te bestuderen: het contact tussen rollende band en vlak wegdek; en de trillingsoverdracht vanuit het wegdek via de band naar de wielas. In het geval van de studie met betrekking tot het contact van een rollende band met wegdek is het bandmodel aangepast door rekening te houden met de stijfheid van het loopvlak in de radiale richting. Een nieuwe benadering gebaseerd op het aangepaste bandmodel met modale decompositie is ontwikkeld om het contactprobleem van de rollende band op te lossen. Met behulp van deze nieuwe benadering kunnen de bandvervorming en contactdruk simultaan opgelost worden voor een bepaalde aangenomen contactlengte. Dit vereenvoudigt de iteratie welke noodzakelijk is om de uiteindelijke contactlengte te vinden voor een voorgeschreven radiale deformatie van de band of een gegeven statische belasting. De nieuwe methode is geimplementeerd in een computersimulatieprogramma. Numerieke uitkomsten zijn vergeleken met experimentele resultaten welke bekend zijn uit de literatuur. Met behulp van deze methode kunnen verschillende vormen van drukverdelingen in het contactvlak van de rollende band voorspeld worden als functie van de bandenspanning en de verticale belasting.

Het probleem van de trillingsoverdracht is bestudeerd aan de hand van een puntcontact veronderstelling. Eerst zijn de overdrachtsfuncties van een vrij band-wiel systeem afgeleid met behulp van het bandmodel. Deze overdrachtsfuncties bepalen de dynamische verplaatsingsresponsie van het systeem op een krachtsexcitatie. Vervolgens worden de randvoorwaarden van het systeem die kunnen voorkomen bij testen op de weg en in het laboratorium, besproken en geformuleerd. De mathematische formuleringen welke betrekking hebben op deze randvoorwaarden worden vastgesteld. Door toe-

passing van deze voorwaarden op een vrij band-wiel systeem kunnen de trillingseigenschappen van een band-wiel systeem onder verschillende randvoorwaarden verkregen worden. De overdrachtsfuncties zijn afgeleid met behulp van de modale synthesemethode. Numerieke resultaten worden gepresenteerd en besproken.

Het bandmodel is tenslotte gevalideerd met behulp van experimentele modale analyse, toegepast op een testband. De modale trilvormen en eigenfrequenties zijn bepaald in het laboratorium. De experimenten zijn uitgevoerd voor twee verschillende bandconfiguraties: een systeem met een ten opzichte van de buitenwereld ingeklemde wielvelg en een systeem met een vrijhangend wiel. Er zijn drie gemeten eigenfrequenties gebruikt van het ingeklemde wielsysteem om de stijfheden van het model af te schatten. De andere eigenfrequenties en trilvormen zijn vergeleken met de berekende waarden van het bandmodel. De resultaten stemmen goed overeen met de gemeten responsies.

Biography

October 6, 1962	born in Pinghu County, Zhejiang Province, China
1969–1974	Chenguang Elementary School, Pinghu County, Zhejiang Province, China
1974–1978	Xincang Secondary School, Pinghu County, Zhejiang Province, China
1978–1982	B. Sc. Student, Beijing Agricultural Engineering University, Beijing, China
1982–1985	M. Sc. Student and Research Assistant, Beijing Agricultural Engineering University, Beijing, China
1985–1988	Lecturer, Beijing Agricultural Engineering University, Beijing, China
1988–1993	Research Assistant, Delft University of Technology, Delft, The Netherlands